Targeting AML dependency on VCP-mediated DNA repair through a selective second-generation small molecule inhibitor

Blandine Roux, Camille Vaganay, Jesse D Vargas, Gabriela Alexe, Chaima Benaksas, Bryann Pardieu, Nina Fenouille, Jana M Ellegast, Edyta Malolepsza, Frank Ling, et al.

Targeting AML dependency on VCP-mediated DNA repair through a selective second-generation small molecule inhibitor

Blandine Roux[1*], Camille Vaganay[1*], Jesse D. Vargas[2], Gabriela Alexe[3,4], Chaima Benaksas[1], Bryann Pardieu[1], Nina Fenouille[1], Jana M. Ellegast[3,4], Edyta Malolepsza[4], Frank Ling[1], Gaetano Sodaro[1], Linda Ross[3,4], Yana Pikman[3,4], Amy S. Conway[3,4], Yangzhong Tang[2], Tony Wu[2], Daniel J. Anderson[2], Ronan Le Moigne[2], Han-Jie Zhou[2], Frédéric Luciano[5], Christina R. Hartigan[4], Ilene Galinsky[6], Daniel J. DeAngelo[6], Richard M. Stone[6], Patrick Auberger[5], Monica Schenone[4], Steven A. Carr[4], Josée Guirouilh-Barbat[7], Bernard Lopez[7], Mehdi Khaled[8], Kasper Lage[4], Olivier Hermine[9], Michael T. Hemann[10], Alexandre Puissant[1#], Kimberly Stegmaier[3,4#] and Lina Benajiba[1#]

[1] Université de Paris, INSERM U944 and CNRS UMR 7212, Institut de Recherche Saint Louis, Hôpital Saint Louis, APHP, Paris, FRANCE;
[2] Cleave Therapeutics, Inc, Burlingame, CA, USA;
[3] Department of Pediatric Oncology, Dana-Farber Cancer Institute and Boston Children's Hospital, Harvard Medical School, Boston, MA, USA;
[4] The Broad Institute of Harvard University and Massachusetts Institute of Technology, Cambridge, MA, USA;
[5] C3M, INSERM U1065, Team Cell Death, Differentiation, Inflammation and Cancer, Nice, FRANCE;
[6] Department of Medical Oncology, Dana-Farber Cancer Institute, Harvard Medical School, Boston, MA, USA;
[7] CNRS UMR 8200, Gustave-Roussy Cancer Center, Université Paris-Saclay, Equipe Labellisée Ligue Contre le Cancer, Villejuif, FRANCE;
[8] INSERM U1186, Gustave-Roussy Cancer Center, Université Paris-Saclay, Villejuif, FRANCE;
[9] Université de Paris, INSERM U1163 and CNRS 8254, Institut Imagine, Hôpital Necker, APHP, Paris, FRANCE;
[10] Koch Institute for Integrative Cancer Research at Massachusetts Institute of Technology, Massachusetts Institute of Technology, Cambridge, MA, USA;

*: These authors contributed equally to this work.
[#]: These senior authors contributed equally to this work.
Corresponding authors:
lina.benajiba@inserm.fr
kimberly_stegmaier@dfci.harvard.edu
alexandre.puissant@inserm.fr

ABSTRACT

The development and survival of cancer cells require adaptive mechanisms to stress. Such adaptations confer intrinsic vulnerabilities, enabling the selective targeting of cancer cells. Through a pooled *in vivo* shRNA screen, we identified the AAA-ATPase VCP as a top stress-related vulnerability in acute myeloid leukemia (AML). We established that AML was the most responsive disease to chemical inhibition of VCP across a panel of 16 cancer types. The sensitivity to VCP inhibition of human AML cell lines, primary patient samples, and syngeneic and xenograft mouse models of AML was validated using VCP-directed shRNAs, overexpression of a dominant negative VCP mutant, and chemical inhibition. By combining a mass spectrometry-based analysis of the VCP interactome and phospho-signaling studies, we determined that VCP is important for ATM kinase activation and subsequent DNA repair in AML. Finally, we report a second-generation, clinical candidate VCP inhibitor, CB-5339, and validate its efficacy in multiple AML models, providing data to support the clinical testing of single agent CB-5339 or its combination with standard of care AML DNA damaging chemotherapy.

Keywords: AML, VCP, DNA damage repair, ATM, CB-5339

Single sentence summary: AML cell dependency on the DNA repair function of the AAA-ATPase VCP offers a therapeutic avenue.

INTRODUCTION

The past two decades of basic and translational cancer research have brought into the clinic a myriad of small molecules targeting oncogenic dependencies driven by oncogene mutations. The treatment of acute myeloid leukemia (AML) has seen recent progress with the FDA-approval of drugs for patients with mutations in *FLT3* (midostaurin and gilteritinib), *IDH2* (enasidenib) and *IDH1* (ivosidenib) (*1*-*3*). Although conceptually attractive and clinically effective in a subset of patients, targeting mutated oncogenes is not always feasible, for reasons such as loss-of-function mutations, difficult to drug oncogenic drivers, or lack of identified mutated drivers. Additionally, clonal evolution under targeted selective pressure frequently results in drug-resistant clonal outgrowth (*4*).

An emerging alternative therapeutic approach relies on targeting non oncogenic driver pathways essential for tumor survival, such as cellular stress response (*5, 6*). Systematic functional genomic screens, using shRNA or CRISPR/Cas9, have recently revealed such new therapeutic targets in a number of cancers not suggested by their mutational profiles (*7*). In some cases, *in vitro* screens are sufficient to identify high fidelity dependencies subsequently validated both *in vitro* and *in vivo*. In other cases, particularly in the context of metabolic, immunologic, proteotoxic, or DNA damage stress response targets, an *in vivo* approach may enhance the identification of true positives.

These evolutionaly conserved stress response pathways are rewired in cancers, such as AML, to permit tumorigenesis and cancer cell survival in the face of oncogenic stress. Indeed, these escape mechanisms allow the clonal selection of cells which can

proliferate despite accumulation of damage, thus increasing the risk of full transformation in a premalignant cell (*8*). Although necessary for leukemogenesis, these adaptive mechanisms also confer an intrinsic vulnerability and an attractive therapeutic opportunity to selectively target AML cells. Indeed, cellular survival under such unfavorable conditions becomes highly dependent on proficient stress response pathways. Disrupting this common hallmark of cancer through stress sensitization and/or stress overload should ultimately result in cancer cell death (*5*). For example, targeting oxidative and metabolic stress through BCL-2 inhibition has been shown to have anti-leukemic activity in multiple preclinical models (*9*). These studies have been recently validated with the promising efficacy of the selective BCL-2 inhibitor venetoclax, now FDA-approved for a subset of patients with AML, combined with low dose cytarabine or hypomethylating agents (*10-13*). Therefore, developing functional approaches to unravel such cellular mechanisms to evade stress surveillance may open new therapeutic avenues for AML treatment. Here, we performed an *in vivo* pooled shRNA screen in an AML mouse model driven by the MLL-AF9 translocation to identify new druggable targets involved in cellular stress reponse pathways.

RESULTS

An *in vivo* shRNA screen identifies VCP as an AML dependency.

To find therapeutic gene candidates in AML, we designed a custom shRNA library of 2,115 shRNAs targeting 429 genes implicated in various adaptive stress response pathways. This library, cloned into a doxycycline-inducible vector, was transduced as a pool into L-GMP primary MLL-AF9 cells reinjected into sub-lethally irradiated secondary syngeneic recipient mice (*14*, *15*) (**Fig. 1A**). Using an EdgeR/RIGER comparative analysis of the relative representation of the library hairpins between the two groups of mice treated with and without doxycycline, we identified *Vcp*, an AAA-ATPase family member, as a top scoring hit (**Fig. 1B and table S1**). As expected, multiple hairpins directed against the tumor suppressor gene, *PTEN* (*16*), as well as a previously described metabolic cancer dependency gene, *LDHA*, scored among the top enriched and depleted genes respectively (*17*), providing support for the overall screen quality. We first validated the dependency of the MLL-AF9 blasts on Vcp using two *Vcp*-directed shRNAs whose efficiency was validated by western blot (**Fig. 1C**). Doxycycline-induced *Vcp* knockdown reduced the MLL-AF9-driven disease burden in mouse bone marrow, spleen and peripheral blood as evaluated by flow cytometry (**Fig. 1D)** and prolonged survival, thereby confirming Vcp dependency in this AML model (**Fig. 1E**). Because mice ultimately succumbed to AML despite the initial disease burden clearance following *Vcp* knockdown, we further evaluated disease relapse characteristics in this murine model. Interestingly, at time of death, *Vcp* knocked down mice harbored a leukemic burden mainly composed of non shRNA-expressing cells, suggesting that disease relapse may result from a positive selection of leukemic cells that have escaped the doxycycline-induced shRNA knock-down (**Fig. 1F and fig. S1, A-C**). These results thus further validate AML cell dependency on *Vcp*.

VCP is an ATPase protein chaperone which adopts a homo-hexameric conformation comprising six identical subunits arranged in a ring. Each monomeric subunit contains two tandem AAA-ATPase domains responsible for ATP binding and hydrolysis (D1 and D2). The main ATPase activity is contained in the D2 domain. We further evaluated the VCP dependency in the MLL-AF9 cells using a previously reported ATPase-deficient, mutant form of VCP (E305Q, E578Q). This mutant VCP is unable to hydrolyze ATP but still incorporates into WT hexamers, and thus exhibits a dominant negative (DN) function on the complex by abrogating its ATPase activity (*18, 19*). VCP DN was tagged with a ligand-dependent destabilization domain (DD) whose function was to constitutively destabilize VCP DN. Treatment with the membrane-permeable DD ligand, Shield-1, was then used to block the DD function and stabilize VCP DN in MLL-AF9 cells (**Fig. 1G**). Shield-1-induced VCP DN overexpression was sufficient to impair the MLL-AF9-driven disease expansion (**Fig. 1H)** *in vivo* and prolonged mice survival, thereby establishing that the ATPase activity of VCP is required for AML progression (**Fig. 1I**).

AML is preferentially sensitive to VCP inhibition.

To evaluate whether VCP inhibition elicited a preferential response in AML, we expanded our investigation to a panel of 131 human cancer cell lines, representing 16 cancer types, with the ATP-competitive, small-molecule VCP inhibitor CB-5083 (*20, 21*). AML was more sensitive to CB-5083 compared to other cancer subtypes, suggesting that AML is highly dependent on VCP (**Fig. 2A and table S2**). To further validate these results, we treated a panel of 16 AML cell lines with CB-5083 and a highly-selective allosteric VCP inhibitor NMS-873 (*22*). The sensitivity of the AML

cell lines to these two VCP inhibitors was strongly correlated (Spearman score = 0.8), supporting their on-target effect (**Fig. 2B**). Moreover, expression of a mutated form of *VCP* (A530T), which confers resistance to NMS-873 (*23*), in UT-7 cells rescued the loss of viability induced by NMS-837, thereby confirming the selectivity of NMS-873 for VCP in an AML context **(Fig. 2C)**.

The anti-leukemic effect of reduced VCP expression and activity was then investigated in three human AML cell lines expressing *VCP*-directed shRNAs **(Fig. 2D)** or overexpressing the WT or DN VCP (**Fig. 2E).** Impairment of VCP expression or function markedly decreased viability of the AML cell lines MV4-11 and UT-7, whereas the NOMO-1 cell line was relatively resistant to VCP inhibition, suggesting that all AML subtypes are not equally dependent on VCP (**Fig. 2, D and E**). The decreased cell viability observed is specific to the loss of VCP function, as the overexpression of WT VCP did not impair cell growth. Of note, the profile of sensitivity of these cell lines to *VCP* knockdown and VCP DN overexpression matched their sensitivity to VCP chemical inhibition, supporting on-target activity of both the genetic and chemical tools.

Additionally, VCP impairment through either chemical inhibition or VCP DN overexpression resulted in a decreased colony forming ability (**Fig. 2F**). Finally, using Annexin V/propidium iodide staining and flow cytometry analysis of the two most VCP-dependent AML cell lines, MV4-11 and UT-7, we determined that inhibition of VCP ATPase activity using either NMS-873 or overexpression of exogenous VCP DN induced Annexin-positive cell death consistent with apoptosis (**Fig. 2G**).

VCP inhibition efficiently targets leukemic cells in multiple *in vivo* AML models and primary AML patient samples.

In order to confirm the anti-leukemic effect of VCP impairment in human AML *in vivo*, we first induced VCP DN overexpression using Shield-1 in MV4-11 cells injected into immunocompromised NSG mice. As we observed in **Fig. 1, G-H** in the MLL-AF9 syngeneic mouse model, VCP DN overexpression delayed disease progression and improved survival in this MV4-11 orthotopic xenograft model (**Fig. 3, A and B**). Because NMS-873 does not possess pharmacokinetic properties suitable for *in vivo* testing, we then evaluated the efficacy of the orally-bioavailable drug candidate recently tested in a phase I clinical trial in patients with advanced solid tumors : CB-5083, in both the MLL-AF9 syngeneic and MV4-11 xenograft mouse models (*20, 21*) (NCT02243917). CB-5083 treatment decreased disease burden (**Fig. 3, C-E**) and prolonged mice survival in both AML models (**Fig. 3, F and G**). Importantly, no major weight loss or hematopoietic toxicity based on complete blood counts was observed upon CB-5083 treatment (**fig. S2, A-D**).

To further demonstrate the clinical potential of VCP inhibition as an anti-AML therapy, we then treated leukemia cells from five patients with AML and established that the blockade of VCP activity, using either NMS-873 or CB-5083, impaired the capacity of AML blasts to form colonies in methylcellulose (**Fig. 3, H-I and table S3**). In line with this data, CB-5083 also substantially decreased disease burden in an orthotopic patient-derived xenograft (PDX) model of therapy-related MLL-AF9 positive AML (**Fig. 3J and table S3**).

Together, these results indicate that primary patient AML blasts and AML cell lines are dependent on the enzymatic activity of VCP for survival and proliferation, both *in vitro* and *in vivo*.

Inhibition of the nuclear function of VCP alters AML cell line viability through impairment of DNA repair.

VCP is reported to have many functions in the cell, but the mechanism promoting the exquisite dependency in AML was unclear. Previous studies demonstrated that VCP inhibition triggers the endoplasmic reticulum (ER)-associated protein degradation pathway, promotes accumulation of poly-ubiquitinated proteins and generation of proteotoxic stress associated with activation of the unfolded protein response pathway (*24*, *25*). In contrast to these reports, neither NMS-873 treatment nor overexpression of VCP DN induced accumulation of poly-ubiquitinated proteins **(Fig. 4A and fig. S3A)** or promoted accumulation of the ER stress marker GRP78 **(fig. S3B)** at a concentration of NMS-873 observed to impair viability in AML. Poly-ubiquitinated proteins start to accumulate when AML cells are exposed to 5 μM (100-fold the IC50) of NMS-873 (**fig. S3C**). Moreover, in the panel of 16 AML cell lines tested, sensitivity to NMS-873 did not correlate with sensitivity to bortezomib, a proteasome inhibitor **(fig. S3D),** and VCP inhibition did not result in any marked changes in the caspase-, trypsin-, or chymotrypsin-like enzymatic activities of the proteasome at concentrations altering cellular viability **(fig. S3E)**.

To further investigate the mechanism of action by which VCP inhibition may alter AML growth, we exploited the fact that VCP is present in both the nucleus and cytoplasm of AML cells in order to ask whether AML cell survival relies more on the

nuclear or the cytoplasmic pool of VCP. Therefore, we depleted endogenous VCP concomitantly with overexpression of a codon optimized non shRNA targetable exogenous VCP WT or VCP WT fused to a Nuclear Export Signal (NES), in the MV4-11 AML cell line. We validated by subcellular fractionation that this NES mutant VCP WT remained largely absent from the nucleus of MV4-11 AML cell lines (**Fig. 4B**). As expected, VCP knockdown decreased cellular viability in the MV4-11 AML cell line. Although this effect was significantly abolished by codon optimized VCP WT overexpression ($p<0.0001$), VCP WT NES failed to restore MV4-11 cell viability to the same extent as its WT counterpart, thus suggesting an essential role for VCP in nuclear signaling pathways in AML (**Fig. 4C**). To further support the nuclear essentiality of VCP in AML, we fused a Nuclear Export Signal (NES) to the VCP DN mutant to drive its constitutive export from the nucleus (**Fig. 4D**). Restricting VCP DN localization to the cytoplasm abrogates its cytotoxic effects on these cells, therefore arguing again for a role of the nuclear fraction of VCP in AML cells survival (**Fig. 4E**).

To investigate the nuclear functions of VCP in AML, we performed an unbiased mass spectrometry-based characterization of the VCP interactome in the MV4-11 AML cell line, one of the most sensitive cell lines to VCP inhibition. MV4-11 cells were infected with either a V5-tagged VCP or an empty control vector before V5 immunoprecipitation and mass-spectrometry analysis. A total of 735 VCP protein partners were identified **(table S4)**. Two previously described critical VCP substrate adapters, NPLOC4 and UFD1L, scored as top VCP interactors in our screen, thereby acting as internal positive controls and validating our mass-spectrometry approach **(fig. S4A)**. The 92 top scoring hits (p-value < 0.05 and $\log_2$ (FC) > 0.5) are represented in the interactome network in **Fig. 4F.** We interrogated this list of top scoring hits with

published, validated gene signatures for enrichment by pathway analysis **(table S5)** and established that VCP interacts with 41 nuclear proteins markedly enriched among DNA damage recognition and repair pathways **(Fig. 4F and table S5)**. To better explore the VCP interactome in an AML context, we compared our data with previously reported VCP interactome data in HEK-293T cells (*26*). The overlap and differences between both cellular contexts are highlighted in **fig. S4, B and C** and **table S6**. Eighty high confidence VCP-interacting proteins were only identified in the MV4-11 AML cell line (**fig. S4C**). Interestingly, this AML interactors were markedly enriched among DNA repair and replication pathways in an unbiased enrichment overlapping analysis (**fig. S4D**). In a similar enrichment analysis, VCP-interacting proteins only detected in the HEK-293T cellular context were mainly enriched among mRNA processing and not DNA repair pathways (**fig. S4E)**.

Based on these results, we then assessed phosphorylation of the histone H2AX (termed as γH2AX), which reflects accumulation of double-strand breaks (DSB) in DNA. Inhibition of VCP using either NMS-873 treatment or VCP DN overexpression increased γH2AX in MV4-11 and UT-7 AML cell lines as was observed in cells treated with etoposide, a topoisomerase inhibitor that induces DSBs (**Fig. 4,G and H**).

Given that the two major DNA repair pathways in response to DSB are homologous recombination (HR) and non-homologous end-joining (NHEJ), we then explored the effects of VCP impairment on these pathways. We used two reporter systems to evaluate induction of either HR or NHEJ in response to I-SceI overexpression. This endonuclease creates a targeted DSB in an eGFP or CD4 reporter sequence. Successful repair of the DSB by either HR or NHEJ results in the reconstitution of functional eGFP

or CD4, which can be quantified using flow cytometry (**Fig. 4, I and J**). As expected, we observed that pharmacological inhibition of the serine/threonine kinase ATM, a key component of the HR repair pathway (*27, 28*), impaired HR-mediated DSB repair. Inhibition of VCP with NMS-873 also led to an impairment of HR, whereas it did not impair NHEJ, suggesting that VCP plays an important role in HR DSB repair.

Taken together, these results suggest that VCP inhibition impedes the activation of HR DNA repair pathways, thereby promoting DNA damage accumulation in leukemic cells.

VCP inhibition impairs ATM phosphorylation and downstream signaling resulting in increased sensitivity to DNA damaging agents.

Many key mammalian DNA damage response signaling pathways stem from activation of the canonical serine/threonine kinase ATM (*27, 28*). Interestingly, we observed that the pattern of sensitivity to pharmacological inhibition of this key genome guardian using the ATM inhibitor KU-55933, in a panel of 16 AML cell lines **(Fig. 5A)** and 16 primary AML patient samples **(Fig. 5B and table S3),** was highly correlated with their sensitivity to NMS-873 (Spearman score = 0.8 and 0.7 respectively). To evaluate the impact of VCP impairment on the DNA damage signaling response, we used etoposide to induce DSBs. We then evaluated the downstream DNA repair signaling cascade after either genetic (VCP DN overexpression) or chemical inhibition of VCP. These experiments were performed using short-term VCP impairment, to allow the evaluation of early effects on DNA repair signaling, before high cellular DNA damage accumulation. Consistent with our previous results, we established that VCP inhibition blocked DSB-induced activation of ATM signaling **(Fig. 5, C and D)** and ATM's well-

reported protein substrates, BRCA1, SMC1 and KAP1 **(Fig. 5E),** suggesting that VCP plays a central role in DNA damage sensing and repair in AML. Moreover, in line with a role for VCP at the crosstalk between DNA damage response pathways and AML growth, we established that VCP inhibition sensitizes AML cells to DNA damaging agents, such as irradiation (**Fig. 5, F and G**) and the anthracycline doxorubicin (**Fig. 5, H and I**).

Together, these results suggest that the anti-leukemic effect of VCP inhibition might result from inefficient DNA damage recognition and repair. Therefore, these findings nominate VCP inhibition as a potential therapeutic avenue to treat patients with AML and support further preclinical studies to test it in combination with standard chemotherapy regimens using anthracyclines.

CB-5339, a second-generation, potent and selective VCP small-molecule inhibitor offers a promising therapeutic avenue for AML.

CB-5083 is a first-in-class ATP-competitive VCP inhibitor that was recently tested in two phase I clinical trials in solid tumors and multiple myeloma (*20, 21*) (NCT02243917, NCT0223598). The clinical development of this drug candidate was halted due to an unexpected off-target inhibitory action on phosphodiesterase 6 (PDE6), a key regulator of the retinal phototransduction cascade (*29*), thus resulting in ophthalmological side effects. This finding is reminiscent of the vision disturbances caused by PDE5 inhibitors, which were developed for the treatment of erectile dysfunction and had cross-reactivity with PDE6 (*30*).

In order to translate our findings into the clinic, a second-generation, highly selective and potent ATP-competitive, oral, small molecule inhibitor of VCP, CB-5339, was developed (**Fig. 6A**). CB-5339 is 15-fold less active on the human cone PDE6 (PDE6C) in *in vitro* biochemical assays, and displays a 31-times lower Cmax *in vivo* in rat retina compared to CB-5083, thus addressing the off-target limitations of the first-generation compound (**Fig. 6B**). Importantly, CB-5339 retains the high on-target potency of CB-5083 and displays a similar sensitivity profile across a panel of 138 cell lines (**Fig. 6C**). To further characterize the molecular inhibition of VCP using this second-generation drug candidate, the previously established HCT116 colon cancer CB-5083 resistant cell lines were treated with either CB-5083 or CB-5339 (*20*). These resistant cell lines harbor *VCP* mutations mainly located in or adjacent to the D2 ATPase domain of VCP. Both compounds showed a comparable biochemical efficacy profile, thus arguing for a similar molecular inhibitory mechanism, and retention of the on-target effect of the first-generation compound on VCP (**Fig. 6D**). The efficacy of CB-5339 was then assessed in our panel of 16 AML cell lines and was accordingly correlated to the first-generation inhibitor CB-5083 (**Fig. 6E**). Importantly, CB-5339 efficacy was also validated on a panel of 16 primary AML patient samples harboring diverse genetic backgrounds (**table S3**). The median IC50 was 375 nM among these samples, thus supporting the translational potential of CB-5339 (**Fig. 6F**).

To further validate our mechanistic hypothesis using the clinical candidate CB-5339, we first studied its effects on polyubiquitin protein accumulation and the activation of the unfolded protein response (UPR) in an AML context. CB-5339 treatment induced dose-dependent polyubiquitin protein accumulation at concentrations ≥ 0.4 µM (**fig. S5A**). Similarly, the ER stress marker GRP78 accumulated at concentrations ≥ 0.4 µM,

while spliced XBP-1 and ATF-4 accumulated after treatment with CB-5339 at concentrations ≥ 1.6 µM and 0.8 µM respectively (**fig. S5B**) arguing for a concentration-dependent increase in proteotoxic stress. We also explored DNA damage response signaling after CB-5339 treatement to evaluate whether CB-5339 also impaired DNA repair at concentrations impacting cellular viability in AML (MV4-11 IC_{50} = 0.18 µM). Importantly, CB-5339 treatment impaired ATM phosphorylation upon etoposide DSBs induction (**fig. S5C**) and increased γH2AX accumulation at 0.2 µM (**fig. S5D**). Accordingly, CB-5339 also synergized with doxorubicin in the MV4-11 AML cell line (**fig. S5E**). CB-5339 thus displays both a nuclear and a cytoplasmic effect on AML cell lines. Lower concentrations impair DNA repair while higher concentrations result in proteotoxic stress, with both potentially contributing to the viability effect observed with CB-5339 treatment of AML cells. To further evaluate the relative importance of each effect on AML cellular viability, we studied the pattern of sensitivity of 16 AML cell lines to CB-5339 compared to either the proteasome inhibitor bortezomib or the ATM inhibitor KU-55933. Cellular sensitivity to CB-5339 across this panel of AML cell lines was not correlated with bortezomib response while it was strongly correlated with KU-55933 sensitivity (Spearman score = 0.67) (**fig. S5, F and G**). These results are similar to those observed with the allosteric inhibitor of VCP; NMS-873 and are in line with our rescue experiments arguing for a strong dependency of AML on the nuclear function of VCP.

Compared to CB-5083, CB-5339 has a lower clearance in preclinical studies in multiple species, thus providing for a higher bioavailability (**fig. S6A**). In order to confirm that the highly conserved on-target activity of CB-5339 against VCP translated into a similar *in vivo* efficacy, we used a MLL-AF9 driven patient derived xenograft (PDX)

AML mouse model. As observed with CB-5083, CB-5339 treatment resulted in decreased bone marrow leukemic infiltration and prolonged mice survival (**Fig. 6,G and H**).

Similar to the results obtained with this PDX model, CB-5339 treatment decreased circulating leukemic cells and prolonged survival in the MLL-AF9 syngeneic mouse model (**Fig. 6, I and J**). Moreover, CB-5339 synergized *in vivo* with standard of care AML chemotherapy, a combination of an anthracycline and cytarabine. This triple combination regimen resulted in decreased leukemia burden and prolonged mouse survival compared to each regimen alone (**Fig. 6, K and L**). Importantly, CB-5339 was well tolerated as evidenced by stable weight curves and absence of substantial myelosuppression (**fig. S6, B-E**).

At time of disease relapse, no marked difference in disease burden or cell surface myeloid differentiation markers were observed (**fig. S6, F and G**). Consistently, differentiation markers were not substantially increased at time of initial disease burden evaluation post-CB-5339 treatment (**fig. S6H**). These results suggest that CB-5339 does not induce phenotypic differentiation of myeloid leukemia cells and are in agreement with our mechanistic model based on leukemic cell apoptosis rather than cell differentiation.

Together, these data suggest that the nuclear function of VCP is critical for AML cell survival and uncover a promising therapeutic avenue for the use of the second-generation inhibitor, CB-5339, in combination with standard of care AML chemotherapy regimens.

Co-occurrence of RAS oncogene activation and TP53 deficiency is associated with impaired response to VCP inhibition.

One fundamental step to accelerate the clinical translation of our findings relies on the identification of the most or least responsive AML subgroups to VCP inhibition. To address this question, we first evaluated *VCP* mRNA expression based on the publicly available Cancer Cell Line Encyclopedia (CCLE) database (https://depmap.org/portal/download/; (*31, 32*)). No correlation was observed between *VCP* expression and cancer cell line sensitivity to CB-5339 in our panel of AML cell lines (12 available in CCLE) nor in our pan-cancer sensitivity screen (91 cell lines available in CCLE) (**Fig. 7, A and B**). VCP is thus ubiquitously expressed with very low variation among different cancer cellular contexts and does not explain the differential sensitivity to VCP inhibition.

Because of the role of DNA repair impairment in the underlying mechanism of AML growth blockade by VCP inhibition, we next evaluated both γ-H2AX and pATM basal expression using a quantitative flow cytometry approach in two sensitive and two resistant AML cell lines. Neither of these DNA damage-related markers was correlated with VCP sensitivity (**Fig. 7, C and D**).

To further assess for biomarkers of VCP sensitivity or resistance in AML, we then analyzed the mutational profiles of the 16 AML cell lines screened for sensitivity to the VCP inhibitor NMS-873 using the CCLE database (https://depmap.org/portal/download/; (*31, 32*)). Because our initial screen was performed in an MLL-driven mouse model, we first evaluated the impact of MLL rearrangement on VCP dependency. The MLL status was not associated with increased

sensitivity to NMS-873. No specific single mutation was associated with VCP sensitivity nor with VCP resistance.

Given the poor prognosis of *TP53* and *RAS* mutations in AML and their potential effect on the DNA repair pathways, we then explored whether the combination of these mutations was associated with resistance to VCP inhibition. We found that harboring co-occurring activating mutations in one of the RAS family genes (*KRAS* or *NRAS*) and deleterious mutations in the *TP53* gene is associated with decreased response to VCP inhibition (two tailed Fisher exact test odds ratio = 2.67, P-value = 0.002) **(Fig. 7E and table S7).** Consistently, the top 4 sensitive cell lines EOL-1, MV4-11, U937 and UT-7 harbor at most a single splice site mutation for *TP53* and no mutation for *KRAS* or *NRAS*. *KRAS/NRAS* and *TP53* mutational co-occurrence was associated with decreased response to VCP inhibition using NMS-873, CB-5083 and CB-5339 **(Fig. 7F)**.

Using the pan-cancer TCGA database (https://cancergenome.nih.gov/publications; (*33*)), we observed that the frequency of *TP53* and *RAS* mutations co-occurrence in AML was among the lowest across the 33 TCGA cancer cohorts **(Fig. 7G and table S8)**, potentially generating a preferential VCP vulnerability in AML. This observation was validated using recently developed functional classifiers allowing identification of *TP53* deficiency (*34*) and *RAS* activation (*35*) **(Fig. 7H and table S8)**.

Together, this data suggests that co-occurrence of *TP53* deficiency and *RAS* pathway activation renders cancer cells less sensitive to VCP inhibition and highlights a useful biomarker that could inform future clinical trials.

DISCUSSION

Our studies revealed a strong dependency of AML on the multifunctional AAA-ATPase VCP. VCP recently has been reported to play a role in solid tumors and multiple myeloma progression through regulation of protein homeostasis and ER stress (*20, 22, 36*). In contrast to these prior studies focused on the role of VCP in proteotoxic stress, our data provide evidence that impairing this multifunctional AAA-ATPase in an AML context also targets another key cancer hallmark: genomic instability (*5, 37*).

Previous studies have determined that the yeast homolog of VCP - Cdc48 - and VCP play a key role in regulation of DNA damage tolerance and repair pathways (*38-41*). VCP has been implicated in extracting proteins, such as trapped Ku70/80 rings and the CMG (Cdc45, MCM2-7, and GINS) replicative helicase from chromatin, to maintain genome stability (*42-47*). Here, we demonstrate that VCP inhibition plays a key upstream function in DNA repair in an AML context, through the impairment of the canonical DNA repair kinase ATM. Using mass spectrometry-based interactome analysis, we highlighted the broad role of VCP in AML as a key interactor at the crosstalk of many nuclear signaling cascades, including DNA repair, synthesis and replication.

Emerging evidence suggests that targeting non-oncogene addictions, such as stress response pathways (*5, 6*), represents a promising cancer therapy. Among these cancer cell vulnerabilities, targeting DNA damage tolerance and repair pathways has emerged as a valuable therapeutic avenue. Indeed, the success of Poly(ADP-ribose) polymerase inhibitors in the treatment of cancers deficient for homologous recombination, such as *BRCA1-2* deficient ovarian and breast cancers, prompted

researchers to develop and test new therapeutic strategies to target the DNA damage response (DDR) in cancer (*48*). In AML, despite the fact that germ-line mutations in DDR genes are very rare, recent reports demonstrate that defective DDR can result from replication and oxidative stress, gene polymorphisms and transcriptional deregulation of key DDR players (*49, 50*). For example, mutations in *IDH1* have been reported to downregulate the DNA damage sensor ATM by altering histone methylation, leading to impaired DNA repair and increased sensitivity to DNA damage (*51*). Recent studies established that pharmacological inhibition of the two serine/threonine kinases ATR and ATM represent potential therapeutic strategies for the treatment of AML, especially MLL-driven leukemias (*52*). Our own results, using genetic and pharmacological tools in primary AML patient samples and cell lines, and in syngeneic and xenografted AML mouse models, uncovered a strong dependency of AML on the nuclear function of the AAA-ATPase VCP through its regulation of ATM kinase signaling and subsequent DNA repair. VCP inhibition thus represents another approach to inhibiting DNA damage repair in AML. Although complete *Vcp* knockout (KO) is embryonic lethal in mice (*53*), *Vcp* heterozygous KO is notably viable and no specific dysfunctional phenotype has been reported (*53*), suggesting a dosage effect, and offering a therapeutic window for the selective targeting of cancer cells particularly addicted to VCP-driven cellular processes. Given the heightened sensitivity of AML cells to VCP inhibition, we hypothesize that impairment of DNA repair through VCP inhibition could offer a therapeutic window to selectively target AML cells while sparing normal tissues. In line with this hypothesis, CB-5083 and CB-5339 treatments did not markedly alter normal peripheral blood counts and weight curves in C57/BL6 mice. Accordingly, CB-5083 was not myelosuppressive in the recently conducted phase I clinical trial (NCT02243917).

The rewiring of DNA repair pathways by cancer cells plays an important role both in disease progression and response to chemotherapy (*49*). On one hand, the impairment of DDR can be beneficial to cancer cells in the initial steps of tumorigenesis and in tumor evolution, leading to the DNA DSBs responsible for genomic rearrangements and accumulation of somatic driver and passenger mutations (*54*). On the other hand, these features can be detrimental to cancer cells exposed to chemotherapeutic drugs, which interfere with DNA replication and cause DNA damage themselves, and render cells vulnerable to damage as they progress through the S-phase of the cell cycle (*55, 56*). Compromised DDR can thus both promote cancer development and influence cancer cell response to chemotherapy. While the molecular basis of the DNA damage and DNA repair coordination that enables a tolerable mutational burden in cancer cells is only partially understood, DNA-damaging agents, such as chemotherapy or radiation, are widely used in the clinic and tend to exploit the inability of cancer cells to correctly repair DNA. DDR upregulation can provide cancer cells with escape mechanisms and explain the chemotherapy resistance of some cancer subtypes. For instance, high expression of the DNA replication checkpoint gene *CHEK1* in AML cells was associated with an increased risk of relapse and poor survival in a cohort of patients with AML who had received first-line cytarabine and anthracycline chemotherapy (*57*). Thus, the combination of standard AML chemotherapy with inhibitors of DNA damage repair, such as VCP inhibitors, is a therapeutic strategy of interest. Our data suggests that targeting the DNA damage response through VCP inhibition might also sensitize AML cells to DNA damaging agents, such as anthracyclines and cytarabine, currently used as frontline therapy in AML (*58*). Such a synergistic combination strategy should thus simultaneously help to avoid compensatory pathways activated in response to either chemotherapy regimens

alone or single agent VCP inhibitors. Additionally, a better understanding of the role of VCP in DDR may implicate synthetic lethal mechanisms in diverse cancers dependent on specific DDR defects.

To more effectively target cancer cells vulnerability to DNA damage, one of the major current translational challenges is the identification of biomarkers predicting response to DNA repair pathway-targeted cancer therapy. Our data demonstrated that the sensitivity to VCP inhibitors varies across and within a tumor type. In our study, we did not identify any specific mutational susceptibility to VCP impairment, suggesting that VCP dependency relies on a broader DDR-mediated vulnerability. However, we did observe a strong correlation of co-occuring *RAS* and *TP53* mutations with resistance to VCP inhibition. RAS/MAPK pathway mutations leading to an oncogenic proliferative signal are frequently observed in myeloid neoplasms. These activating mutations induce oncogenic replicative stress and can result in DDR pathways activation and modulation (*59-61*). For example, it has been recently reported that *KRAS* mutated leukemic cells rely on the error prone alt-NHEJ pathway to repair their DNA and present a delayed DSB resolution (*62*). *TP53* inactivating mutations are mainly reported in secondary myeloid malignancies and result in delayed DNA DSB resolution and a better DNA damage tolerability (*63*). Oncogenic RAS activates a TP53 dependent DNA damage response and checkpoints resulting in cellular senescence (*64*). *TP53* deficiency could thus cooperate with RAS through overcoming TP53-mediated senescence in order to promote tumorigenesis (*65, 66*). Taken together, this data suggests that such a double mutated context results in a modulated DDR and a better DNA damage tolerability potentially explaining resistance to VCP inhibition. Association of both *TP53* and *RAS* mutations is only described in a small number of

patients with AML (0.6 to 3.1%) (*66*) suggesting that a large majority of patients with AML may benefit from VCP inhibition. Our findings could thus inform future VCP inhibitor clinical trials by excluding patients harboring both *TP53* and *RAS* pathway mutations.

Translating preclinical studies into the clinic is challenging and relies on the ability to develop tractable drug candidates (*67*). Many small molecule inhibitors have been reported to target the AAA-ATPase VCP (*20, 21, 68-70*). Among these, the most selective reported to date are two mechanistically divergent small molecules: NMS-873 and CB-5083. NMS-873 is a highly selective allosteric inhibitor that lacks appropriate pharmacological and bioavailability properties and thus is not expected to move forward into clinical trials (*22*). CB-5083 is an ATP-competitive, highly selective VCP inhibitor that has been recently tested into a phase I clinical trial in solid tumors, based on promising preclinical data (*21*) (NCT02243917). This small molecule's drug development journey was unfortunately curtailed by an unanticipated off-target ophthalmological toxicity. A comprehensive set of biochemical studies pointed to a PDE6 inhibitory off-target action as responsible for this side effect. Strongly encouraged by our preclinical data in AML, a second-generation VCP inhibitor, CB-5339, was characterized for advancement into clinical studies. We report here the structure and biochemical properties of CB-5339, the lead drug candidate for future clinical trials. Beyond the dissection of the PDE6 off-target effect, CB-5339 drug development will also benefit from the lessons learned from the CB-5083 previous phase I trial. The current study offers an opportunity to repurpose this unique class of VCP inhibitors, potentially at a lower dose, for AML, a disease highly dependent on VCP and with a strong unmet clinical need. Moreover, future studies will evaluate CB-

5339's therapeutic potential in solid tumors and neurodegenerative disorders where VCP represents a promising therapeutic target (*36, 71*).

Limitations of our study include a potentially narrow therapeutic window given the essential and ubiquitous role of VCP in various biological processes. Careful pharmacokinetic and pharmacodynamic studies will be needed to account for inter-individual variability and ensure exposure to an effective and non-toxic dose of CB-5339. Additionaly, redundance in the DNA repair pathways may be responsible for resistance mechanisms that will need to be carefully monitored and mechanistically dissected during future clinical trials.

In conclusion, we identified and validated VCP as a therapeutic target in AML using multiple *in vivo* and *in vitro* models. Dissecting the molecular mechanisms underpinning this dependency in AML led us to the identification of a nuclear DNA repair function of VCP in leukemia, thereby providing a therapeutic avenue for AML. Our findings thus provide the preclinical and physiopathological basis for the CB-5339 AML phase I clinical trial as a single agent and in combination with standard of care AML chemotherapy regimens.

MATERIALS AND METHODS

Experimental design

This study sought to identify stress-related AML dependencies and validate the use of a second-generation clinical candidate VCP inhibitor as a targeted therapy in AML. An *in vivo* pooled shRNA screen pointed to the ATPase VCP as an exquisite dependency in AML. Biochemical and functional studies, in murine models, human AML cell lines, and primary patient AML samples, using genetic and chemical tools, were developed to validate the critical role of this ATPase in leukemia. A mass spectrometry-based analysis of the VCP interactome, combined with phospho-signaling studies revealed the essential role of VCP's involvement in DNA replication, damage recognition and repair pathways for leukemic cells survival. To further translate these results to the clinic, a selective ATP-competitive VCP inhibitor was identified. Effects of first-generation (CB-5083) and second-generation (CB-5339) VCP inhibitors in AML were studied *in vitro* in AML cell lines and primary patient AML samples and *in vivo* in human cell line or patient-derived orthotopic xenograft and syngeneic mouse models. Sample size was chosen in light of the fact that these *in vivo* models were historically highly penetrant, aggressive, and consistent. Blinded observers visually inspected mice for obvious signs of illness, such as loss of appetite, hunched posture, and lethargy. Mice were randomly assigned to each treatment group. The number of experimental replicates is specified in each figure legend.

Statistical analysis

Statistical analysis was performed using PRISM 8.0.1 (GraphPad), or the indicated software for more dedicated analysis. Data were analyzed using a nonparametric Mann-Whitney test (with the assumption of no Gaussian distribution of the group) unless otherwise specified, and the threshold of significance (α) was always set at 0.05.

SUPPLEMENTARY MATERIALS LIST

Materials and Methods

REFERENCES

1. R. M. Stone, S. J. Mandrekar, B. L. Sanford, K. Laumann, S. Geyer, C. D. Bloomfield, C. Thiede, T. W. Prior, K. Dohner, G. Marcucci, F. Lo-Coco, R. B. Klisovic, A. Wei, J. Sierra, M. A. Sanz, J. M. Brandwein, T. de Witte, D. Niederwieser, F. R. Appelbaum, B. C. Medeiros, M. S. Tallman, J. Krauter, R. F. Schlenk, A. Ganser, H. Serve, G. Ehninger, S. Amadori, R. A. Larson, H. Dohner, Midostaurin plus Chemotherapy for Acute Myeloid Leukemia with a FLT3 Mutation. *N Engl J Med* **377**, 454-464 (2017); published online EpubAug 3 (10.1056/NEJMoa1614359).
2. C. D. DiNardo, E. M. Stein, S. de Botton, G. J. Roboz, J. K. Altman, A. S. Mims, R. Swords, R. H. Collins, G. N. Mannis, D. A. Pollyea, W. Donnellan, A. T. Fathi, A. Pigneux, H. P. Erba, G. T. Prince, A. S. Stein, G. L. Uy, J. M. Foran, E. Traer, R. K. Stuart, M. L. Arellano, J. L. Slack, M. A. Sekeres, C. Willekens, S. Choe, H. Wang, V. Zhang, K. E. Yen, S. M. Kapsalis, H. Yang, D. Dai, B. Fan, M. Goldwasser, H. Liu, S. Agresta, B. Wu, E. C. Attar, M. S. Tallman, R. M. Stone, H. M. Kantarjian, Durable Remissions with Ivosidenib in IDH1-Mutated Relapsed or Refractory AML. *N Engl J Med* **378**, 2386-2398 (2018); published online EpubJun 21 (10.1056/NEJMoa1716984).
3. E. M. Stein, C. D. DiNardo, D. A. Pollyea, A. T. Fathi, G. J. Roboz, J. K. Altman, R. M. Stone, D. J. DeAngelo, R. L. Levine, I. W. Flinn, H. M. Kantarjian, R. Collins, M. R. Patel, A. E. Frankel, A. Stein, M. A. Sekeres, R. T. Swords, B. C. Medeiros, C. Willekens, P. Vyas, A. Tosolini, Q. Xu, R. D. Knight, K. E. Yen, S. Agresta, S. de Botton, M. S. Tallman, Enasidenib in mutant IDH2 relapsed or refractory acute myeloid leukemia. *Blood* **130**, 722-731 (2017); published online EpubAug 10 (10.1182/blood-2017-04-779405).
4. L. M. Ellis, D. J. Hicklin, Resistance to Targeted Therapies: Refining Anticancer Therapy in the Era of Molecular Oncology. *Clin Cancer Res* **15**, 7471-7478 (2009); published online EpubDec 15 (10.1158/1078-0432.CCR-09-1070).
5. J. Luo, N. L. Solimini, S. J. Elledge, Principles of cancer therapy: oncogene and non-oncogene addiction. *Cell* **136**, 823-837 (2009); published online EpubMar 06 (10.1016/j.cell.2009.02.024).
6. R. Nagel, E. A. Semenova, A. Berns, Drugging the addict: non-oncogene addiction as a target for cancer therapy. *EMBO Rep* **17**, 1516-1531 (2016); published online EpubNov (10.15252/embr.201643030).
7. J. Zuber, J. Shi, E. Wang, A. R. Rappaport, H. Herrmann, E. A. Sison, D. Magoon, J. Qi, K. Blatt, M. Wunderlich, M. J. Taylor, C. Johns, A. Chicas, J. C. Mulloy, S. C. Kogan, P. Brown, P. Valent, J. E. Bradner, S. W. Lowe, C. R. Vakoc, RNAi screen identifies Brd4 as a therapeutic target in acute myeloid leukaemia. *Nature* **478**, 524-528 (2011); published online EpubAug 3 (10.1038/nature10334).
8. M. Greaves, Evolutionary determinants of cancer. *Cancer Discov* **5**, 806-820 (2015); published online EpubAug (10.1158/2159-8290.CD-15-0439).
9. E. D. Lagadinou, A. Sach, K. Callahan, R. M. Rossi, S. J. Neering, M. Minhajuddin, J. M. Ashton, S. Pei, V. Grose, K. M. O'Dwyer, J. L. Liesveld, P. S. Brookes, M. W. Becker, C. T. Jordan, BCL-2 inhibition targets oxidative phosphorylation and selectively eradicates quiescent human leukemia stem cells. *Cell Stem Cell* **12**, 329-341 (2013); published online EpubMar 7 (10.1016/j.stem.2012.12.013).

10. C. D. DiNardo, C. R. Rausch, C. Benton, T. Kadia, N. Jain, N. Pemmaraju, N. Daver, W. Covert, K. R. Marx, M. Mace, E. Jabbour, J. Cortes, G. Garcia-Manero, F. Ravandi, K. N. Bhalla, H. Kantarjian, M. Konopleva, Clinical Experience with the BCL2-inhibitor Venetoclax in Combination Therapy for Relapsed and Refractory Acute Myeloid Leukemia and Related Myeloid Malignancies. *Am J Hematol*, (2017); published online EpubDec 8 (10.1002/ajh.25000).
11. M. Konopleva, D. A. Pollyea, J. Potluri, B. Chyla, L. Hogdal, T. Busman, E. McKeegan, A. H. Salem, M. Zhu, J. L. Ricker, W. Blum, C. D. DiNardo, T. Kadia, M. Dunbar, R. Kirby, N. Falotico, J. Leverson, R. Humerickhouse, M. Mabry, R. Stone, H. Kantarjian, A. Letai, Efficacy and Biological Correlates of Response in a Phase II Study of Venetoclax Monotherapy in Patients with Acute Myelogenous Leukemia. *Cancer Discov* **6**, 1106-1117 (2016); published online EpubOct (10.1158/2159-8290.CD-16-0313).
12. D. A. Pollyea, B. M. Stevens, C. L. Jones, A. Winters, S. Pei, M. Minhajuddin, A. D'Alessandro, R. Culp-Hill, K. A. Riemondy, A. E. Gillen, J. R. Hesselberth, D. Abbott, D. Schatz, J. A. Gutman, E. Purev, C. Smith, C. T. Jordan, Venetoclax with azacitidine disrupts energy metabolism and targets leukemia stem cells in patients with acute myeloid leukemia. *Nat Med* **24**, 1859-1866 (2018); published online EpubDec (10.1038/s41591-018-0233-1).
13. C. D. DiNardo, K. Pratz, V. Pullarkat, B. A. Jonas, M. Arellano, P. S. Becker, O. Frankfurt, M. Konopleva, A. H. Wei, H. M. Kantarjian, T. Xu, W. J. Hong, B. Chyla, J. Potluri, D. A. Pollyea, A. Letai, Venetoclax combined with decitabine or azacitidine in treatment-naive, elderly patients with acute myeloid leukemia. *Blood* **133**, 7-17 (2019); published online EpubJan 3 (10.1182/blood-2018-08-868752).
14. A. Puissant, N. Fenouille, G. Alexe, Y. Pikman, C. F. Bassil, S. Mehta, J. Du, J. U. Kazi, F. Luciano, L. Ronnstrand, A. L. Kung, J. C. Aster, I. Galinsky, R. M. Stone, D. J. DeAngelo, M. T. Hemann, K. Stegmaier, SYK is a critical regulator of FLT3 in acute myeloid leukemia. *Cancer Cell* **25**, 226-242 (2014); published online EpubFeb 10 (10.1016/j.ccr.2014.01.022).
15. P. G. Miller, F. Al-Shahrour, K. A. Hartwell, L. P. Chu, M. Jaras, R. V. Puram, A. Puissant, K. P. Callahan, J. Ashton, M. E. McConkey, L. P. Poveromo, G. S. Cowley, M. G. Kharas, M. Labelle, S. Shterental, J. Fujisaki, L. Silberstein, G. Alexe, M. A. Al-Hajj, C. A. Shelton, S. A. Armstrong, D. E. Root, D. T. Scadden, R. O. Hynes, S. Mukherjee, K. Stegmaier, C. T. Jordan, B. L. Ebert, In Vivo RNAi screening identifies a leukemia-specific dependence on integrin beta 3 signaling. *Cancer Cell* **24**, 45-58 (2013); published online EpubJul 8 (10.1016/j.ccr.2013.05.004).
16. V. Stambolic, A. Suzuki, J. L. de la Pompa, G. M. Brothers, C. Mirtsos, T. Sasaki, J. Ruland, J. M. Penninger, D. P. Siderovski, T. W. Mak, Negative regulation of PKB/Akt-dependent cell survival by the tumor suppressor PTEN. *Cell* **95**, 29-39 (1998); published online EpubOct 2 (
17. H. Xie, J. Hanai, J. G. Ren, L. Kats, K. Burgess, P. Bhargava, S. Signoretti, J. Billiard, K. J. Duffy, A. Grant, X. Wang, P. K. Lorkiewicz, S. Schatzman, M. Bousamra, 2nd, A. N. Lane, R. M. Higashi, T. W. Fan, P. P. Pandolfi, V. P. Sukhatme, P. Seth, Targeting lactate dehydrogenase--a inhibits tumorigenesis and tumor progression in mouse models of lung cancer and impacts tumor-initiating cells. *Cell Metab* **19**, 795-809 (2014); published online EpubMay 06 (10.1016/j.cmet.2014.03.003).

18. Q. Wang, C. Song, C. C. Li, Hexamerization of p97-VCP is promoted by ATP binding to the D1 domain and required for ATPase and biological activities. *Biochem Biophys Res Commun* **300**, 253-260 (2003); published online EpubJan 10 (
19. S. Dalal, M. F. Rosser, D. M. Cyr, P. I. Hanson, Distinct roles for the AAA ATPases NSF and p97 in the secretory pathway. *Mol Biol Cell* **15**, 637-648 (2004); published online EpubFeb (10.1091/mbc.E03-02-0097).
20. D. J. Anderson, R. Le Moigne, S. Djakovic, B. Kumar, J. Rice, S. Wong, J. Wang, B. Yao, E. Valle, S. Kiss von Soly, A. Madriaga, F. Soriano, M. K. Menon, Z. Y. Wu, M. Kampmann, Y. Chen, J. S. Weissman, B. T. Aftab, F. M. Yakes, L. Shawver, H. J. Zhou, D. Wustrow, M. Rolfe, Targeting the AAA ATPase p97 as an Approach to Treat Cancer through Disruption of Protein Homeostasis. *Cancer Cell* **28**, 653-665 (2015); published online EpubNov 09 (10.1016/j.ccell.2015.10.002).
21. H. J. Zhou, J. Wang, B. Yao, S. Wong, S. Djakovic, B. Kumar, J. Rice, E. Valle, F. Soriano, M. K. Menon, A. Madriaga, S. Kiss von Soly, A. Kumar, F. Parlati, F. M. Yakes, L. Shawver, R. Le Moigne, D. J. Anderson, M. Rolfe, D. Wustrow, Discovery of a First-in-Class, Potent, Selective, and Orally Bioavailable Inhibitor of the p97 AAA ATPase (CB-5083). *J Med Chem* **58**, 9480-9497 (2015); published online EpubDec 24 (10.1021/acs.jmedchem.5b01346).
22. P. Magnaghi, R. D'Alessio, B. Valsasina, N. Avanzi, S. Rizzi, D. Asa, F. Gasparri, L. Cozzi, U. Cucchi, C. Orrenius, P. Polucci, D. Ballinari, C. Perrera, A. Leone, G. Cervi, E. Casale, Y. Xiao, C. Wong, D. J. Anderson, A. Galvani, D. Donati, T. O'Brien, P. K. Jackson, A. Isacchi, Covalent and allosteric inhibitors of the ATPase VCP/p97 induce cancer cell death. *Nat Chem Biol* **9**, 548-556 (2013); published online EpubSep (10.1038/nchembio.1313).
23. N. G. Her, J. I. Toth, C. T. Ma, Y. Wei, K. Motamedchaboki, E. Sergienko, M. D. Petroski, p97 Composition Changes Caused by Allosteric Inhibition Are Suppressed by an On-Target Mechanism that Increases the Enzyme's ATPase Activity. *Cell Chem Biol* **23**, 517-528 (2016); published online EpubApr 21 (10.1016/j.chembiol.2016.03.012).
24. C. Wojcik, M. Rowicka, A. Kudlicki, D. Nowis, E. McConnell, M. Kujawa, G. N. DeMartino, Valosin-containing protein (p97) is a regulator of endoplasmic reticulum stress and of the degradation of N-end rule and ubiquitin-fusion degradation pathway substrates in mammalian cells. *Mol Biol Cell* **17**, 4606-4618 (2006); published online EpubNov (10.1091/mbc.E06-05-0432).
25. R. M. Dai, C. C. Li, Valosin-containing protein is a multi-ubiquitin chain-targeting factor required in ubiquitin-proteasome degradation. *Nat Cell Biol* **3**, 740-744 (2001); published online EpubAug (10.1038/35087056).
26. M. Raman, M. Sergeev, M. Garnaas, J. R. Lydeard, E. L. Huttlin, W. Goessling, J. V. Shah, J. W. Harper, Systematic proteomics of the VCP-UBXD adaptor network identifies a role for UBXN10 in regulating ciliogenesis. *Nat Cell Biol* **17**, 1356-1369 (2015); published online EpubOct (10.1038/ncb3238).
27. Y. Shiloh, ATM and related protein kinases: safeguarding genome integrity. *Nat Rev Cancer* **3**, 155-168 (2003); published online EpubMar (10.1038/nrc1011).
28. Y. Shiloh, Y. Ziv, The ATM protein kinase: regulating the cellular response to genotoxic stress, and more. *Nat Rev Mol Cell Biol* **14**, 197-210 (2013); published online EpubApr (

29. V. Y. Arshavsky, T. D. Lamb, E. N. Pugh, Jr., G proteins and phototransduction. *Annu Rev Physiol* **64**, 153-187 (2002)10.1146/annurev.physiol.64.082701.102229).
30. K. E. Andersson, PDE5 inhibitors - pharmacology and clinical applications 20 years after sildenafil discovery. *Br J Pharmacol* **175**, 2554-2565 (2018); published online EpubJul (10.1111/bph.14205).
31. J. Barretina, G. Caponigro, N. Stransky, K. Venkatesan, A. A. Margolin, S. Kim, C. J. Wilson, J. Lehar, G. V. Kryukov, D. Sonkin, A. Reddy, M. Liu, L. Murray, M. F. Berger, J. E. Monahan, P. Morais, J. Meltzer, A. Korejwa, J. Jane-Valbuena, F. A. Mapa, J. Thibault, E. Bric-Furlong, P. Raman, A. Shipway, I. H. Engels, J. Cheng, G. K. Yu, J. Yu, P. Aspesi, Jr., M. de Silva, K. Jagtap, M. D. Jones, L. Wang, C. Hatton, E. Palescandolo, S. Gupta, S. Mahan, C. Sougnez, R. C. Onofrio, T. Liefeld, L. MacConaill, W. Winckler, M. Reich, N. Li, J. P. Mesirov, S. B. Gabriel, G. Getz, K. Ardlie, V. Chan, V. E. Myer, B. L. Weber, J. Porter, M. Warmuth, P. Finan, J. L. Harris, M. Meyerson, T. R. Golub, M. P. Morrissey, W. R. Sellers, R. Schlegel, L. A. Garraway, The Cancer Cell Line Encyclopedia enables predictive modelling of anticancer drug sensitivity. *Nature* **483**, 603-607 (2012); published online EpubMar 28 (10.1038/nature11003).
32. C. Cancer Cell Line Encyclopedia, C. Genomics of Drug Sensitivity in Cancer, Pharmacogenomic agreement between two cancer cell line data sets. *Nature* **528**, 84-87 (2015); published online EpubDec 3 (10.1038/nature15736).
33. M. H. Bailey, C. Tokheim, E. Porta-Pardo, S. Sengupta, D. Bertrand, A. Weerasinghe, A. Colaprico, M. C. Wendl, J. Kim, B. Reardon, P. K. Ng, K. J. Jeong, S. Cao, Z. Wang, J. Gao, Q. Gao, F. Wang, E. M. Liu, L. Mularoni, C. Rubio-Perez, N. Nagarajan, I. Cortes-Ciriano, D. C. Zhou, W. W. Liang, J. M. Hess, V. D. Yellapantula, D. Tamborero, A. Gonzalez-Perez, C. Suphavilai, J. Y. Ko, E. Khurana, P. J. Park, E. M. Van Allen, H. Liang, M. C. W. Group, N. Cancer Genome Atlas Research, M. S. Lawrence, A. Godzik, N. Lopez-Bigas, J. Stuart, D. Wheeler, G. Getz, K. Chen, A. J. Lazar, G. B. Mills, R. Karchin, L. Ding, Comprehensive Characterization of Cancer Driver Genes and Mutations. *Cell* **173**, 371-385 e318 (2018); published online EpubApr 5 (10.1016/j.cell.2018.02.060).
34. T. A. Knijnenburg, L. Wang, M. T. Zimmermann, N. Chambwe, G. F. Gao, A. D. Cherniack, H. Fan, H. Shen, G. P. Way, C. S. Greene, Y. Liu, R. Akbani, B. Feng, L. A. Donehower, C. Miller, Y. Shen, M. Karimi, H. Chen, P. Kim, P. Jia, E. Shinbrot, S. Zhang, J. Liu, H. Hu, M. H. Bailey, C. Yau, D. Wolf, Z. Zhao, J. N. Weinstein, L. Li, L. Ding, G. B. Mills, P. W. Laird, D. A. Wheeler, I. Shmulevich, N. Cancer Genome Atlas Research, R. J. Monnat, Jr., Y. Xiao, C. Wang, Genomic and Molecular Landscape of DNA Damage Repair Deficiency across The Cancer Genome Atlas. *Cell Rep* **23**, 239-254 e236 (2018); published online EpubApr 3 (10.1016/j.celrep.2018.03.076).
35. G. P. Way, F. Sanchez-Vega, K. La, J. Armenia, W. K. Chatila, A. Luna, C. Sander, A. D. Cherniack, M. Mina, G. Ciriello, N. Schultz, N. Cancer Genome Atlas Research, Y. Sanchez, C. S. Greene, Machine Learning Detects Pan-cancer Ras Pathway Activation in The Cancer Genome Atlas. *Cell Rep* **23**, 172-180 e173 (2018); published online EpubApr 3 (10.1016/j.celrep.2018.03.046).
36. R. Le Moigne, B. T. Aftab, S. Djakovic, E. Dhimolea, E. Valle, M. Murnane, E. M. King, F. Soriano, M. K. Menon, Z. Y. Wu, S. T. Wong, G. J. Lee, B. Yao, A. P. Wiita, C. Lam, J. Rice, J. Wang, M. Chesi, P. L. Bergsagel, M. Kraus, C.

Driessen, S. Kiss von Soly, F. M. Yakes, D. Wustrow, L. Shawver, H. J. Zhou, T. G. Martin, 3rd, J. L. Wolf, C. S. Mitsiades, D. J. Anderson, M. Rolfe, The p97 Inhibitor CB-5083 Is a Unique Disrupter of Protein Homeostasis in Models of Multiple Myeloma. *Mol Cancer Ther* **16**, 2375-2386 (2017); published online EpubNov (10.1158/1535-7163.MCT-17-0233).

37. S. Negrini, V. G. Gorgoulis, T. D. Halazonetis, Genomic instability--an evolving hallmark of cancer. *Nat Rev Mol Cell Biol* **11**, 220-228 (2010); published online EpubMar (10.1038/nrm2858).
38. N. Jiang, Y. Shen, X. Fei, K. Sheng, P. Sun, Y. Qiu, J. Larner, L. Cao, X. Kong, J. Mi, Valosin-containing protein regulates the proteasome-mediated degradation of DNA-PKcs in glioma cells. *Cell Death Dis* **4**, e647 (2013); published online EpubMay 30 (10.1038/cddis.2013.171).
39. I. Gibbs-Seymour, Y. Oka, E. Rajendra, B. T. Weinert, L. A. Passmore, K. J. Patel, J. V. Olsen, C. Choudhary, S. Bekker-Jensen, N. Mailand, Ubiquitin-SUMO circuitry controls activated fanconi anemia ID complex dosage in response to DNA damage. *Mol Cell* **57**, 150-164 (2015); published online EpubJan 8 (10.1016/j.molcel.2014.12.001).
40. J. He, Q. Zhu, G. Wani, N. Sharma, C. Han, J. Qian, K. Pentz, Q. E. Wang, A. A. Wani, Ubiquitin-specific protease 7 regulates nucleotide excision repair through deubiquitinating XPC protein and preventing XPC protein from undergoing ultraviolet light-induced and VCP/p97 protein-regulated proteolysis. *J Biol Chem* **289**, 27278-27289 (2014); published online EpubSep 26 (10.1074/jbc.M114.589812).
41. A. Franz, L. Ackermann, T. Hoppe, Ring of Change: CDC48/p97 Drives Protein Dynamics at Chromatin. *Front Genet* **7**, 73 (2016)10.3389/fgene.2016.00073).
42. B. Vaz, S. Halder, K. Ramadan, Role of p97/VCP (Cdc48) in genome stability. *Front Genet* **4**, 60 (2013)10.3389/fgene.2013.00060).
43. S. Bergink, T. Ammon, M. Kern, L. Schermelleh, H. Leonhardt, S. Jentsch, Role of Cdc48/p97 as a SUMO-targeted segregase curbing Rad51-Rad52 interaction. *Nat Cell Biol* **15**, 526-532 (2013); published online EpubMay (10.1038/ncb2729).
44. K. Acs, M. S. Luijsterburg, L. Ackermann, F. A. Salomons, T. Hoppe, N. P. Dantuma, The AAA-ATPase VCP/p97 promotes 53BP1 recruitment by removing L3MBTL1 from DNA double-strand breaks. *Nat Struct Mol Biol* **18**, 1345-1350 (2011); published online EpubNov 27 (10.1038/nsmb.2188).
45. J. van den Boom, M. Wolf, L. Weimann, N. Schulze, F. Li, F. Kaschani, A. Riemer, C. Zierhut, M. Kaiser, G. Iliakis, H. Funabiki, H. Meyer, VCP/p97 Extracts Sterically Trapped Ku70/80 Rings from DNA in Double-Strand Break Repair. *Mol Cell* **64**, 189-198 (2016); published online EpubOct 06 (10.1016/j.molcel.2016.08.037).
46. E. J. Davis, C. Lachaud, P. Appleton, T. J. Macartney, I. Nathke, J. Rouse, DVC1 (C1orf124) recruits the p97 protein segregase to sites of DNA damage. *Nat Struct Mol Biol* **19**, 1093-1100 (2012); published online EpubNov (10.1038/nsmb.2394).
47. M. Maric, T. Maculins, G. De Piccoli, K. Labib, Cdc48 and a ubiquitin ligase drive disassembly of the CMG helicase at the end of DNA replication. *Science* **346**, 1253596 (2014); published online EpubOct 24 (10.1126/science.1253596).

48. P. C. Fong, D. S. Boss, T. A. Yap, A. Tutt, P. Wu, M. Mergui-Roelvink, P. Mortimer, H. Swaisland, A. Lau, M. J. O'Connor, A. Ashworth, J. Carmichael, S. B. Kaye, J. H. Schellens, J. S. de Bono, Inhibition of poly(ADP-ribose) polymerase in tumors from BRCA mutation carriers. *N Engl J Med* **361**, 123-134 (2009); published online EpubJul 9 (10.1056/NEJMoa0900212).
49. M. T. Esposito, C. W. So, DNA damage accumulation and repair defects in acute myeloid leukemia: implications for pathogenesis, disease progression, and chemotherapy resistance. *Chromosoma* **123**, 545-561 (2014); published online EpubDec (10.1007/s00412-014-0482-9).
50. M. T. Esposito, L. Zhao, T. K. Fung, J. K. Rane, A. Wilson, N. Martin, J. Gil, A. Y. Leung, A. Ashworth, C. W. So, Synthetic lethal targeting of oncogenic transcription factors in acute leukemia by PARP inhibitors. *Nat Med* **21**, 1481-1490 (2015); published online EpubDec (10.1038/nm.3993).
51. S. Inoue, W. Y. Li, A. Tseng, I. Beerman, A. J. Elia, S. C. Bendall, F. Lemonnier, K. J. Kron, D. W. Cescon, Z. Hao, E. F. Lind, N. Takayama, A. C. Planello, S. Y. Shen, A. H. Shih, D. M. Larsen, Q. Li, B. E. Snow, A. Wakeham, J. Haight, C. Gorrini, C. Bassi, K. L. Thu, K. Murakami, A. R. Elford, T. Ueda, K. Straley, K. E. Yen, G. Melino, L. Cimmino, I. Aifantis, R. L. Levine, D. D. De Carvalho, M. Lupien, D. J. Rossi, G. P. Nolan, R. A. Cairns, T. W. Mak, Mutant IDH1 Downregulates ATM and Alters DNA Repair and Sensitivity to DNA Damage Independent of TET2. *Cancer Cell* **30**, 337-348 (2016); published online EpubAug 8 (10.1016/j.ccell.2016.05.018).
52. I. Morgado-Palacin, A. Day, M. Murga, V. Lafarga, M. E. Anton, A. Tubbs, H. T. Chen, A. Ergan, R. Anderson, A. Bhandoola, K. G. Pike, B. Barlaam, E. Cadogan, X. Wang, A. J. Pierce, C. Hubbard, S. A. Armstrong, A. Nussenzweig, O. Fernandez-Capetillo, Targeting the kinase activities of ATR and ATM exhibits antitumoral activity in mouse models of MLL-rearranged AML. *Sci Signal* **9**, ra91 (2016); published online EpubSep 13 (10.1126/scisignal.aad8243).
53. J. M. Muller, K. Deinhardt, I. Rosewell, G. Warren, D. T. Shima, Targeted deletion of p97 (VCP/CDC48) in mouse results in early embryonic lethality. *Biochem Biophys Res Commun* **354**, 459-465 (2007); published online EpubMar 9 (10.1016/j.bbrc.2006.12.206).
54. J. Libura, D. J. Slater, C. A. Felix, C. Richardson, Therapy-related acute myeloid leukemia-like MLL rearrangements are induced by etoposide in primary human CD34+ cells and remain stable after clonal expansion. *Blood* **105**, 2124-2131 (2005); published online EpubMar 1 (10.1182/blood-2004-07-2683).
55. N. J. Curtin, DNA repair dysregulation from cancer driver to therapeutic target. *Nat Rev Cancer* **12**, 801-817 (2012); published online EpubDec (10.1038/nrc3399).
56. M. Dobbelstein, C. S. Sorensen, Exploiting replicative stress to treat cancer. *Nat Rev Drug Discov* **14**, 405-423 (2015); published online EpubJun (10.1038/nrd4553).
57. L. David, A. Fernandez-Vidal, S. Bertoli, S. Grgurevic, B. Lepage, D. Deshaies, N. Prade, M. Cartel, C. Larrue, J. E. Sarry, E. Delabesse, C. Cazaux, C. Didier, C. Recher, S. Manenti, J. S. Hoffmann, CHK1 as a therapeutic target to bypass chemoresistance in AML. *Sci Signal* **9**, ra90 (2016); published online EpubSep 13 (10.1126/scisignal.aac9704).

58. M. Kastan, Ataxia-telangiectasia--broad implications for a rare disorder. *N Engl J Med* **333**, 662-663 (1995); published online EpubSep 7 (10.1056/NEJM199509073331014).
59. P. Kotsantis, E. Petermann, S. J. Boulton, Mechanisms of Oncogene-Induced Replication Stress: Jigsaw Falling into Place. *Cancer Discov* **8**, 537-555 (2018); published online EpubMay (10.1158/2159-8290.CD-17-1461).
60. E. Grabocka, Y. Pylayeva-Gupta, M. J. Jones, V. Lubkov, E. Yemanaberhan, L. Taylor, H. H. Jeng, D. Bar-Sagi, Wild-type H- and N-Ras promote mutant K-Ras-driven tumorigenesis by modulating the DNA damage response. *Cancer Cell* **25**, 243-256 (2014); published online EpubFeb 10 (10.1016/j.ccr.2014.01.005).
61. Z. Tu, K. M. Aird, B. G. Bitler, J. P. Nicodemus, N. Beeharry, B. Xia, T. J. Yen, R. Zhang, Oncogenic RAS regulates BRIP1 expression to induce dissociation of BRCA1 from chromatin, inhibit DNA repair, and promote senescence. *Dev Cell* **21**, 1077-1091 (2011); published online EpubDec 13 (10.1016/j.devcel.2011.10.010).
62. P. S. Hahnel, B. Enders, D. Sasca, W. P. Roos, B. Kaina, L. Bullinger, M. Theobald, T. Kindler, Targeting components of the alternative NHEJ pathway sensitizes KRAS mutant leukemic cells to chemotherapy. *Blood* **123**, 2355-2366 (2014); published online EpubApr 10 (10.1182/blood-2013-01-477620).
63. M. A. Jacoby, R. E. De Jesus Pizarro, J. Shao, D. C. Koboldt, R. S. Fulton, G. Zhou, R. K. Wilson, M. J. Walter, The DNA double-strand break response is abnormal in myeloblasts from patients with therapy-related acute myeloid leukemia. *Leukemia* **28**, 1242-1251 (2014); published online EpubJun (10.1038/leu.2013.368).
64. G. Ferbeyre, E. de Stanchina, A. W. Lin, E. Querido, M. E. McCurrach, G. J. Hannon, S. W. Lowe, Oncogenic ras and p53 cooperate to induce cellular senescence. *Mol Cell Biol* **22**, 3497-3508 (2002); published online EpubMay (
65. M. Serrano, A. W. Lin, M. E. McCurrach, D. Beach, S. W. Lowe, Oncogenic ras provokes premature cell senescence associated with accumulation of p53 and p16INK4a. *Cell* **88**, 593-602 (1997); published online EpubMar 7 (
66. J. Zhang, G. Kong, A. Rajagopalan, L. Lu, J. Song, M. Hussaini, X. Zhang, E. A. Ranheim, Y. Liu, J. Wang, X. Gao, Y. I. Chang, K. D. Johnson, Y. Zhou, D. Yang, B. Bhatnagar, D. M. Lucas, E. H. Bresnick, X. Zhong, E. Padron, J. Zhang, p53-/- synergizes with enhanced NrasG12D signaling to transform megakaryocyte-erythroid progenitors in acute myeloid leukemia. *Blood* **129**, 358-370 (2017); published online EpubJan 19 (10.1182/blood-2016-06-719237).
67. B. Munos, Lessons from 60 years of pharmaceutical innovation. *Nat Rev Drug Discov* **8**, 959-968 (2009); published online EpubDec (10.1038/nrd2961).
68. S. Banerjee, A. Bartesaghi, A. Merk, P. Rao, S. L. Bulfer, Y. Yan, N. Green, B. Mroczkowski, R. J. Neitz, P. Wipf, V. Falconieri, R. J. Deshaies, J. L. Milne, D. Huryn, M. Arkin, S. Subramaniam, 2.3 A resolution cryo-EM structure of human p97 and mechanism of allosteric inhibition. *Science* **351**, 871-875 (2016); published online EpubFeb 19 (10.1126/science.aad7974).
69. T. F. Chou, S. J. Brown, D. Minond, B. E. Nordin, K. Li, A. C. Jones, P. Chase, P. R. Porubsky, B. M. Stoltz, F. J. Schoenen, M. P. Patricelli, P. Hodder, H. Rosen, R. J. Deshaies, Reversible inhibitor of p97, DBeQ, impairs both ubiquitin-dependent and autophagic protein clearance pathways. *Proc Natl*

Acad Sci U S A **108**, 4834-4839 (2011); published online EpubMar 22 (10.1073/pnas.1015312108).

70. R. Pohler, J. H. Krahn, J. van den Boom, G. Dobrynin, F. Kaschani, H. M. Eggenweiler, F. T. Zenke, M. Kaiser, H. Meyer, A Non-Competitive Inhibitor of VCP/p97 and VPS4 Reveals Conserved Allosteric Circuits in Type I and II AAA ATPases. *Angew Chem Int Ed Engl* **57**, 1576-1580 (2018); published online EpubFeb 5 (10.1002/anie.201711429).
71. A. Kakizuka, Roles of VCP in human neurodegenerative disorders. *Biochem Soc Trans* **36**, 105-108 (2008); published online EpubFeb (10.1042/BST0360105).
72. Z. Dai, J. M. Sheridan, L. J. Gearing, D. L. Moore, S. Su, S. Wormald, S. Wilcox, L. O'Connor, R. A. Dickins, M. E. Blewitt, M. E. Ritchie, edgeR: a versatile tool for the analysis of shRNA-seq and CRISPR-Cas9 genetic screens. *F1000Res* **3**, 95 (2014)10.12688/f1000research.3928.2).
73. M. D. Robinson, D. J. McCarthy, G. K. Smyth, edgeR: a Bioconductor package for differential expression analysis of digital gene expression data. *Bioinformatics* **26**, 139-140 (2010); published online EpubJan 01 (10.1093/bioinformatics/btp616).
74. B. Luo, H. W. Cheung, A. Subramanian, T. Sharifnia, M. Okamoto, X. Yang, G. Hinkle, J. S. Boehm, R. Beroukhim, B. A. Weir, C. Mermel, D. A. Barbie, T. Awad, X. Zhou, T. Nguyen, B. Piqani, C. Li, T. R. Golub, M. Meyerson, N. Hacohen, W. C. Hahn, E. S. Lander, D. M. Sabatini, D. E. Root, Highly parallel identification of essential genes in cancer cells. *Proc Natl Acad Sci U S A* **105**, 20380-20385 (2008); published online EpubDec 23 (10.1073/pnas.0810485105).
75. C. Fellmann, T. Hoffmann, V. Sridhar, B. Hopfgartner, M. Muhar, M. Roth, D. Y. Lai, I. A. Barbosa, J. S. Kwon, Y. Guan, N. Sinha, J. Zuber, An optimized microRNA backbone for effective single-copy RNAi. *Cell Rep* **5**, 1704-1713 (2013); published online EpubDec 26 (10.1016/j.celrep.2013.11.020).
76. V. Banerji, S. M. Frumm, K. N. Ross, L. S. Li, A. C. Schinzel, C. K. Hahn, R. M. Kakoza, K. T. Chow, L. Ross, G. Alexe, N. Tolliday, H. Inguilizian, I. Galinsky, R. M. Stone, D. J. DeAngelo, G. Roti, J. C. Aster, W. C. Hahn, A. L. Kung, K. Stegmaier, The intersection of genetic and chemical genomic screens identifies GSK-3alpha as a target in human acute myeloid leukemia. *J Clin Invest* **122**, 935-947 (2012); published online EpubMar (10.1172/JCI46465).
77. J. Rappsilber, M. Mann, Y. Ishihama, Protocol for micro-purification, enrichment, pre-fractionation and storage of peptides for proteomics using StageTips. *Nat Protoc* **2**, 1896-1906 (2007)10.1038/nprot.2007.261).
78. N. D. Udeshi, D. R. Mani, T. Eisenhaure, P. Mertins, J. D. Jaffe, K. R. Clauser, N. Hacohen, S. A. Carr, Methods for quantification of in vivo changes in protein ubiquitination following proteasome and deubiquitinase inhibition. *Mol Cell Proteomics* **11**, 148-159 (2012); published online EpubMay (10.1074/mcp.M111.016857).
79. H. Wickham, *ggplot2: Elegant Graphics for Data Analysis.* . (Springer-Verlag New York., 2009).
80. A. Subramanian, P. Tamayo, V. K. Mootha, S. Mukherjee, B. L. Ebert, M. A. Gillette, A. Paulovich, S. L. Pomeroy, T. R. Golub, E. S. Lander, J. P. Mesirov, Gene set enrichment analysis: a knowledge-based approach for interpreting genome-wide expression profiles. *Proc Natl Acad Sci U S A* **102**, 15545-15550 (2005); published online EpubOct 25 (10.1073/pnas.0506580102).

81. E. Y. Chen, C. M. Tan, Y. Kou, Q. Duan, Z. Wang, G. V. Meirelles, N. R. Clark, A. Ma'ayan, Enrichr: interactive and collaborative HTML5 gene list enrichment analysis tool. *BMC Bioinformatics* **14**, 128 (2013); published online EpubApr 15 (10.1186/1471-2105-14-128).
82. M. V. Kuleshov, M. R. Jones, A. D. Rouillard, N. F. Fernandez, Q. Duan, Z. Wang, S. Koplev, S. L. Jenkins, K. M. Jagodnik, A. Lachmann, M. G. McDermott, C. D. Monteiro, G. W. Gundersen, A. Ma'ayan, Enrichr: a comprehensive gene set enrichment analysis web server 2016 update. *Nucleic Acids Res* **44**, W90-97 (2016); published online EpubJul 8 (10.1093/nar/gkw377).
83. A. Muslimovic, I. H. Ismail, Y. Gao, O. Hammarsten, An optimized method for measurement of gamma-H2AX in blood mononuclear and cultured cells. *Nat Protoc* **3**, 1187-1193 (2008)10.1038/nprot.2008.93).
84. A. J. Pierce, R. D. Johnson, L. H. Thompson, M. Jasin, XRCC3 promotes homology-directed repair of DNA damage in mammalian cells. *Genes Dev* **13**, 2633-2638 (1999); published online EpubOct 15 (
85. J. Guirouilh-Barbat, S. Huck, P. Bertrand, L. Pirzio, C. Desmaze, L. Sabatier, B. S. Lopez, Impact of the KU80 pathway on NHEJ-induced genome rearrangements in mammalian cells. *Mol Cell* **14**, 611-623 (2004); published online EpubJun 04 (10.1016/j.molcel.2004.05.008).
86. T. C. Chou, Drug combination studies and their synergy quantification using the Chou-Talalay method. *Cancer Res* **70**, 440-446 (2010); published online EpubJan 15 (10.1158/0008-5472.CAN-09-1947).
87. T. C. Chou, Theoretical basis, experimental design, and computerized simulation of synergism and antagonism in drug combination studies. *Pharmacol Rev* **58**, 621-681 (2006); published online EpubSep (10.1124/pr.58.3.10).

ACKNOWLEDGEMENTS

We thank Timur Yusufzai, Raphael Ceccaldi, Sebastian Oeck, Benjamin Manning, Neil Umbreit and Peter Bruno for advice and discussions. We are indebted to Veronique Montcuquet, Nicolas Setterblad, Christelle Doliger, and Sophie Duchez from the Saint-Louis Research Institute Core Facility for their technical support.

FUNDING: This research was supported with grants from the US National Cancer Institute (NCI) (NIH R35 CA210030; KS, and NIH K08 CA222684 ; YP), the Children's Leukemia Research Foundation (CLRF) (KS), the Bettencourt Schueller foundation (CCA-INSERM-Bettencourt; LB) and the Bridge Project, a collaboration between the Koch Institute for Integrative Cancer Research at MIT and the Dana-Farber–Harvard Cancer Center (DF-HCC) (KS and MTH). KS was a Leukemia and Lymphoma Society Scholar. AP is a recipient of support from the starting grant form ERC (Horizon 2020), the ATIP–AVENIR and LNCC French research programs, the EHA research grant for a non-clinical advanced fellow, the FSER foundation grant, the Emergence ville de Paris grant and is supported by the St. Louis Association for leukemia research. LB is a CCA-INSERM-Bettencourt laureate and a recipient of Philippe Foundation and GPM fellowships, and research funding from Association Laurette Fugain, LNCC (Comité de Paris) and Gilead Sciences as a "Gilead Research Scholars award" recipient. JME is a recipient of a Swiss National Science Foundation, a Lady Tata Memorial Trust and a Pediatric Cancer Research Foundation fellowships.

AUTHOR CONTRIBUTIONS: BR and CV established conditions for *in vivo* and *in vitro* experiments, acquired and analyzed the data, and wrote the manuscript. JDV, YT,

TW, DJA, RLM and HJZ screened for CB-5339, designed and performed the *in vitro* CB-5083 cancer cell lines screening and biochemical *in vitro* and pharmacological assays for CB-5339. GA performed analysis of the *in vivo* shRNA screening data and the bioinformatics analysis of publicly available databases. CB, BP, GS and ASC performed *in vivo* experiments. NF designed, performed, and analyzed the *in vivo* pooled shRNA screening. EM and KL performed analysis of the proteomics data. JME, FLi and LR performed *in vitro* experiments. FLu and PA designed, performed, and analyzed experiments related to proteotoxic and ER stress. CRH, MS and SAC designed and performed the mass spectrometry-based proteomics experiments and performed subsequent data analysis. JGB, BL and MK contributed to experiments related to DNA damage and repair. IG, DJD, and RMS provided patient samples. YP analyzed patient samples and performed *in vitro* experiments. OH and MTH designed experiments and interpreted data. LB developed the study, acquired and analyzed *in vivo* and *in vitro* data. AP, KS and LB supervised the study, designed the *in vitro* and *in vivo* experiments, analyzed the data, wrote and revised the manuscript, and provided funding for the study.

Correspondence and requests for materials should be addressed to lina.benajiba@inserm.fr, Kimberly_Stegmaier@dfci.harvard.edu and alexandre.puissant@inserm.fr.

COMPETING INTERESTS: JDV is an employee of Cleave Therapeutics and YT, TW, DA, RLM and HJZ are former employees of Cleave Therapeutics, a biopharmaceutical company developing VCP inhibitors for therapeutic use in oncology. KS has consulted for Rigel Pharmaceuticals, Kronos Bio, and Auron Therapeutics on unrelated topics, receives grant funding from Novartis which did not

fund this project, and holds stock options with Auron Therapeutics on unrelated topics. LB receives grant support from Gilead Sciences as a "Gilead Research Scholars award recipient". The other authors declare no competing financial interests. The following patents are held by Cleave Therapeutics (formerly Cleave Biosciences): (U.S. Patent Nos.: 9,828,363 and 10,174,005); HJZ is a listed inventor on these patents. Cleave Therapeutics has filed additional provisional patent applications concerning CB-5339 and its uses. JDV, DJA, RLM and HJZ are listed as inventors on the provisional patents.

DATA AND MATERIALS AVAILABILITY: All data associated with this study are available in the main text or the supplementary materials. CB-5339 can be obtained by request to Cleave Therapeutics (contact email: jadvargas@cleavetherapeutics.com).

FIGURE TITLES AND LEGENDS

Figure 1. An *in vivo* shRNA screen identifies VCP as an AML dependency.

(A) Model of the doxycycline-inducible shRNA screening.

(B) Waterfall plot of all screened hairpins analyzed using the EdgeR/RIGER method. Top scoring *Vcp, Ldha* (positive control), and *Pten* (negative control) hairpins are highlighted in red, black and blue respectively.

(C) Western blot for *Vcp* and *Actin* in MLL-AF9 cells expressing one control (shControl) and two *Vcp*-directed shRNAs (shVcp #1 and #2).

(D) Proportion of $shRNA^+$ MLL-AF9 cells in bone marrow, spleen and peripheral blood respectively 19, 19 and 16 days post-injection of MLL-AF9 cells expressing either shControl, sh*Vcp*#1 or sh*Vcp*#2 (n=3 mice per condition). Welch's t-test in comparison with control condition. Error bars represent mean ± SEM.

(E) Kaplan-Meier curves showing overall survival of mice (n=5 for shControl and n=4 for each sh*Vcp* group) transplanted with cells expressing shControl, sh*Vcp*#1 or sh*Vcp*#2. Arrow indicates the beginning of doxycycline treatment. Log-rank (Mantel-Cox) test. * $p < 0.05$ by comparison with shControl within the *shVcp#1* or the *shVcp#2* group.

(F) Percentage of $shRNA^+$ and $shRNA^-$ MLL-AF9 cells in mice bone marrow 14 days post-injection (Early Bone Marrow) of MLL-AF9 cells expressing either shControl, sh*Vcp*#1 or sh*Vcp*#2, and in bone marrow and spleen at time of death (n=7 mice per condition). Mann-Whitney test in comparison with the shControl condition. Error bars represent mean ± SEM.

(G) Western blot for *Vcp* and *Actin* indicating exogenous (Exo) dominant negative (DN) VCP in MLL-AF9 cells treated with Shield-1 for 24 hours.

(H) Percentage in peripheral blood of MLL-AF9 cells expressing either an empty or a VCP DN-encoding vector 16 days post-transplantation (n=3 mice per condition). Welch's t-test in comparison with empty condition. Error bars represent mean ± SEM.
(I) Kaplan-Meier curves showing overall survival of mice (n=5 per condition) transplanted with MLL-AF9 cells expressing either an empty vector or VCP DN. Arrow indicates beginning of Shield-1 and red squares indicate days of Shield-1 injection. Log-rank (Mantel-Cox) test. * $p < 0.05$ by comparison with empty vector.

Figure 2. AML is preferentially sensitive to VCP inhibition.

(A) Distribution of IC_{50} (concentrations of CB-5083 at which viability was reduced by 50%) in a panel of 131 cancer cell lines treated with CB-5083 for three days in duplicate. Cell lines derived from non-oncogenic tissues and cancer types represented by only one cell line were excluded from this analysis. Error bars represent mean ± SEM of all cell lines within each cancer subtype. Kruskal-Wallis Anova test.
(B) Linear regression analysis of the distribution of IC_{50} of a panel of 16 AML cell lines treated with various concentrations of NMS-873 or CB-5083 for four and five days respectively, with four replicates for each condition. Non-parametric Spearman correlation coefficients (ρ) and associated P-value.
(C) Growth inhibition of UT-7 AML cells infected with the indicated Shield-1-inducible constructs and treated with increasing concentrations of NMS-873 for four days. Western blot for VCP and actin indicating VCP WT and a NMS-873-resistant mutant form of VCP (A530T) after Shield-1 treatment for 24 hours. Error bars represent mean of 4 replicates ± SEM.
(D) Growth inhibition of indicated AML cell lines infected with either a control or two *VCP*-directed shRNAs. Western blot for VCP and actin, 6 days post-doxycycline**.** Data

are normalized to the control shRNA and shown relative to day two of doxycycline induction (time of seeding). Welch's t-test in comparison with control condition. Error bars represent mean of 4 to 8 replicates ± SEM. *p<0.05.

(E) Growth inhibition of indicated human AML cell lines infected with a Shield-1-inducible overexpression vector either empty or encoding WT or dominant negative (DN) VCP**.** Western blot for VCP and actin indicating VCP WT or DN overexpression**,** in MV4-11 cells 24 hours post-Shield-1. Growth inhibition after four days of Shield-1 treatment is normalized to the empty vector and shown relative to non-induced conditions. Welch's t-test in comparison with empty condition. Error bars represent mean of 4 to 8 replicates ± SEM. *p<0.05.

(F) Colony-forming assay for MV4-11 AML cell line either treated with DMSO or NMS-873 (NMS) at 0.4 μM, or infected with an empty, a VCP WT or DN overexpression construct and treated with Shield-1. Welch's t-test in comparison with control conditions (DMSO or empty). Error bars represent mean of 3 replicates ± SEM. *p<0.05.

(G) Representative FACS plots for annexin V (AV) and propidium iodide (PI) staining of indicated AML cell lines either treated with DMSO or NMS-873 (NMS) at 0.2 μM for 8 days, or infected with an empty or a VCP DN overexpression construct and treated two days with Shield-1. Data representative of two independent experiments.

Figure 3. VCP is a dependency in multiple *in vivo* AML models and primary AML patient samples.

(A) Bioluminescence measurements of mice transplanted with MV4-11-luc cells infected with either an empty or a VCP DN-encoding vector (n=5 mice per condition).

Welch's t-test in comparison with empty condition. Error bars represent mean ± SEM. * $p < 0.05$.

(B) Kaplan-Meier curves showing overall survival of mice (n=5 per condition) transplanted with MV4-11-luc cells expressing either an empty or a VCP DN-encoding vector. Arrow indicates beginning of Shield-1 and red squares indicate days of Shield-1 injection. Log-rank (Mantel-Cox) test. * $p < 0.05$ by comparison with empty vector.

(C-D) Proportion of MLL-AF9 cells in peripheral blood (n=5 mice per condition) **(C)** and bone marrow (n=4 mice per condition) **(D)**, respectively 18 and 20 days post-injection of MLL-AF9 cells. CB-5083 treatment was started at day 14. Mann-Whitney test in comparison with vehicle. Error bars represent mean ± SEM.

(E) Bioluminescence measurements of mice transplanted with MV4-11-luc cells and treated with CB-5083 or vehicle (n=5 mice per condition). CB-5083 treatment was started at day 9. Welch's t-test in comparison with vehicle. Error bars represent mean ± SEM. * $p < 0.05$.

(F) Kaplan-Meier curves showing overall survival of mice (n=5 per condition) transplanted with MLL-AF9 and treated with CB-5083. Red squares indicate days of CB-5083 treatment. Log-rank (Mantel-Cox) test. * $p < 0.05$ by comparison with vehicle.

(G) Kaplan-Meier curves showing overall survival of mice (n=5 per condition) transplanted with MV4-11-luc cells and treated with CB-5083 or vehicle. Red squares indicate days of CB-5083 treatment. Log-rank (Mantel-Cox) test. * $p < 0.05$ by comparison with vehicle.

(H-I) Colony-forming assay for primary patient AML samples treated with NMS-873 (n=5) **(H)** or CB-5083 (n=4) **(I)**. Results represent mean of three replicates for each

patient. Welch's t-test in comparison with the control condition. Error bars represent mean ± SEM.

(J) Proportion of hCD45+ leukemic cells in mice peripheral blood 24 days post-injection of patient derived primary AML cells (n=6 mice per condition). CB-5083 treatment was started 20 days post-injection, after engraftment validation. Mann-Whitney test in comparison with vehicle. Error bars represent mean ± SEM.

Figure 4. Inhibition of the nuclear function of VCP alters AML cell line viability through impairment of DNA repair.

(A) Western blot for ubiquitin and actin in the indicated AML cell lines treated with 0.4 μM NMS-873 or 10 nM bortezomib for 24 hours.

(B) Western blot for VCP, lamin B1 (nucleus loading control) and tubulin A (cytoplasm loading control) after nuclear/cytoplasmic fractionation of the MV4-11 cell line expressing either a codon optimized "wild-type" VCP (WT) or a NES (nuclear export signal) flanked-WT VCP.

(C) Growth inhibition of the indicated MV4-11 cell lines treated with Shield-1 for six days, and five days post-doxycycline supplementation. Data are normalized to shControl for each condition. Mann-Whitney test in comparison to empty vector condition. Error bars represent mean of 10 replicates ± SEM.

(D) Western blot for VCP, lamin B1 and tubulin A after nuclear/cytoplasmic fractionation of MV4-11 and UT-7 cell lines expressing either a DN or a NES (nuclear export signal) flanked-DN VCP.

(E) Growth inhibition of indicated AML cell lines treated with Shield-1 for four days. Data are normalized to the empty vector and are shown relative to non-induced

conditions. Mann-Whitney test in comparison to VCP DN condition. Error bars represent mean of two independent experiments with 6 replicates each ± SEM.

(F) Network depicting the VCP interactome established by quantitative mass spectrometry-based analysis of MV4-11 cells stably expressing V5-tagged WT VCP. Results achieving statistical significance (log2FC>0.5 and P-value<0.05) in two biological replicates are shown. VCP interactome was interrogated in a functional enrichment overlapping analysis across the MSigDB database (C2 collection). Protein partners involved in DNA repair, synthesis and cell cycle checkpoints pathways are highlighted in red. -log10FDR calculated through overlapping analysis >1 is defined as threshold of significance.

(G-H) FACS analysis of the intracellular expression of γH2AX in MV4-11 and UT-7 AML cells treated for 72 hours with 0.4 μM NMS-873 or expressing either an empty or a VCP DN vector and treated with Shield-1 for 48 hours**.** Etoposide treatment was used as a positive control. Error bars represent mean ± SEM of 3 to 4 replicates. 10,000 cellular events were measured for each replicate condition. Welch's t-test in comparison with control condition. * p<0.001.

(I-J) FACS analysis of GFP and CD4 expression in RG37-DR-GFP and GC92-NHEJ-CD4 cells respectively at 48 hours post-transfection with I-SceI endonuclease and treated with either 0.4 μM NMS-873, 5 μM KU-55933 (ATMi), or 2.5 μM KU-57788 (DNAPKi). Error bars represent mean ± SEM of three biological replicates. 10,000 cellular events were measured for each replicate. Welch's t-test in comparison with control condition. * p<0.005.

Figure 5. VCP inhibition impairs ATM phosphorylation and downstream signaling resulting in increased sensitivity to DNA damaging agents.

(A-B) Linear regression analysis of the distribution of IC_{50} of a panel of 16 AML cell lines **(A)** and 16 primary patient AML samples **(B)** treated with various concentrations of NMS-873 or KU-55933 (ATMi) for four and three days respectively, four replicates for each condition. Non-parametric Spearman correlation coefficient (ρ) and associated P-value.

(C-D) FACS analysis of the intracellular expression of P-ATM (S1981) in MV4-11 and UT-7 AML cells treated with NMS-873 for two hours **(C)** or with Shield-1 for 12 hours to stabilize VCP DN **(D).** Etoposide treatment was used to induce DNA damage in order to evaluate the DNA repair signaling response under VCP impairment. Error bars represent mean ± SEM of three replicates. 10,000 cellular events were measured for each replicate. Welch's t-test in comparison with etoposide conditions for each cell line. * $p<0.05$.

(E) Western blot for P-ATM (S1981), ATM, P-BRCA1 (S1524), BRCA1, P-KAP1 (S824), KAP1, P-SMC1 (S957), SMC1 and actin, from MV4-11 cells treated with NMS-873 for two hours. Etoposide treatment was used to induce DNA damage, to evaluate the DNA repair signaling response under VCP impairment.

(F-G) Colony-forming assay for MV4-11 AML cell line treated with 0.2 μM NMS-873 for 24H or infected with a Shield-1 inducible empty or VCP DN overexpression construct, and then irradiated with the indicated doses. Welch's t-test in comparison with each control condition. Error bars represent mean of 3 replicates ± SEM.

(H-I) Isobologram representation **(H)** or Combination Index (CI) plots **(I)** for the combination of NMS-873 with doxorubicin in MV4-11 cell line after four days of treatment. Doxorubicin treatment was added after 24 hours of NMS-873 pre-treatment. Results represent the average of four replicates for each dose combination. Dx denotes the drug concentration required to produce x percentage effect alone, and d denotes the

drug concentration required to produce the same x percentage effect in combination with the second drug.

Figure 6. Targeting VCP in AML through a second-generation VCP inhibitor: CB-5339.

(A) Chemical structure and properties of CB-5339 compared to CB-5083.

(B) CB-5339 *in vitro* biochemical selectivity towards PDE6 and retina/plasma tissue distribution compared to CB-5083.

(C) Linear regression analysis of IC_{50} distribution of a panel of 138 cell lines treated with CB-5339 or CB-5083 for three days in duplicates. Non-parametric Spearman correlation coefficient (ρ) and associated P-value.

(D) Linear regression analysis of IC_{50} distribution of a panel of 11 HCT116 cell lines carrying resistance mutations to CB-5083, treated with CB-5339 or CB-5083 for three days in duplicates. Results are presented as fold resistance compared to the parental HCT116 cell line. Non-parametric Spearman correlation coefficient (ρ) and associated P-value.

(E) Linear regression analysis of IC_{50} distribution of a panel of 16 AML cell lines treated with CB-5339 or CB-5083 (four replicates for each condition). Non-parametric Spearman correlation coefficient (ρ) and associated P-value.

(F) Growth inhibition of 16 primary patient AML samples treated with increasing concentrations of CB-5339 for six days. Error bars represent mean of two replicates ± SEM.

(G) Proportion of $hCD45^+$ leukemic cells in mice bone marrow (n=5 mice per condition) 21 days post-injection of patient-derived primary AML cells. CB-5339

treatment was started 10 days post-injection, after engraftment validation. Mann-Whitney test in comparison with vehicle. Error bars represent mean ± SEM.

(H) Kaplan-Meier curves showing overall survival of mice (n=5 mice per condition) transplanted with patient-derived primary AML cells and treated with CB-5339 at 90 mg/kg. Red squares indicate days of CB-5339 treatment. Log-rank (Mantel-Cox) test. * $p < 0.05$ by comparison with vehicle.

(I) Proportion of MLL-AF9 cells in peripheral blood (n=6 mice per condition) 12 days post-injection of MLL-AF9 cells. CB-5339 treatment was started at day 8. Mann-Whitney test in comparison with vehicle. Error bars represent mean ± SEM.

(J) Kaplan-Meier curves showing overall survival of mice (n=6 per condition) transplanted with MLL-AF9 and treated with CB-5339 at 90 mg/kg. Red squares indicate days of CB-5339 treatment. Log-rank (Mantel-Cox) test. * $p < 0.05$ by comparison with vehicle.

(K) Proportion of MLL-AF9 cells in peripheral blood (n=3 mice per condition) 11 days post-injection of MLL-AF9 cells. Treatment was started at day 9 (CB-5339 at 50 mg/kg for 4 days, Chemo : Doxorubicin at 0.5 mg/kg for 3 days and cytarabine at 75 mg/kg for 5 days). Mann-Whitney test. Error bars represent mean ± SEM. * $p < 0.05$ by comparison with vehicle. $^{\#}$ $p < 0.05$ by comparison with CB-5339 or Chemo groups.

(L) Kaplan-Meier curves showing overall survival of mice (n=5 per condition) transplanted with MLL-AF9 and treated as indicated. Red squares indicate days of CB-5339 treatment. Log-rank (Mantel-Cox) test. * $p < 0.05$ by comparison with vehicle. $^{\#}$ $p < 0.05$ by comparison with CB-5339 or Chemo groups.

Figure 7. Co-occurrence of RAS oncogene activation and TP53 deficiency is associated with decreased response to VCP inhibition.

(A-B) Linear regression analysis of IC_{50} distributions of a panel of 91 cancer cell lines **(A)** or 12 AML cell lines **(B)** treated with CB-5339 for three days compared to VCP mRNA expression data extracted from the CCLE database. Cell lines with no available transcriptional data were excluded from this analysis. R-square coefficient and associated P-value. NS=Not Significant. TPM=Transcripts per Million.

(C-D) FACS analysis of the intracellular expression of γH2AX **(C)** or P-ATM (S1981) **(D)** in the indicated AML cell lines. Error bars represent mean of 2 to 3 replicates ± SEM. 10,000 cellular events were measured for each replicate. Welch's t-test. NS=Not Significant.

(E) *KRAS, NRAS* and *TP53* mutational profiles (extracted from CCLE database) of the 16 AML cell lines screened for sensitivity to NMS-873. Cell lines harboring both RAS (*KRAS* or *NRAS*) and *TP53* mutations are highlighted in red.

(F) Distribution of IC_{50} in a panel of 13 AML cell lines treated with various concentrations of NMS-873, CB-5083 or CB-5339 (four replicates for each condition). The 3 AML cell lines with no available *RAS-TP53* mutational status were excluded from this analysis. Mann-Whitney test. * $p<0.05$.

(G-H) *RAS* and *TP53* mutational **(G)** or RAS activation and TP53 deficiency **(H)** co-occurrence frequency across pan-cancer TCGA database (10, 294 patient samples, 33 tumor lineages). Functional RAS activation and TP53 deficiency scores were determined based on two previously validated classifiers. AML subtype is highlighted in red. TCGA acronyms are detailed in **Table S8**.

Figure 1

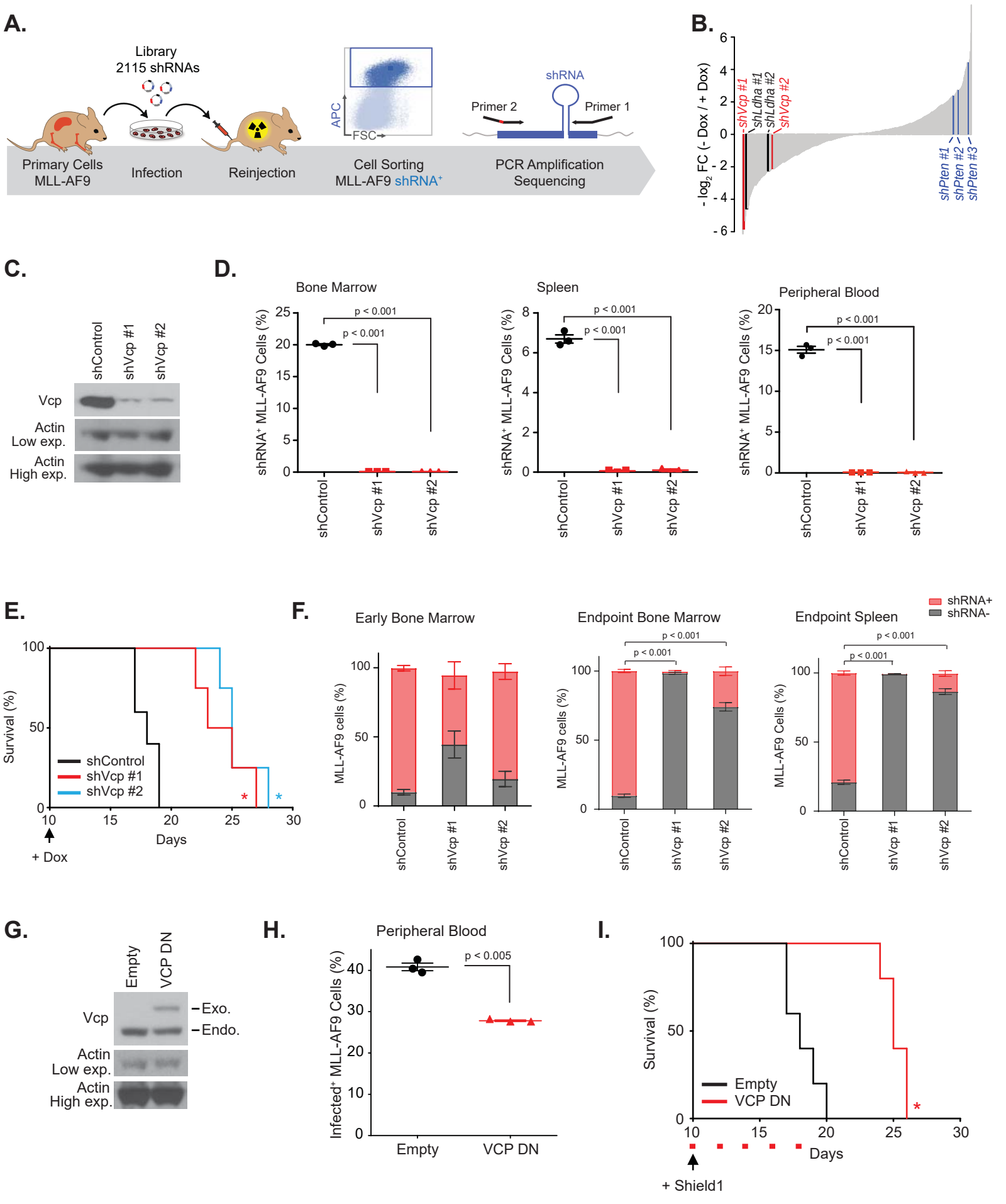
A.
Library
2115 shRNAs
Primary Cells
MLL-AF9
Infection
Reinjection
APC
FSC
Cell Sorting
MLL-AF9 shRNA+
shRNA
Primer 2
Primer 1
PCR Amplification
Sequencing
B.
- log2 FC (- Dox / + Dox)
shVcp #1
shLdha #1
shLdha #2
shVcp #2
shPten #1
shPten #2
shPten #3
C.
shControl
shVcp #1
shVcp #2
Vcp
Actin
Low exp.
Actin
High exp.
D.
Bone Marrow
Spleen
Peripheral Blood
shRNA+ MLL-AF9 Cells (%)
p < 0.001
E.
Survival (%)
shControl
shVcp #1
shVcp #2
Days
+ Dox
F.
Early Bone Marrow
Endpoint Bone Marrow
Endpoint Spleen
shRNA+
shRNA-
MLL-AF9 cells (%)
G.
Empty
VCP DN
Vcp
Exo.
Endo.
Actin
Low exp.
Actin
High exp.
H.
Peripheral Blood
Infected+ MLL-AF9 Cells (%)
p < 0.005
Empty
VCP DN
I.
Survival (%)
Empty
VCP DN
Days
+ Shield1

Figure 2

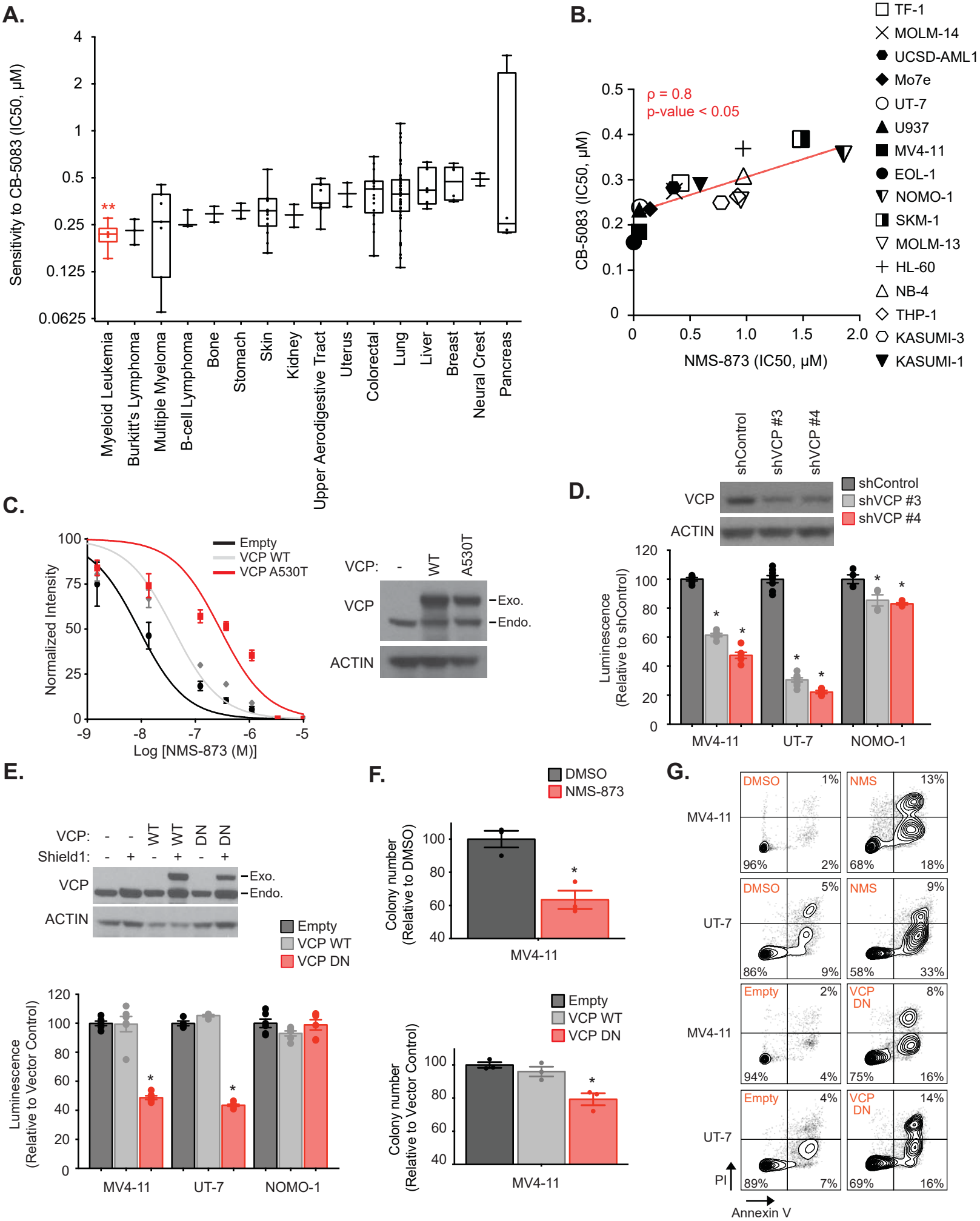
A.
Sensitivity to CB-5083 (IC50, μM)
4
2
1
0.5
0.25
0.125
0.0625
**
Myeloid Leukemia
Burkitt's Lymphoma
Multiple Myeloma
B-cell Lymphoma
Bone
Stomach
Skin
Kidney
Upper Aerodigestive Tract
Uterus
Colorectal
Lung
Liver
Breast
Neural Crest
Pancreas
B.
ρ = 0.8
p-value < 0.05
CB-5083 (IC50, μM)
NMS-873 (IC50, μM)
TF-1
MOLM-14
UCSD-AML1
Mo7e
UT-7
U937
MV4-11
EOL-1
NOMO-1
SKM-1
MOLM-13
HL-60
NB-4
THP-1
KASUMI-3
KASUMI-1
C.
Normalized Intensity
Log [NMS-873 (M)]
Empty
VCP WT
VCP A530T
VCP:
WT
A530T
VCP
ACTIN
Exo.
Endo.
D.
shControl
shVCP #3
shVCP #4
VCP
ACTIN
Luminescence (Relative to shControl)
MV4-11
UT-7
NOMO-1
E.
VCP:
Shield1:
WT
DN
VCP
ACTIN
Exo.
Endo.
Empty
VCP WT
VCP DN
Luminescence (Relative to Vector Control)
MV4-11
UT-7
NOMO-1
F.
DMSO
NMS-873
Colony number (Relative to DMSO)
MV4-11
Empty
VCP WT
VCP DN
Colony number (Relative to Vector Control)
MV4-11
G.
DMSO
NMS
MV4-11
UT-7
96%
2%
68%
18%
86%
9%
58%
33%
Empty
VCP DN
94%
4%
75%
16%
89%
7%
69%
16%
PI
Annexin V

Figure 3

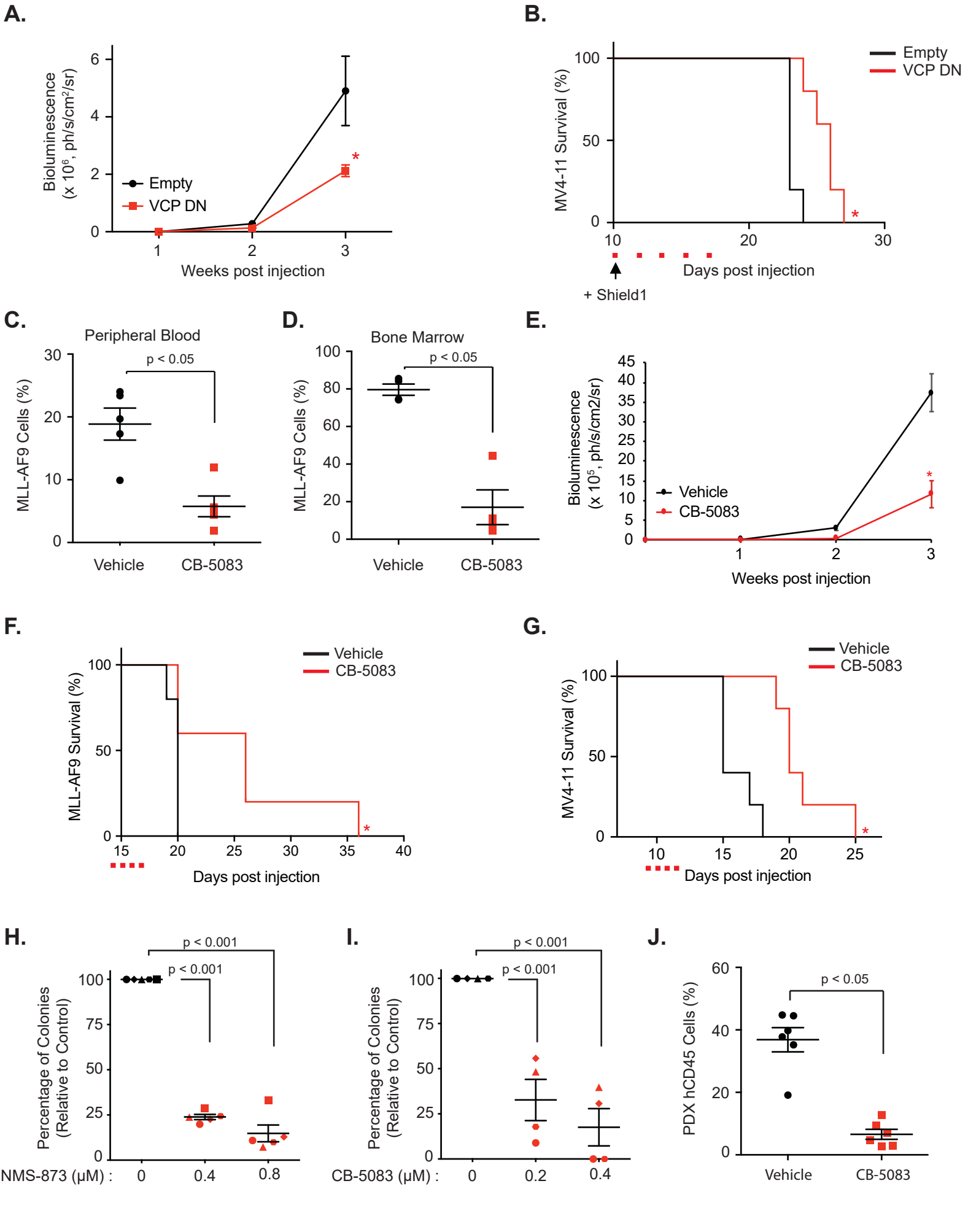
A.
Bioluminescence (x 10^6, ph/s/cm^2/sr)
Empty
VCP DN
Weeks post injection
B.
MV4-11 Survival (%)
Empty
VCP DN
Days post injection
+ Shield1
C.
Peripheral Blood
p < 0.05
MLL-AF9 Cells (%)
Vehicle
CB-5083
D.
Bone Marrow
p < 0.05
MLL-AF9 Cells (%)
Vehicle
CB-5083
E.
Bioluminescence (x 10^5, ph/s/cm2/sr)
Vehicle
CB-5083
Weeks post injection
F.
MLL-AF9 Survival (%)
Vehicle
CB-5083
Days post injection
G.
MV4-11 Survival (%)
Vehicle
CB-5083
Days post injection
H.
p < 0.001
p < 0.001
Percentage of Colonies (Relative to Control)
NMS-873 (μM) :
I.
p < 0.001
p < 0.001
Percentage of Colonies (Relative to Control)
CB-5083 (μM) :
J.
p < 0.05
PDX hCD45 Cells (%)
Vehicle
CB-5083

Figure 4

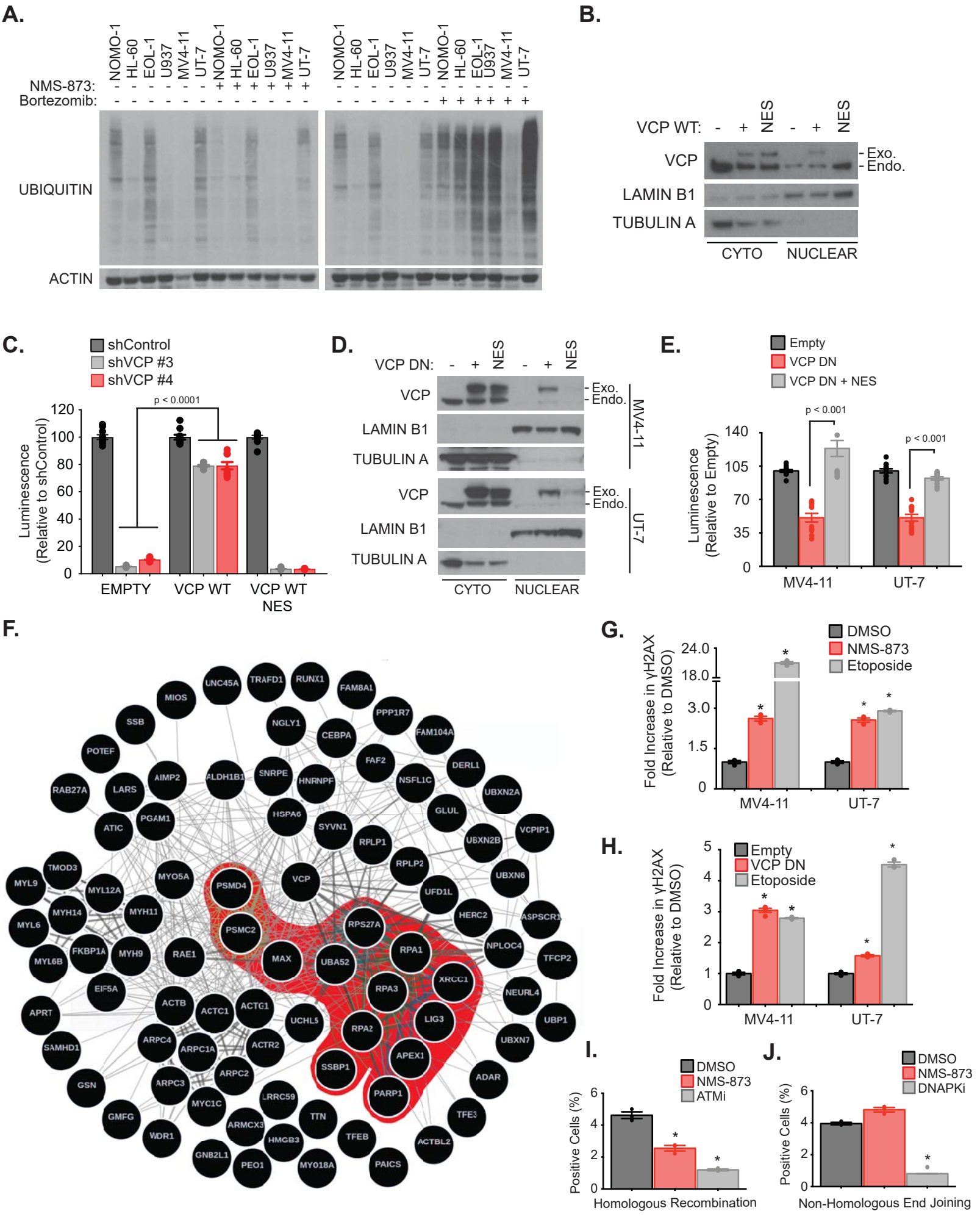
A.
NOMO-1
HL-60
EOL-1
U937
MV4-11
UT-7
NMS-873:
Bortezomib:
UBIQUITIN
ACTIN
B.
VCP WT:
NES
VCP
LAMIN B1
TUBULIN A
Exo.
Endo.
CYTO
NUCLEAR
C.
shControl
shVCP #3
shVCP #4
p < 0.0001
Luminescence (Relative to shControl)
EMPTY
VCP WT
VCP WT NES
D.
VCP DN:
MV4-11
UT-7
E.
Empty
VCP DN
VCP DN + NES
p < 0.001
Luminescence (Relative to Empty)
F.
G.
DMSO
NMS-873
Etoposide
Fold Increase in γH2AX (Relative to DMSO)
H.
I.
ATMi
Positive Cells (%)
Homologous Recombination
J.
DNAPKi
Non-Homologous End Joining

Figure 5

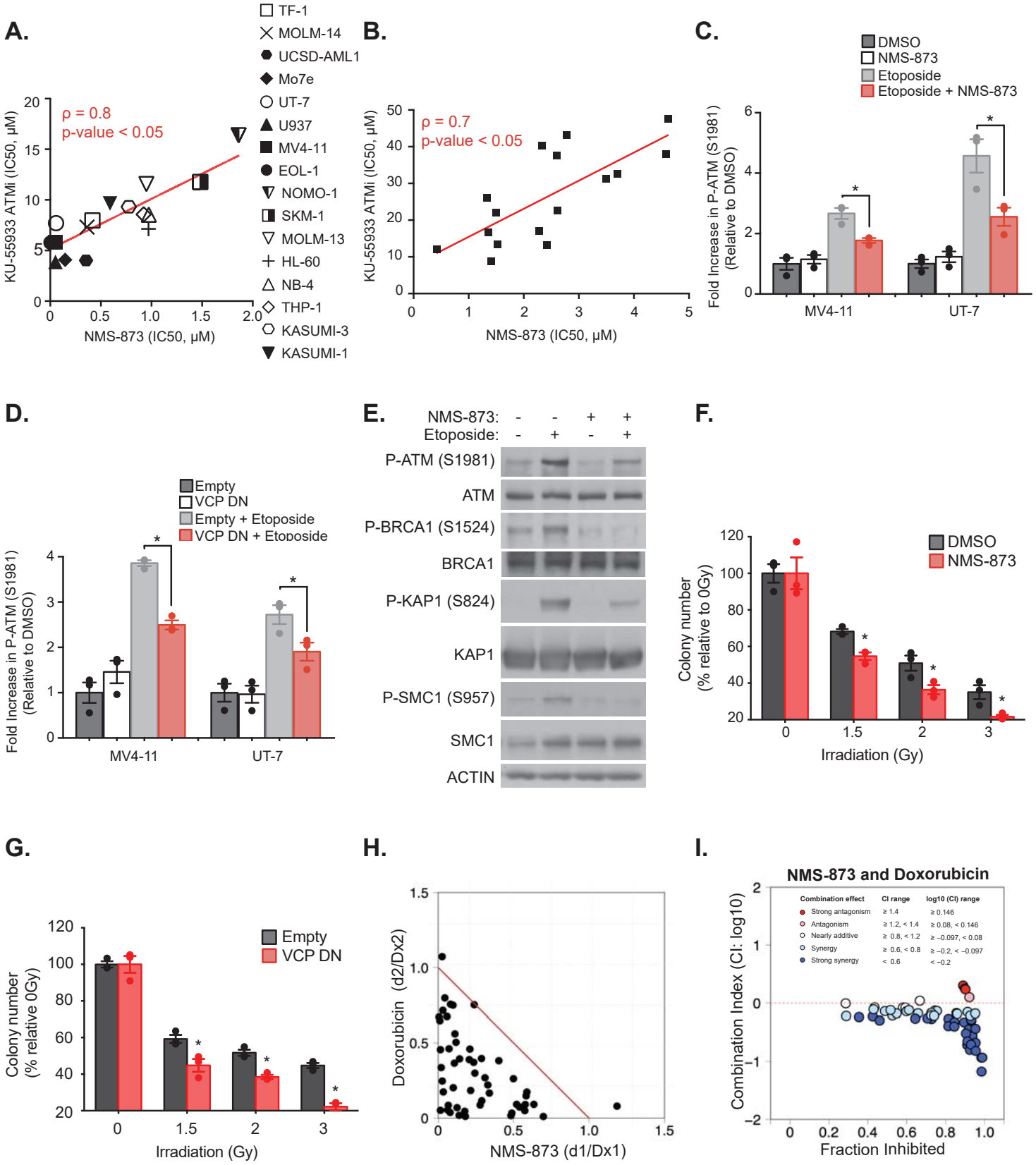
A.
ρ = 0.8
p-value < 0.05
KU-55933 ATMi (IC50, μM)
NMS-873 (IC50, μM)
TF-1
MOLM-14
UCSD-AML1
Mo7e
UT-7
U937
MV4-11
EOL-1
NOMO-1
SKM-1
MOLM-13
HL-60
NB-4
THP-1
KASUMI-3
KASUMI-1
B.
ρ = 0.7
p-value < 0.05
KU-55933 ATMi (IC50, μM)
NMS-873 (IC50, μM)
C.
DMSO
NMS-873
Etoposide
Etoposide + NMS-873
Fold Increase in P-ATM (S1981) (Relative to DMSO)
MV4-11
UT-7
D.
Empty
VCP DN
Empty + Etoposide
VCP DN + Etoposide
Fold Increase in P-ATM (S1981) (Relative to DMSO)
MV4-11
UT-7
E.
NMS-873:
Etoposide:
P-ATM (S1981)
ATM
P-BRCA1 (S1524)
BRCA1
P-KAP1 (S824)
KAP1
P-SMC1 (S957)
SMC1
ACTIN
F.
DMSO
NMS-873
Colony number (% relative to 0Gy)
Irradiation (Gy)
G.
Empty
VCP DN
Colony number (% relative 0Gy)
Irradiation (Gy)
H.
Doxorubicin (d2/Dx2)
NMS-873 (d1/Dx1)
I.
NMS-873 and Doxorubicin
Combination effect
CI range
log10 (CI) range
Strong antagonism
Antagonism
Nearly additive
Synergy
Strong synergy
Combination Index (CI: log10)
Fraction Inhibited

Figure 6

A.

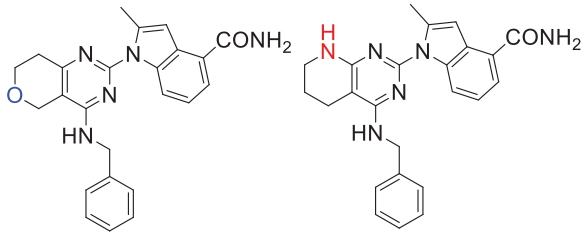

	Molecular Weight	log P	H-bond donors	H-bond acceptors	pKa	pKa type
CB-5339	412.49	3.57	3	5	6.56	Basic
CB-5083	413.47	2.72	2	5	4.74	Basic

B.

***In vitro* biochemical selectivity**	**CB-5083**	**CB-5339**
VCP IC50 (nM)	11	9
PDE6 IC50 (bovine, nM)	33	384
PDE6C IC50 (human, nM)	261	3900

***In vivo* tissue distribution**	**CB-5083**	**CB-5339**
Cmax (retina/plasma ratio)	2.5	0.08
AUC (retina/plasma ratio)	4.3	1.1

C.

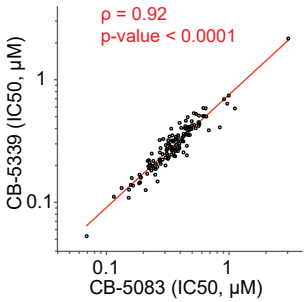

D.

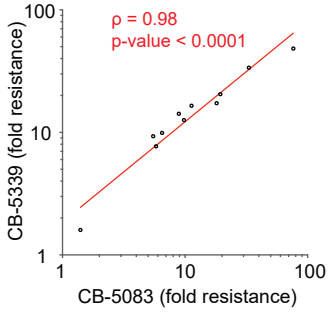

E.

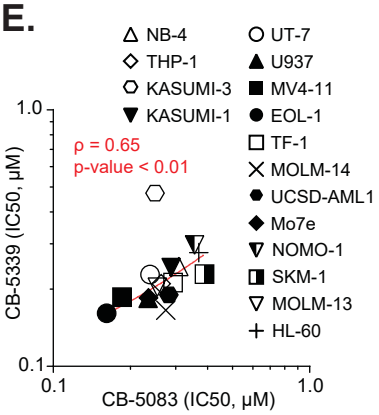

F.

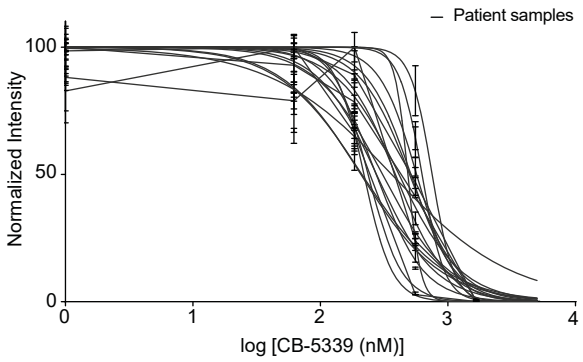

G.

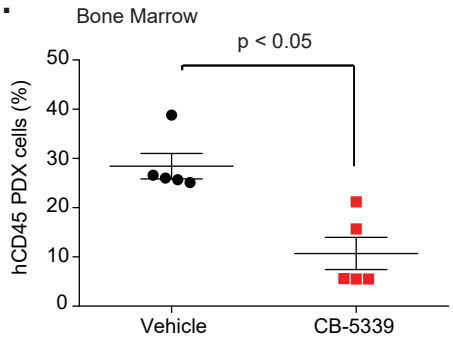

I.

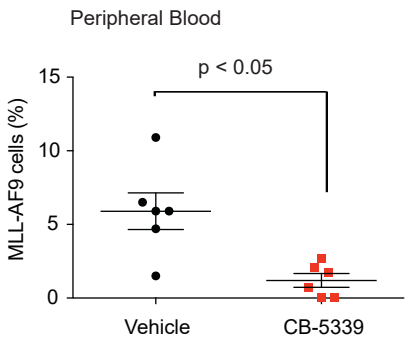

K.

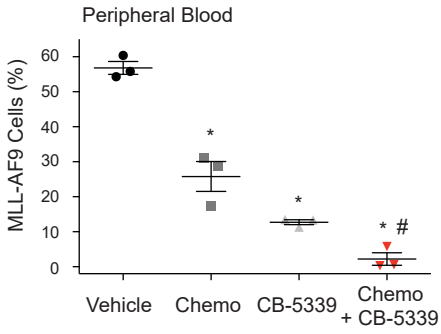

H.

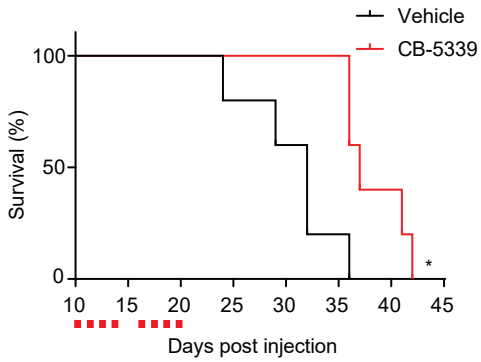

J.

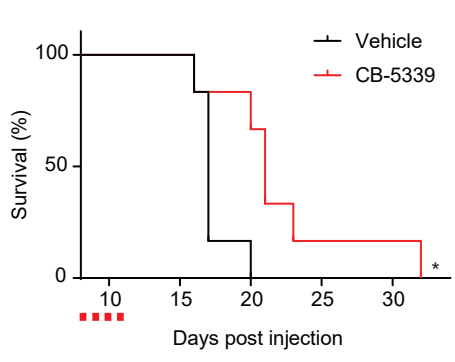

L.

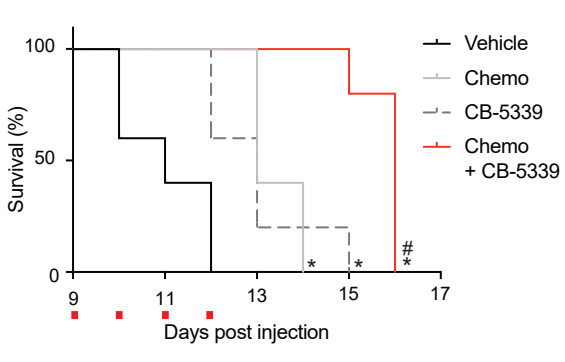

Figure 7

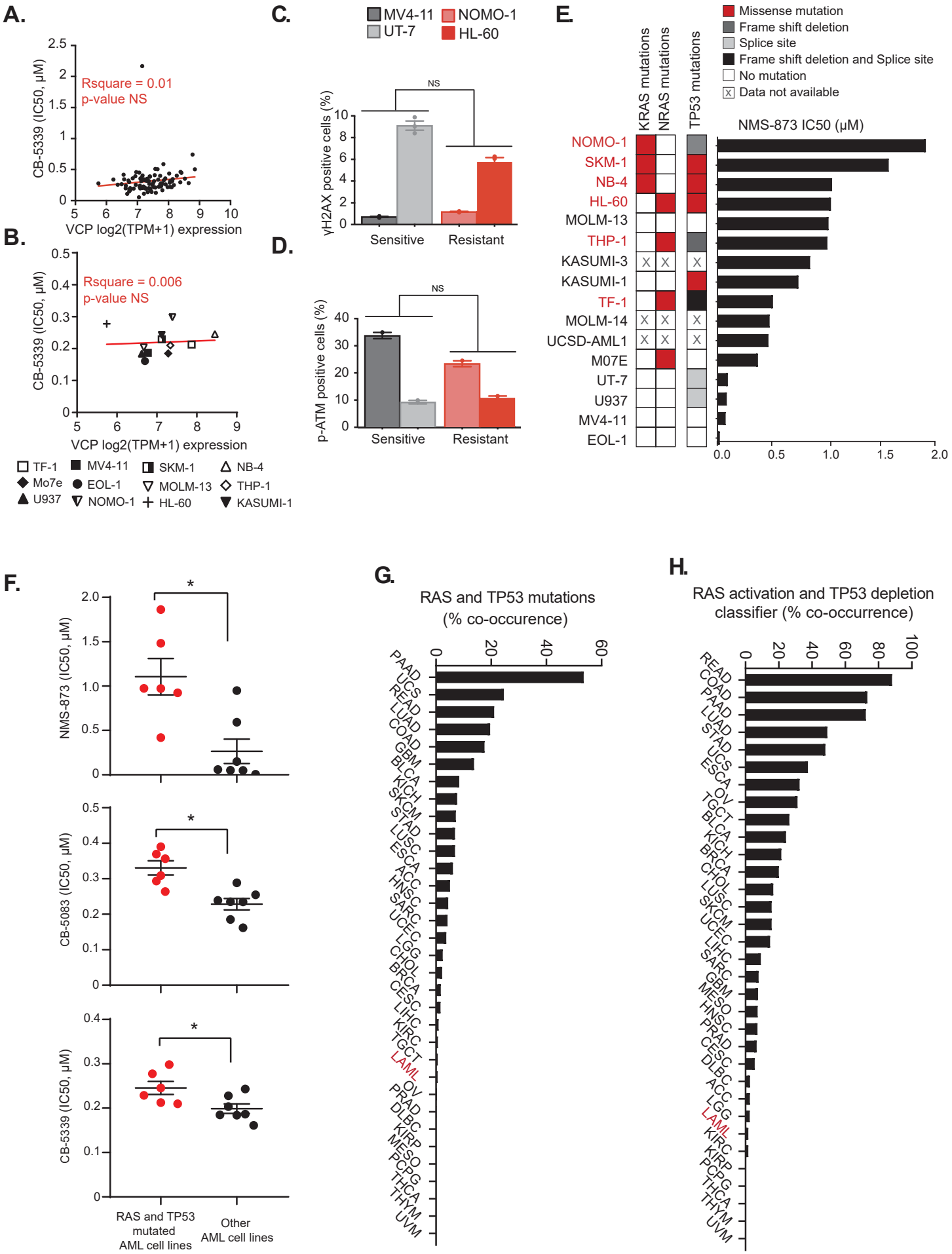
A.
Rsquare = 0.01
p-value NS
CB-5339 (IC50, µM)
VCP log2(TPM+1) expression
B.
Rsquare = 0.006
p-value NS
CB-5339 (IC50, µM)
VCP log2(TPM+1) expression
TF-1
MV4-11
SKM-1
NB-4
Mo7e
EOL-1
MOLM-13
THP-1
U937
NOMO-1
HL-60
KASUMI-1
C.
MV4-11
NOMO-1
UT-7
HL-60
γH2AX positive cells (%)
NS
Sensitive
Resistant
D.
p-ATM positive cells (%)
NS
Sensitive
Resistant
E.
Missense mutation
Frame shift deletion
Splice site
Frame shift deletion and Splice site
No mutation
Data not available
KRAS mutations
NRAS mutations
TP53 mutations
NMS-873 IC50 (µM)
NOMO-1
SKM-1
NB-4
HL-60
MOLM-13
THP-1
KASUMI-3
KASUMI-1
TF-1
MOLM-14
UCSD-AML1
M07E
UT-7
U937
MV4-11
EOL-1
F.
NMS-873 (IC50, µM)
CB-5083 (IC50, µM)
CB-5339 (IC50, µM)
RAS and TP53 mutated AML cell lines
Other AML cell lines
G.
RAS and TP53 mutations (% co-occurence)
PAAD
UCS
READ
LUAD
COAD
GBM
BLCA
KICH
SKCM
STAD
LUSC
ESCA
ACC
HNSC
SARC
UCEC
LGG
CHOL
BRCA
CESC
LIHC
KIRC
TGCT
LAML
OV
PRAD
DLBC
KIRP
MESO
PCPG
THCA
THYM
UVM
H.
RAS activation and TP53 depletion classifier (% co-occurrence)
READ
COAD
PAAD
LUAD
STAD
UCS
ESCA
OV
TGCT
BLCA
KICH
BRCA
CHOL
LUSC
SKCM
UCEC
LIHC
SARC
GBM
MESO
HNSC
PRAD
CESC
DLBC
ACC
LGG
LAML
KIRC
KIRP
PCPG
THCA
THYM
UVM

SUPPLEMENTARY MATERIALS

SUPPLEMENTARY MATERIALS AND METHODS

***In Vivo* Transplantation**

Saint-Louis Research Institute, Dana Farber Cancer Institute and the Massachusetts Institute of Technology Committee on Animal Care reviewed and approved all mouse experiments described in this study.

In vivo pooled shRNA screening. A custom library of 2,115 hairpins directed against 429 murine genes involved in cellular stress response with a minimum of 4 hairpins per gene, which were synthesized as an Oligomix from LC Sciences, was cloned into a retroviral TRMPVIR/E2Crimson vector. To preserve library complexity, a minimum of 500-fold coverage of the shRNA library was maintained at each step of the screen. 6-week-old C57BL/6 male donor mice (The Jackson Laboratory) were injected with 200,000 MLL-AF9-DsRed-L-GMP cells into the tail vein. Bone marrow was harvested from femur, tibia and humerus, and red blood cells were lysed (Sigma). DsRed sorted cells were resuspended in transplant medium made with 20 ng/ml IL-3 (#213-13, Peprotech), 20 ng/mL IL-6 (#216-16, Peprotech), 100 ng/mL FLT3-ligand (#250-31L, Peprotech) and 100 ng/mL SCF (#250-03, Peprotech) in StemSpan SFEM (#09650, StemCell Technologies Inc.) and then transduced with TRMPVIR/E2Crimson-library vector by one round of spin-infection. 10×10^6 cells in 3 mL transplant medium containing 5 μg/mL polybrene (Sigma) and 7.5 mM HEPES buffer (Sigma) were centrifuged in the presence of virus for 4 hours at 1800g to promote cell transduction. After 24 hours, cells were sorted based on expression of the GFP fluorescent protein and then reinjected into 15 secondary recipient mice. These mice were randomized into

3 groups i) one group "input", ii) one group treated with doxycycline for two days, and iii) one group treated with doxycycline throughout the experiment. Doxycycline induction was started 7 days post-injection by supplementation of the drinking water with 1 mg/mL doxycycline and 5% sucrose. MLL-AF9 cells were harvested and sorted based on the expression of the crimson fluorescent dye. The antisense strand of shRNA was amplified from genomic DNA using primers that include 1-basepair mutation to barcode individual samples. Hairpins were amplified in multiple 50 μl reactions using HotStar Taq (Qiagen). After PCR amplification, samples were pooled and prepared for sequencing with Illumina's genomic adaptor kit. At least 41 bases of the PCR product were sequenced with an Illumina HiSeq 2000 machine and then aligned with bowtie2 to the mouse mm9 genome at the Swanson Biotechnology Center, Koch Institute, Massachusetts Institute of Technology. shRNAs with less than 100 reads in the input sample were excluded from further analysis, and read numbers for each shRNA were normalized to the total read numbers per sample to allow for cross-comparison between samples.

The genes whose depletion blocked (or enhanced) the cell proliferation between the groups of mice (doxycycline vs vehicle, n=5 per group) were determined based on the EdgeR (*72*, *73*) method followed by the RIGER method (*74*) (https://software.broadinstitute.org/GENE-E/extensions/RIGER.jar).

EdgeR was used to perform the differential analysis on the shRNA count data between the groups of mouse samples. RIGER ranked all the 2,115 shRNAs according to their differential score between the two classes of samples, then identified the genes targeted by the shRNAs at the top of the list, by computing a gene Normalized Enrichment Score

(NES), based on the Kolmogorov-Smirnov statistic for gene enrichment in the top hairpins. The significance of the normalized enrichment score was estimated through a permutation P-value ($n=10^9$ repetitions) adjusted for false discovery based on the Benjamini-Hochberg method, with a significance cut-off ≤ 0.10. The significance cut-off was estimated as 0.10 instead of 0.05 due to the small size of the hairpin library. In this way, the EdgeR/RIGER methods identified 34 significantly depleted genes.

Low-throughput in vivo Vcp dependency validation in the MLL-AF9 mouse model: For shRNA and VCP-DN overexpression experiments, 6 to 8 week-old C57BL/6 male mice (The Jackson Laboratory) were injected with 200,000 MLL-AF9-DsRed-L-GMP cells after infection with either TRMPVIR/E2Crimson, TRMPVIR/E2Crimson-shVCP#1, TRMPVIR/E2Crimson-shVCP#2, pRetroX-pTUNER-Empty or pRetroX-pTUNER-VCP-DN. For the relapse evaluation experiment, Venus positive MLL-AF9-DsRed-L-GMP cells were sorted to purify the successfully infected population before tail vein injection of 150,000 MLL-AF9-DsRed-L-GMP $Venus^+$ cells. Hairpins and VCP-DN expression was induced by supplementing the drinking water with 1 mg/ml doxycycline and 5% sucrose throughout the experiment, and by IP. injection of 40 µL with 10 mg/kg Shield-1 in 50% N,N-dimethylacetamide, 45% PEG400 and 5% Tween-80 at days 10, 12, 14, 16 and 18, respectively. Peripheral blood mononuclear cells were collected by sub-mandibular bleeding while bone marrow biopsies were performed on mice femurs at the indicated time points to collect bone marrow mononuclear cells. Bone marrow and spleen mononuclear cells were also harvested after mice sacrifice . For *in vivo* knockdown or overexpression experiments, Vcp extinction was evaluated by western blot.

Low-throughput in vivo Vcp dependency validation in the MV-411-Luc mouse model: MV4-11 cells were transduced with the pMMP-LucNeo retrovirus and selected with neomycin at 1 mg/mL. MV4-11-luc cells were then stably infected wit either pRetroX-pTUNER-Empty or pRetroX-pTUNER-VCP-DN. $1x10^6$ cells were subsequently injected via tail vein into 8-week-old male NSG mice (The Jackson Laboratory). VCP-DN expression was induced by IP as described. Mice were imaged at the indicated time points on an IVIS Spectrum (Caliper Life Sciences) to assess bioluminescence.

In vivo drug treatment studies: $1x10^6$ MV4-11-luc cells, 100,000 or 200,000 MLL-AF9-DsRed-L-GMP cells, or 500,000 patient derived primary AML cells were injected via tail vein into 8-week-old male NSG mice, 6-week-old C57BL/6 male mice, or 6-week-old male and female NSGS or NOG-EXL mice respectively (The Jackson Laboratory and Taconic Biosciences). After disease engraftment confirmation, mice were randomized to be treated with CB-5083 (50 mg/kg, oral gavage, 4 days on - 3 days off schedule) or vehicle (0.5% methylcellulose) as previously described (*20*). CB-5339 was delivered through oral gavage at the indicated doses. Doxorubicin and cytarabine were used intraperitoneally, respectively at 0.5 mg/kg for 3 days and 75 mg/kg for 5 days. Mice were imaged at the indicated time points on an IVIS Spectrum (Caliper Life Sciences) to assess bioluminescence. Peripheral blood mononuclear cells were collected by sub-mandibular bleeding and bone marrow mononuclear cells were harvested by bone marrow biopsy at the indicated time points. Bone marrow and spleen mononuclear cells were also harvested after mice were sacrificed for the relapse experiment. Complete blood counts were measured at the indicated time point.

Cell Culture

HL-60, U937, Kasumi-1, Kasumi-3, and TF-1 cell lines were purchased from the American Type Culture Collection. NOMO-1, UT-7 and UCSD-AML were purchased from DSMZ. EOL-1 were purchased from Sigma-Aldrich. NB-4, MV4-11, SKM-1 and Mo7e were provided by Ross Levine, MOLM-13 by Benjamin Ebert, THP-1 and MOLM-14 by Scott Armstrong and U2OS by David Pellman. All cell lines except MOLM-13, SKM-1, Kasumi-1, TF-1, UT-7, Kasumi-3, Mo7e, UCSD-AML1 and U2OS were maintained in RPMI 1640 (Cellgro) supplemented with 1% penicillin-streptomycin (PS, Invitrogen) and 10% fetal bovine serum (FBS, Sigma-Aldrich) at 37 °C with 5% CO2. MOLM-13, SKM-1 and Kasumi-1 cells were maintained in RPMI 1640 supplemented with 1% penicillin-streptomycin and 20% FBS. TF-1, UT-7, Kasumi-3, Mo7e and UCSD-AML1 were maintained in RPMI 1640 supplemented with 1% penicillin-streptomycin and 10% FBS with 20 ng per ml GM-CSF (Peprotech). All AML cell lines were confirmed by STR genotyping.

Cancer cell lines for the large scale cell lines screening were obtained from American Type Culture Collection and cultured according to the supplier's instructions. HEK-293T and U2OS were maintained in Dulbecco's modified Eagle's medium (Cellgro) supplemented with 10% fetal bovine serum (FBS, Sigma-Aldrich) and 1% penicillin-streptomycin (PS, Invitrogen). MLL-AF9-DsRed-L-GMP cells were maintained in StemSpan SFEM (#09650, StemCell Technologies Inc.) with 20 ng/ml IL-3 (#213-13, Peprotech), 20 ng/ml IL-6 (#216-16, Peprotech), 100 ng/ml FLT3-ligand (#250-31L, Peprotech) and 100 ng/ml SCF (#250-03, Peprotech).

Primary patient AML blasts were collected from bone marrow aspirates after obtaining patient informed consent under a Dana-Farber Cancer Institute Internal Review Board-approved protocol. Mononuclear cells were isolated using Ficoll-Paque Plus (Amersham Biosciences) and red blood cells were lysed (eBioscience). These cells were maintained in StemSpan SFEM (StemCell Technologies Inc.) medium supplemented with 20 ng/ml IL-3 (Peprotech), 20 ng/ml IL-6 (Peprotech), 20 ng/ml GM-CSF (Peprotech), 100 ng/ml FLT3-ligand (Peprotech) and 100 ng/ml SCF (Peprotech). For CB-5339 *in vitro* assays, primary patient AML blasts were obtained from leukapheresis, following Champions Oncology institutional committee protocols. Samples were cultured in cytokine enriched media (StemSpan SFEM, StemSpan TM CC110 (StemCell Technologies Inc.) and recombinant human IL-3 (R&D Systems)).

Chemicals

NMS-873, KU-57788, etoposide, bortezomib and MG-132 were purchased from Selleckchem, KU-55933 from Abcam, Shield-1 from Aobious, TLCK hydrochloride and epoxomicin from Santa Cruz Biotechnology, tunicamycin from EMD Millipore or Sigma, thapsigargin from Sigma, doxycycline from Clontech, and doxorubicin from Cell Signaling. CB-5083 was purchased from Selleckchem or provided by Cleave Therapeutics. CB-5339 was provided by Cleave Therapeutics.

Biochemical assays

CB-5083 and CB-5339 *in vitro* biochemical analyses for VCP were performed using a standard NADH-based coupled kinetic ATPase assay as previously described (*20, 21*). CB-5083 and CB-5339 *in vitro* biochemical analyses for bovine retina PDE6 and recombinant human PDE6C were performed by Eurofins Cerep, Celle l'Evescault

France and BPS Bioscience, San Diego, CA USA, respectively, using their standard enzymatic inhibition assays. Briefly, VCP inhibition activity on PDE6C from human retina was determined by enzymatic reactions conducted at room temperature for 60 minutes in a 50 µl reaction mixture consisting of PDE assay buffer (BPS Biosciences), 100 nM FAM-cGMP, 0.5 ng PDE6 enzyme and a 0.001 to 10 µM dilution range of VCP inhibitor. After the enzymatic reaction, 100 µl of cGMP binding solution (BPS Biosciences) was added and allowed to incubate at room temperature for 60 minutes. Fluorescence intensity was measured at an excitation of 485 nm and an emission of 528 nm using a Tecan Infinite M1000 microplate reader. The effect of VCP inhibition on PDE6 isolated from bovine retina was determined by measuring the conversion of [3H]-cGMP to the [3H]-5'-GMP mononucleotide by radiometric scintillation counts after a 60 minutes incubation of a [3H]-cGMP + cGMP (2uM)(Eurofins – CEREP) 100 µl reaction mixture with an 8 point dilution series of inhibitor.

Pharmacological assays

Metabolic stability was assessed in liver microsomes from rat, dog, monkey and human, and clearance was calculated. *In vivo* tissue distribution and bioavailability (F%) was determined from pharmacokinetic measurements. For bioavailability, pharmacokinetic assessement of the areas under the plasma concentration versus time curves following iv and oral administration in rat (Cleave Therapeutics), dog (BioDuro) and monkey (Charles River) was used. Tissue distribution was determined from analysis of tissue samples after oral administration (WuXi Apptec).

Cleave Therapeutics IACUC or contracted company Committee on Animal Care reviewed and approved the rat, dog and monkey experiments described in this study.

Plasmids, shRNA Constructs and cell infection

The pMMP LUC-NEO vector was a kind gift from Andrew Kung. (WT)-EGFP and VCP(DK0)-EGFP (a gift from Nico Dantuma, Addgene plasmids # 23971 and # 23974) were amplified using primers listed below and then cloned into pRetroX-pTUNER (Clontech).

cDNA	Primer	Sequence
VCP	Forward	CTCGTGATACCGCGGCCGCTGGCTTCTGGAGCCGATTC AAAAGGTGATGACC
	Reverse	GCAGTGAGAAGATCTTTACGTAGAATCGAGACCGAGG AGAGGGTTAGGGATAGGCTTACCGCCATACAGGTCAT CATCATTGTCTTCTGTG

The codon optimized VCP geneblock was designed and synthesized by Integrated DNA Technologies, before cloning into pRetroX-pTUNER (Clontech).

shRNA constructs targeting murine VCP (shVCP#1 and shVCP#2) and human *VCP* (shVCP#3, shVCP#4) – sequences listed below – were designed by adapting BIOPREDsi small interfering RNA predictions. shRNAs were cloned into the REVIR retroviral vector following instructions from a previously published protocol (*75*). Briefly, 97-mer oligonucleotides (IDT Ultramers) coding for the shRNAs were PCR amplified using the forward (5′-TGAACTCGAGAAGGTATATTGCTGTTGACAGTGAGCG-3′) and the reverse (5′-TCTCGAATTCTAGCCCCTTGAAGTCCGAGGCAGTAGGC-3′) primers, 0.05 ng oligonucleotide template, and the PfuUltra HF kit (Agilent), and cloned into miRE recipient vectors.

Designation	shRNA 97-mer oligo sequence
shVCP#1	TGCTGTTGACAGTGAGCGAAACAGCCATTCTCAAACAGAA TAGTGAAGCCACAGATGTATTCTGTTTGAGAATGGCTGTT GTGCCTACTGCCTCGGA
shVCP#2	TGCTGTTGACAGTGAGCGCGCCGTACTTCCTGGAAGCTTA TAGTGAAGCCACAGATGTATAAGCTTCCAGGAAGTACGGC TTGCCTACTGCCTCGGA
shVCP#3	TGCTGTTGACAGTGAGCGCCACAGTGTTGCTGAAAGGAAA TAGTGAAGCCACAGATGTATTTCCTTTCAGCAACACTGTG TTGCCTACTGCCTCGGA
shVCP#4	TGCTGTTGACAGTGAGCGACAGTGTATACACAGAAGACAA TAGTGAAGCCACAGATGTATTGTCTTCTGTGTATACACTGC TGCCTACTGCCTCGGA

For virus production, 12 μg of the above plasmids and 6 μg ψ-eco (for retroviral infection of murine cells), 6 μg pCMV-GAG/POL and pCMV-VSVG (for retroviral infection), or 6 μg pCMV8.9 or psPAX2 and pCMV-VSVG (for lentiviral infection) packaging vectors were transfected into the 293T packaging cell line using X-tremeGENE 9 (Roche), and the resulting viral supernatants were harvested as previously described (*76*). The lentiviral and retroviral viruses were then concentrated using PEG-it™ Virus Precipitation Solution or Retro-concentin (SBI System Biosciences) respectively. Cells were infected using RetroNectin (Clontech) following the manufacturer's recommendations for retroviral vectors and as previously described for lentiviral plasmids (*76*). At least 72h post infection, cells were selected for stable expression of the corresponding plasmids through GFP sorting. Doxycycline inducible constructs were sorted for DsRed induced population 24 to 48h post doxycycline treatment at 1 μg/mL.

Site-directed Mutagenesis

The different point mutations and deletions in the *VCP* sequence were obtained using a QuikChange XL Site-directed Mutagenesis kit (Stratagene). The sequence of primers used for these mutagenesis reactions are listed below.

Target	Mutant	Primer	Sequence
VCP	A530T	Forward	GGAAAACTTTGTTGGCCAAAACCATTGCTAATGAATGCCAG
		Reverse	CTGGCATTCATTAGCAATGGTTTTGGCCAACAAAGTTTTCC
VCP	NES	Forward	TACCGAGCTCGGATCTCACGTGGGCCCGCGGATGTTGCTCGAACTCCTGGAAGATCTCGATCTTGGAGTGCAGGTGGAAACCATCTCCCCAGGAGACG
		Reverse	CGTCTCCTGGGGAGATGGTTTCCACCTGCACTCCAAGATCGAGATCTTCCAGGAGTTCGAGCAACATCCGCGGGCCCACGTGAGATCCGAGCTCGGTA

Growth Measurement

To assess growth, cells were plated in 384-well or 96-well cell-culture coated white plates for cell lines and patient samples respectively. Ten and six concentrations of each chemical were tested respectively for AML cell lines and primary patient samples. ATP content was then measured using CellTiter-Glo (Promega) per the manufacturer's instructions. Briefly, CellTiter-Glo reagent was added to each well and incubated at room temperature for 10 minutes prior to luminescence reading at the indicated time points. PRISM GraphPad software was used for statistical analysis.

Western Blotting

Cells were lysed in Cell Signaling Lysis Buffer (Cell Signaling Technology), EDTA-free Protease Inhibitor Cocktail tablets (Roche Diagnostics), and PhosSTOP

Phosphatase Inhibitor (Roche Diagnostics), resolved by gel electrophoresis using Novex 4%–12% Bis-Tris or 3-8% Tris-acetate gels (Invitrogen), transferred to nitrocellulose membranes (Bio-Rad), and blocked for 1 hour in 5% BSA (Sigma-Aldrich). Blots were incubated with primary antibodies, followed by secondary antibodies. Bound antibody was detected using Western Lightning Chemiluminescence Reagent (Perkin Elmer). Nuclear/cytoplasmic extraction was performed using a Biovision kit per the manufacturer's protocol.

Mass Spectrometry and Proteomics Analysis

Cellular preparation and immune-precipitation: MV4-11 cells were first infected with either pRetroX-pTUNER-Empty (control) or pRetroX-pTUNER-VCP-WT-V5, allowing immunoprecipitation of a V5-tagged form of VCP. Cells were then lysed using 150 mM NaCl, 50 mM Tris pH 7.5, 1% IGPAL-CA-630 (Sigma) and EDTA-free Protease Inhibitor Cocktail tablets and PhosSTOP Phosphatase Inhibitor (Roche Diagnostics). 1.5 mg of input protein lysates were then incubated for 12-18 hours with anti-V5-tag magnetic beads (MBL) or sepharose beads (Life Technologies) pre-incubated with the indicated antibodies (normal mouse or rabbit IgG from Santa Cruz were used as controls). Two washes using 150 mM NaCl, 50 mM Tris pH 7.5, 0.05% IGPAL-CA-630 buffer were followed by 2 washes using 150 mM NaCl, 50 mM Tris pH 7.5 buffer.

On-bead digest: Beads from immunopurification were washed once with IP lysis buffer, then 3 times with PBS, and the 3 different lysates of each replicate were resuspended in 90 µL digestion buffer (2 M Urea, 50 mM Tris HCl), 2 µg of sequencing grade trypsin added, 1 hour shaking at 700rpm. Supernatant was removed and placed

in a fresh tube. Beads were then washed twice with 50 µL digestion buffer and combined with the supernatant. The combined supernatants were reduced (2 µL 500 mM DTT, 30 minutes, RT), alkylated (4 uL 500 mM IAA, 45 minutes, dark) and a longer overnight digestion performed: 2 µg (4 µL) trypsin, shake o/n, the samples were then quenched with 20 µL 10% FA and desalted on 10 mg Oasis cartridges.

TMT6 labeling of peptides and basic reversed phase (brp) fractionation: Desalted peptides were labeled with TMT6 reagents. Peptides were dissolved in 25 µL of fresh 100 mM HEPES buffer. The labeling reagent was resuspended in 42 µl of acetonitrile and 10 µl added to each sample as described below. After 1 h incubation the reaction was stopped with 8 µL of 5 mM hydroxylamine. Differentially labeled peptides were mixed and subsequently fractionated on StAGE tips as previously described (*77*). BRP fractionation of the differentially labelled was performed and combined. Samples were dried down and resuspended in 3% acetonitrile (ACN), 5% formic acid, loaded onto the cartridge washed twice with 1 mL of 3% ACN in 5 mM ammonium formate pH10- save as fraction 0. Step-wise elution as follows:

Fraction 1 (Collect)- Elute samples with 10% ACN in 5 mM ammonium formate 300 µL. Fraction 2 (Collect)- Elute samples with 15% ACN in 5 mM ammonium formate 300 µL. Fraction 3 (Collect)- Elute samples with 20% ACN in 5 mM ammonium formate 300 µL. Fraction 4 (Collect)- Elute samples with 30% ACN in 5 mM ammonium formate 300 µL. Fraction 5 (Collect)- Elute samples with 40% ACN in 5 mM ammonium formate 300 µL. Fraction 6 (Collect)- Elute samples with 50% ACN in 5 mM ammonium formate 300 µL. Empore SDB disk used to make StageTips as described in the paper (*77*).

Mass Spectrometry analysis: Reconstituted peptides were separated on an online nanoflow EASY-nLC 1000 UHPLC system (Thermo Fisher Scientific) and analyzed on a benchtop Orbitrap Q Exactive Plus mass spectrometer (Thermo Fisher Scientific). The peptide samples were injected onto a capillary column (Picofrit with 10 μm tip opening / 75 μm diameter, New Objective, PF360-75-10-N-5) packed in-house with 20 cm C18 silica material (1.9 μm ReproSil-Pur C18-AQ medium, Dr. Maisch GmbH, r119.aq). The UHPLC setup was connected with a custom-fit microadapting tee (360 μm, IDEX Health & Science, UH-753), and capillary columns were heated to 50 °C in column heater sleeves (Phoenix-ST) to reduce backpressure during UHPLC separation. Injected peptides were separated at a flow rate of 200 nL/min with a linear 80 min gradient from 100% solvent A (3% acetonitrile, 0.1% formic acid) to 30% solvent B (90% acetonitrile, 0.1% formic acid), followed by a linear 6 min gradient from 30% solvent B to 90% solvent B. Each sample was run for 120 min, including sample loading and column equilibration times. The Q Exactive instrument was operated in the data-dependent mode acquiring HCD MS/MS scans (R=17,500) after each MS1 scan (R=70,000) on the 12 top most abundant ions using an MS1 ion target of $3x\ 10^6$ ions and an MS2 target of $5x10^4$ ions. Isolation width of 0.7. The maximum ion time utilized for the MS/MS scans was 120 ms; the HCD-normalized collision energy was set to 31; the dynamic exclusion time was set to 20s, and the peptide match and isotope exclusion functions were enabled.

Quantification, identification of peptides and proteins and data analysis: All mass spectra were processed using the Spectrum Mill software package v6.0 pre-release (Agilent Technologies) which includes modules developed by us for TMT -based

quantification. Precursor ion quantification was done using extracted ion chromatograms (XIC's) for each precursor ion. The peak area for the XIC of each precursor ion subjected to MS/MS was calculated automatically by the Spectrum Mill software in the intervening high-resolution MS1 scans of the LC-MS/MS runs using narrow windows around each individual member of the isotope cluster. Peak widths in both the time and *m*/*z* domains were dynamically determined based on MS scan resolution, precursor charge and *m*/*z*, subject to quality metrics on the relative distribution of the peaks in the isotope cluster vs theoretical. Similar MS/MS spectra acquired on the same precursor m/z in the same dissociation mode within +/- 60 sec were merged. MS/MS spectra with precursor charge >7 and poor quality MS/MS spectra, which failed the quality filter by not having a sequence tag length > 1 (i.e., minimum of 3 masses separated by the in-chain mass of an amino acid) were excluded from searching.

For peptide identification MS/MS spectra were searched against human Uniprot database to which a set of common laboratory contaminant proteins was appended. Search parameters included: ESI-QEXACTIVE-HCD scoring parameters, trypsin enzyme specificity with a maximum of two missed cleavages, 40% minimum matched peak intensity, +/- 20 ppm precursor mass tolerance, +/- 20 ppm product mass tolerance, and carbamidomethylation of cysteines and iTRAQ labeling of lysines and peptide n-termini as fixed modifications. Allowed variable modifications were oxidation of methionine, N-terminal acetylation, Pyroglutamic acid (N-termQ), Deamidated (N), Pyro Carbamidomethyl Cys (N-termC), with a precursor MH+ shift range of -18 to 64 Da. Identities interpreted for individual spectra were automatically designated as valid by optimizing score and delta rank1-rank2 score thresholds

separately for each precursor charge state in each LC-MS/MS while allowing a maximum target-decoy-based false-discovery rate (FDR) of 1.0% at the spectrum stage.

In calculating scores at the protein stage and reporting the identified proteins, redundancy is addressed in the following manner: the protein score is the sum of the scores of distinct peptides. A distinct peptide is the single highest scoring instance of a peptide detected through an MS/MS spectrum. MS/MS spectra for a particular peptide may have been recorded multiple times, (i.e. as different precursor charge states, isolated from adjacent brp fractions, modified by oxidation of Met) but are still counted as a single distinct peptide. When a peptide sequence >8 residues long is contained in multiple protein entries in the sequence database, the proteins are grouped together and the highest scoring one and its accession number are reported. In some cases when the protein sequences are grouped in this manner there are distinct peptides which uniquely represent a lower scoring member of the group (isoforms or family members). Each of these instances spawns a subgroup and multiple subgroups are reported and counted towards the total number of proteins. TMT6 ratios (protein enrichment between channels) were obtained from the protein-comparisons export table in Spectrum Mill.

Before final analyses non human proteins and proteins with less than two unique peptides identified were removed and the data were median normalized. Resulting data were analysed and visualized using R (http://www.R-project.org). First, statistical analyses were performed via moderated t-test from R package limma (*78*) to estimate P-values for each gene/protein, next the false discovery rate corrections (FDR) were applied to account for multiple hypothesis testing. Plots were created using *ggplot2 (79)* and in-house R scripts. The gene networks were created using InWeb - Genets

(http://apps.broadinstitute.org/genets). The C2 tier of pathways from Molecular Signatures Database (*80*) was chosen to perform pathways analysis enrichment in R. The statistical significance of pathway enrichment was based on hypergeometric distribution further corrected by applying FDR.

To compare our MV4-11 VCP interactome with the previously reported HEK-293T cells interactome (*26*), we extracted the union of the lists of interacting proteins detected after stable overexpression of N or C terminal HA or Flag tagged VCP in HEK-293T cells. This list was first compared to the full list of detected proteins in our mass spectrometry experiment before filtering for high confidence interacting proteins. We then filtered the HEK-293T cells mass-spectrometry data to highlight the high confidence VCP candidate interacting proteins as previously reported (NWD-score ≥ 0.98, Z-score ≥ 4, and average assembled peptide spectral matches (APSMs) ≥ 2) (*26*). This filtered list was compared to our high-confidence VCP interacting proteins in the MV4-11 cell line applying the following significance thresholds: log2FC>0.5 and P-value<0.05.

Enrichr overlapping analysis across the KEGG_2019, Reactome_2016, Bioplanet_2019 and Elsevier_Pathways gene-sets was performed on the 80 “MV4-11 only” or on the 26 “HEK-293T only” VCP-interacting proteins (*81*, *82*). Results were ranked by enrichment combined scores and the top-scoring pathways were plotted as bar graphs. Pathways with an adjusted p-value > 0.05 were excluded.

Proteasome Activity Quantitative Assays

Cells were treated for 24 hours with 0.4 μM of NMS-873. Bortezomib (10 nM), MG132 (1 μM), epoxomycin (100 nM) or Tlck (100 μM) were used as positive controls. Then, the cells were collected, washed, and lysed for 30 min at 4°C in an ATP-containing lysis buffer (50 mM HEPES pH 7.8, 5 mM ATP, 0.5 mM DTT, 5 mM MgCl2 and 0.2 % Triton X-100). Cell lysates were cleared at 16,000 ×g for 15 min at 4°C. Normalized protein lysates (10 μg/well) were incubated in a 96-well plate with 0.1 mM of either Z-Leu- Leu-Glu-AMC, Suc-Leu-Leu-Val-Tyr-AMC or Ac-Arg-Leu-Arg-AMC to measure caspase-, chymotrypsin- and trypsin-like activities, respectively (Enzo). Proteasome activities were measured by following emission at 460 nm (excitation at 390 nm). Each experiment was performed in quadruplicate. PRISM GraphPad software was used for statistical analysis.

Flow cytometry

Cell surface marker staining was performed as follows. Cell lines were washed in PBS-0.1% BSA-2 mM EDTA before a 35-minute incubation with cell surface marker antibodies. Murine peripheral blood, bone marrow and spleen were collected from each organ, washed with PBS-0.1% BSA-2 mM EDTA and lysed for 10 minutes with red blood cell lysis buffer (Sigma). After two washing steps with PBS-0.1% BSA-2 mM EDTA, bone marrow cells were stained for 30 minutes at 4°C with corresponding cell surface antibodies. Cells were then washed twice with PBS-0.1%BSA-2 mM EDTA before analysis of 10,000 cells for each condition with BD FACSCanto II (BD Biosciences).

Intracellular protein staining for p-ATM and γH2AX was performed as previously described (*83*).

Annexin V / PI staining was performed using the Annexin V apoptosis detection kit per the manufacturer's protocol (Affymetrix, eBioscience). Cells were immediately analyzed on BD FACScanto II (BD Biosciences).

A list of antibodies used for western blotting, immunoflourescence and flow cytometry is provided below.

Targets	**Conjugate**	**References**	**Manufacturer**
ACTIN	No	MS-1295-P	Neomarkers
Anti-Mouse HRP	HRP	NA9310V	Amersham
Anti-Rabbit HRP	HRP	NA9340V	Amersham
Anti-Rat HRP	HRP	7077S	Cell Signaling Technology
ATF-4	No	11815S	Cell Signaling Technology
ATM	No	2873S	Cell Signaling Technology
BRCA1	No	9010S	Cell Signaling Technology
BrDU	No	RPN202	GE healthcare
CD4	APC	17-0042-83	Affymetrix
CD45	APC	17-9459-42	Invitrogen
CD45	PE-Cy7	130-113-119	Miltenyi Biotec
CD11b	FITC	IM0530U	Beckman Coulter
CD33	PE-Cy7	25-0338-42	ThermoFisher
CD14	PE	12-0149-42	ThermoFisher
Donkey anti-Mouse	AF568	A10037	Life Technologies
Donkey anti-Rabbit	AF568	A10042	Life Technologies
γH2AX	AF647	05636AF647	ThermoFisher
γH2AX	No	9718P	Cell Signaling Technology
Goat anti-Mouse	AF647	A21236	Life Technologies
GRP-78	No	3183	Cell Signaling Technology
HSP60	No	sc-1722	Santa Cruz
KAP1	No	A300-274A	Bethyl
LAMIN B1	No	12586S	Cell Signaling Technology
pATM (S1981)	No	5883P	Cell Signaling Technology
pATM (S1981)	PE	651204	BioLegend
pBRCA1(S1524)	No	9009S	Cell Signaling Technology
pKAP1 (S824)	No	A-300-767A	Bethyl
UBIQUITIN	No	sc-8017	Santa Cruz

pSMC1(S957)	No	A304-147A	Bethyl
SMC1	No	A300-055A	Bethyl
TUBULIN A	No	T6199	Sigma Aldrich
V5	No	R960-25	Invitrogen
VCP	No	2648S	Cell Signaling Technology
VCP	No	Ab11433	Abcam
VINCULIN	No	Ab18058	Abcam
XBP-1 spliced	No	647502	BioLegend

HR and NHEJ Reporter Assays

RG37-DR-GFP (*84*) and GC92-NHEJ-CD4 (*85*) cells were transiently transfected with I-SceI endonuclease and then treated with 0.4 µM NMS-873, 5 µM KU-55933, or 2.5 µM KU-57788. 48 hours post transfection, HR (GFP) and NHEJ (CD4) activities were measured by flow cytometry on BC FACScanto II (BD Biosciences). PRISM GraphPad software was used for statistical analysis.

Methylcellulose colony formation assay

Five thousand primary patient cells were plated in triplicate into semisolid methylcellulose medium (MethoCult H4236, StemCell Technologies) supplemented with 20 ng/ml IL-3 (Peprotech), 20 ng/ml IL-6 (Peprotech), 20 ng/ml GM-CSF (Peprotech), and 100 ng/ml SCF (Peprotech). After at least 10 days, the colony number was evaluated after MTT staining of the colonies (R&D Systems). For irradiation sensitivity evaluation, 250 to 500 cells were seeded in methylcellulose-based medium (ClonaCell-TCS Medium) with NMS-873 and irradiated at the indicated dose after 24H of NMS-873 pre-treatment. Colony number was evaluated after 4 days. PRISM GraphPad software was used for statistical analysis.

Drug interaction analysis

Estimation of the dose-inhibitory fraction relationship for the combination of NMS-873 or CB-5339 and doxorubicin was based on a dose–effect strategy: the Chou–Talalay combination index (CI) for Loewe additivity, based on the Chou-Talalay Median Effect model (*86, 87*) as implemented in CalcuSyn v2.11 (http://www.biosoft.com/w/calcusyn.htm). If CI < 1, the drugs have a synergistic effect, and if CI > 1, the drugs have an antagonistic effect. CI = 1 means the drugs have additive effect.

CCLE mRNA expression analysis

VCP mRNA expression (TPM= Transcripts per Million) was obtained from the publicly available Cancer Cell Line Encyclopedia (CCLE) database (https://depmap.org/portal/download/) (*31, 32*). A linear regression analysis of IC50 distribution of a panel of 91 cancer cell lines or 12 AML cell lines treated with CB-5339 and VCP mRNA expression was then performed. R-square coefficient and associated P-value were calculated.

CCLE mutations analysis

KRAS, NRAS and *TP53* detailed mutational profiles of AML cell lines were extracted from the CCLE (Cancer Cell Line Encyclopedia) database (*31, 32*) mutation data version 18Q4 (depmap_18Q4_mutation_calls.csv), publicly available from the Depmap portal (https://depmap.org/portal/download/).

TCGA pan-cancer analysis

The pan-cancer TCGA database accounting for 10,294 patient samples across 33 tumor lineages (https://cancergenome.nih.gov/publications; (*33*)) was interrogated to identify the frequency of co-occurrence of *TP53* and *RAS* non-silent mutations across tumor types. In addition, the co-occurrence of *RAS* activation and *TP53* depletion across the pan-cancer TCGA cohorts was computed based on functional classifiers as previously described (*34, 35*).

SUPPLEMENTARY FIGURES

Figure S1

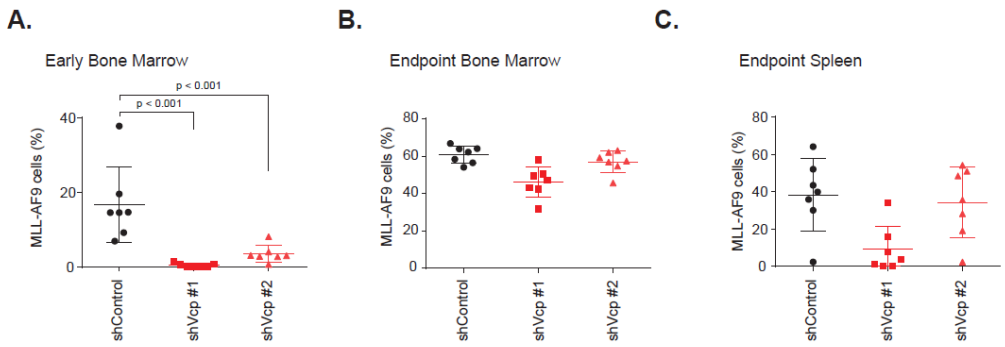

Figure S1. MLL-AF9 AML disease burden evolution after VCP knock-down.

(A-C) Percentage of MLL-AF9 cells in mice bone marrow 14 days post-injection **(A)** of MLL-AF9 cells expressing either shControl, sh*Vcp*#1 or sh*Vcp*#2, and in bone marrow **(B)** and spleen **(C)** at time of death (n=7 mice per condition). Statistical significance determined using Mann-Whitney test in comparison with the shControl condition. Error bars represent mean ± SEM.

Figure S2

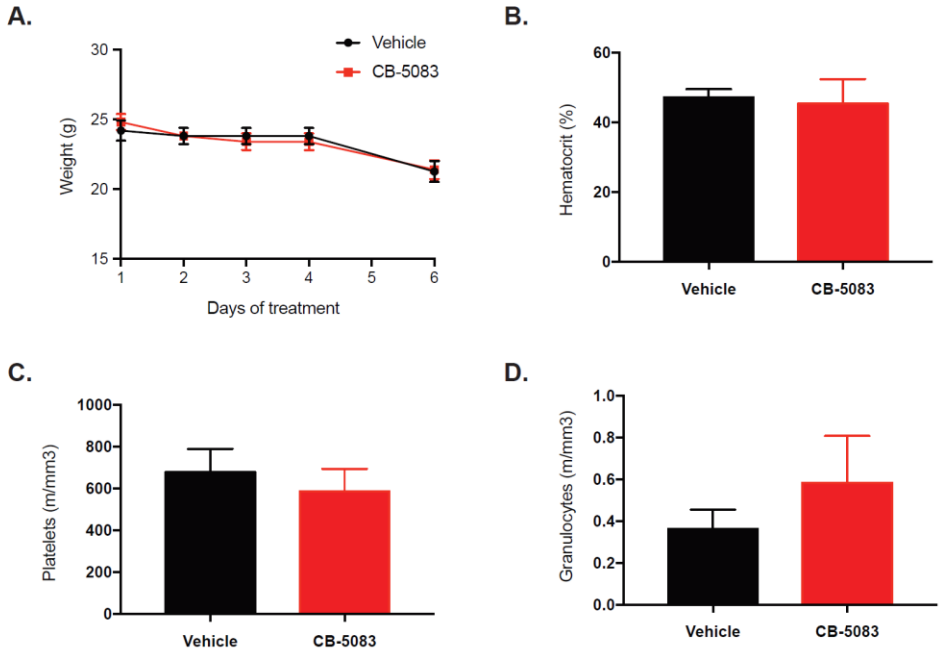

Figure S2. CB-5083 tolerability profile.

(A) Weight was measured starting from day 1 of CB-5083 treatment at 50 mg/kg and until vehicle mice death, in C57/BL6 mice injected with MLL-AF9 cells (n=5 mice per condition).

(B-D) Complete blood counts were measured at day 5 of treatment with CB-5083 at 50 mg/kg in C57/BL6 mice (n=4 mice per condition).

Figure S3

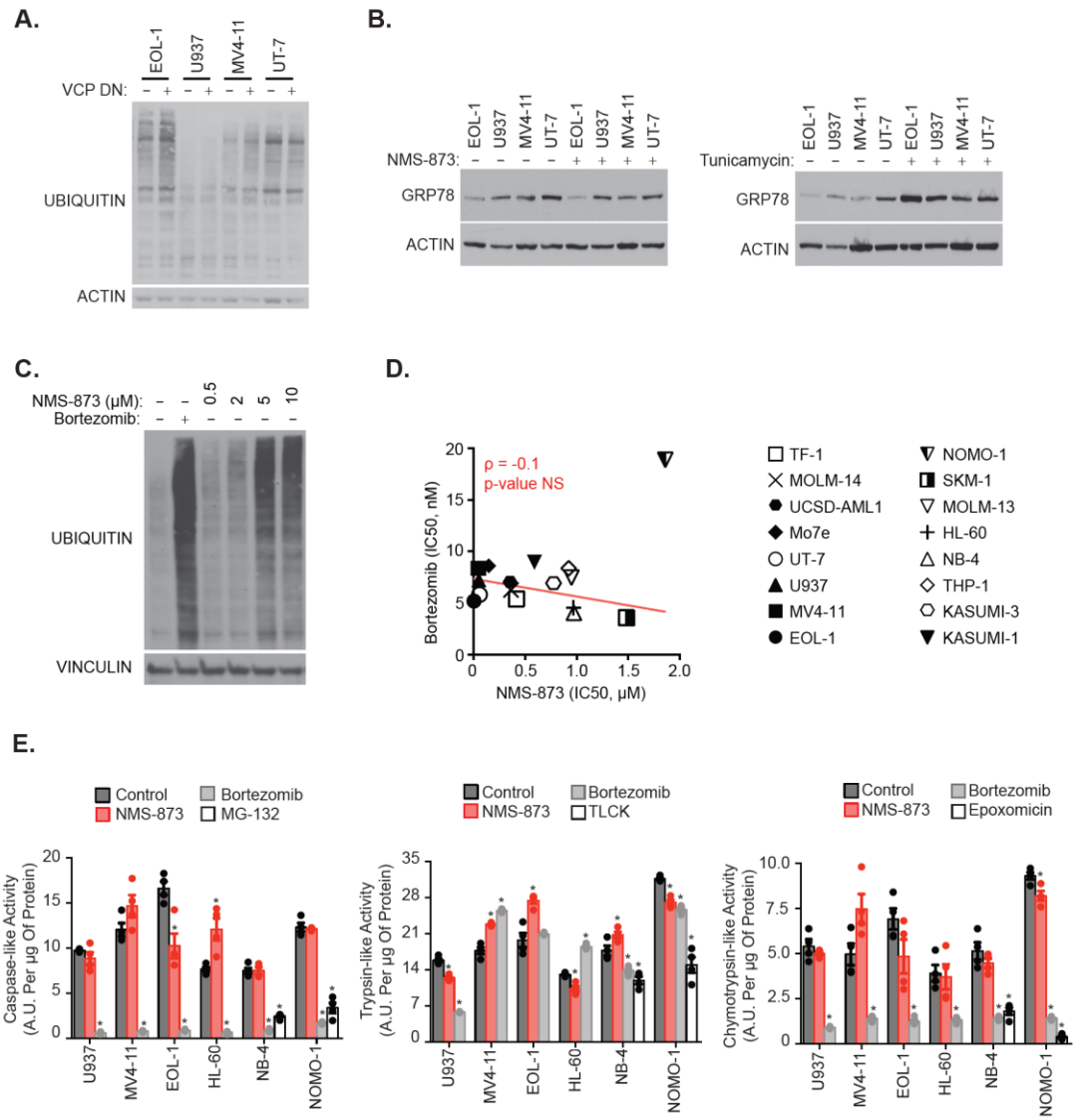

Figure S3. VCP inhibition does not primarily impair AML cell growth through induction of proteotoxic/ER stress.

(A) Western blot for ubiquitin and actin (loading control) from the indicated AML cell lines overexpressing VCP DN construct.

(B) Western blot for GRP78 and actin (loading control) from the indicated AML cell lines treated with 0.4 μM NMS-873 for 24 hours. Tunicamycin 1 μg/mL was used as positive control.

(C) Western blot for ubiquitin and vinculin (loading control) in MV4-11 AML cell line treated with the indicated dose of NMS-873 or 10 nM bortezomib for 24 hours.

(D) Linear regression analysis of IC_{50} distribution of a panel of 16 AML cell lines treated with NMS-873 or bortezomib for four days (4 replicates for each condition). Non-parametric Spearman correlation coefficient (ρ) and associated P-value are calculated. NS=Not Significant.

(E) Caspase-, trypsin- and chymotrypsin-like proteasome activities from the indicated cell lines treated with 0.4 μM NMS-873 for 24 hours. Data are represented as mean of four replicates +/- SEM. Bortezomib is used as a positive control for all cell lines and MG-132, TLCK and epoxomicin are used as positive controls in NB-4 and NOMO-1.

Figure S4

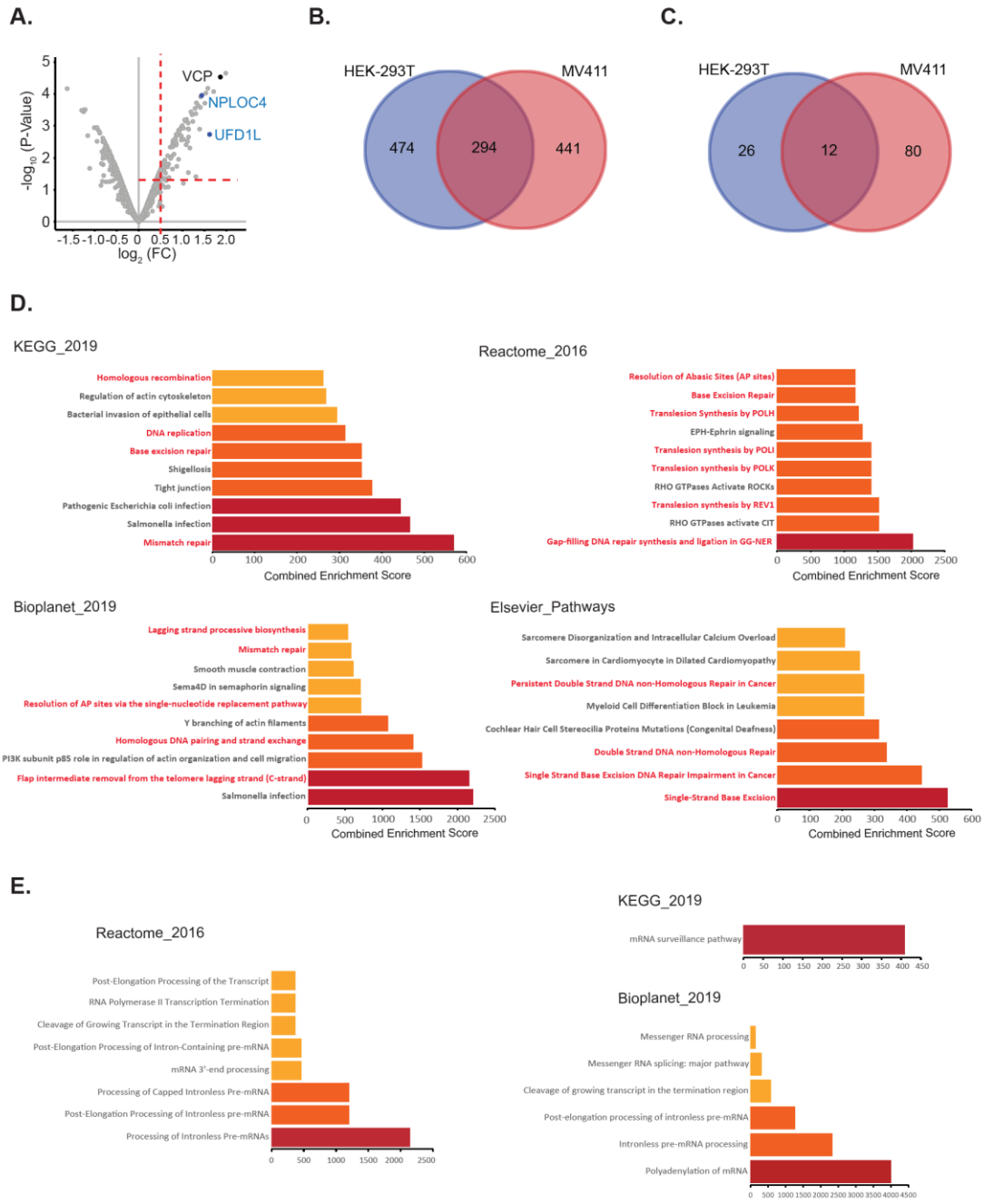

Figure S4. Comparative proteomic analysis identifies VCP-interacting proteins in an AML context.

(A) VCP-interacting proteins identified by mass spectrometry-based interactome analysis from MV4-11 cells stably expressing a V5-tagged wild-type VCP construct (Gray dots). Data are presented as a volcano plot of –log10 (P-value) versus average log2FC of two biological replicates. Black dot and blue dots represent VCP itself and

two known critical VCP-interacting partners, UFD1L and NPLOC4, respectively. log2FC>0.5 and P-value<0.05 are defined as thresholds for significance.

(B,C) Venn diagrams of VCP-interacting proteins in the MV4-11 AML cell line compared to the HEK-293T cell line, including either all mass-spectrometry detected proteins **(B)** or restricted to high confidence interacting proteins in each cellular context **(C)**.

(D) Enrichr overlapping analysis of high confidence AML context VCP interacting proteins. Bar graphs represent the top-ranked overlapping pathways among each gene sets database. Results are presented as combined enrichment scores. DNA repair and replication pathways are highlighted in red.

(E) Enrichr overlapping analysis of high confidence HEK-293T context VCP interacting proteins. Bar graphs represent the top-ranked overlapping pathways among each gene sets database. Results are presented as combined enrichment scores.

Figure S5

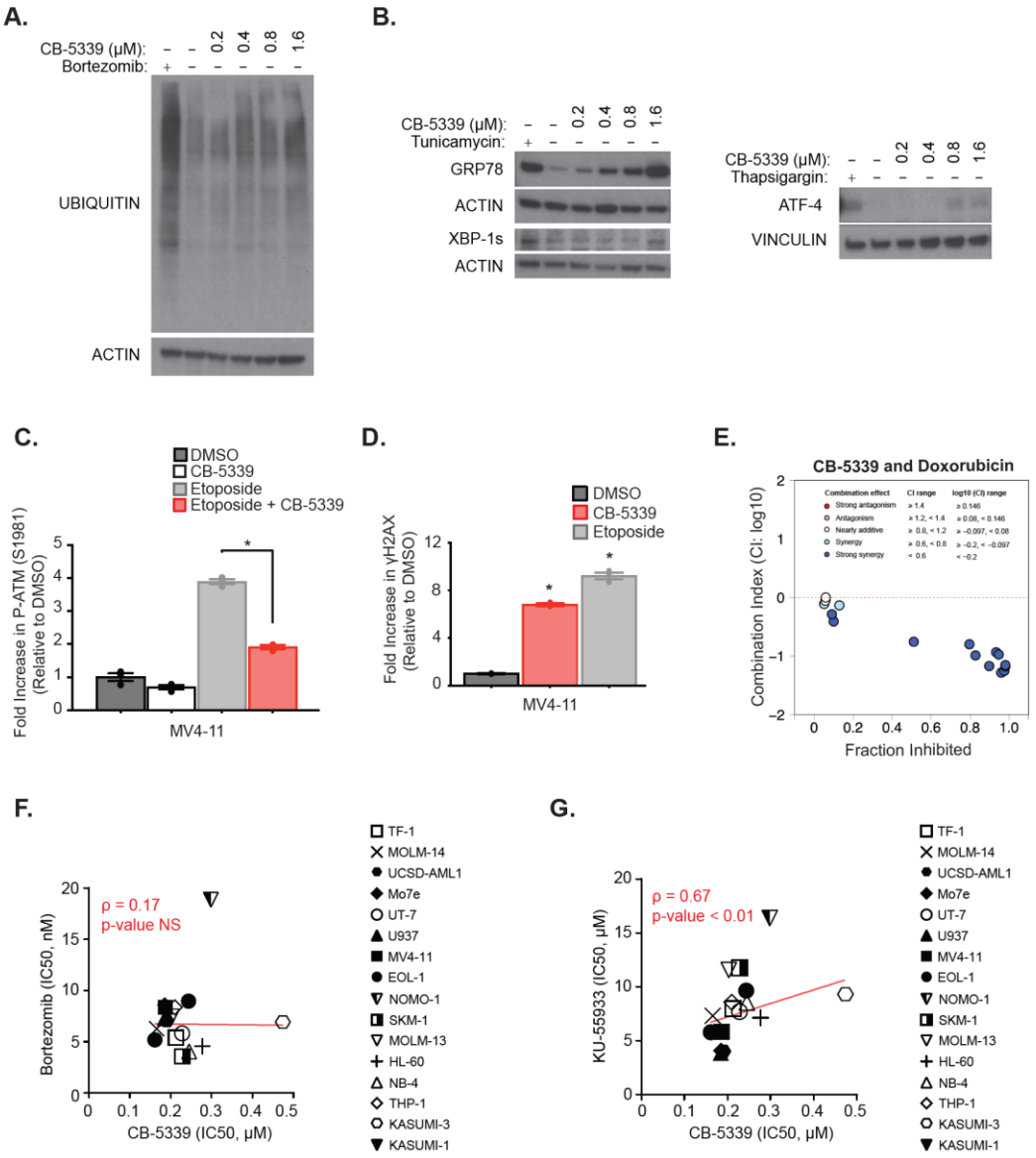

Figure S5. CB-5339 impairs DNA repair and induces proteotoxic stress in AML.

(A) Western blot for ubiquitin and actin (loading control) in MV4-11 AML cell line treated with the indicated concentration of CB-5339 or 10 nM bortezomib for 24 hours. **(B)** Western blot for GRP78, spliced XBP1, ATF4 and actin or vinculin (loading control) from the MV4-11 AML cell line treated with the indicated concentration of CB-5339 for 48 hours. Tunicamycin 1 μg/mL and thapsigargin 1 μM were used as positive controls.

(C) FACS analysis of the intracellular expression of P-ATM (S1981) in the MV4-11 AML cell line treated with CB-5339 for two hours**.** Etoposide treatment was used to induce DNA damage in order to evaluate the DNA repair signaling response under VCP impairment. Error bars represent mean of three replicates ± SEM. 10,000 cellular events were measured for each replicate condition. P-value calculated using Welch's t-test in comparison with etoposide condition. * $p<0.0001$.

(D) FACS analysis of the intracellular expression of γH2AX in the MV4-11 AML cell line treated for 48 hours with 0.2 μM CB-5339**.** Etoposide treatment was used as a positive control. Error bars represent mean ± SEM of 3 replicates. 10,000 cellular events were measured for each replicate condition. P-value calculated using Welch's t-test in comparison with control condition. * $p<0.001$.

(E) Combination Index (CI) plot for the combination of CB-5339 with doxorubicin in MV4-11 cell line after six days of treatment. Doxorubicin treatment was added after 24 hours of CB-5339 pre-treatment. Results represent the average of four replicates for each dose combination.

(F) Linear regression analysis of the IC_{50} distribution of a panel of 16 AML cell lines treated with CB-5339 or bortezomib (4 replicates for each condition). Non-parametric Spearman correlation coefficient (ρ) and associated P-value are calculated. NS=Not Significant.

(G) Linear regression analysis of the IC_{50} distribution of a panel of 16 AML cell lines treated with CB-5339 or KU-55933 (4 replicates for each condition). Non-parametric Spearman correlation coefficient (ρ) and associated P-value are calculated. NS=Not Significant.

Figure S6

A.

Clearance (mL/min/kg)		
	CB-5083	**CB-5339**
Rat	64	34
Dog	38	20
Monkey	34	14
Human (projected)	24.8	6.3

Bioavailability (%)		
	CB-5083	**CB-5339**
Rat	78	42
Dog	10	103
Monkey	22	46

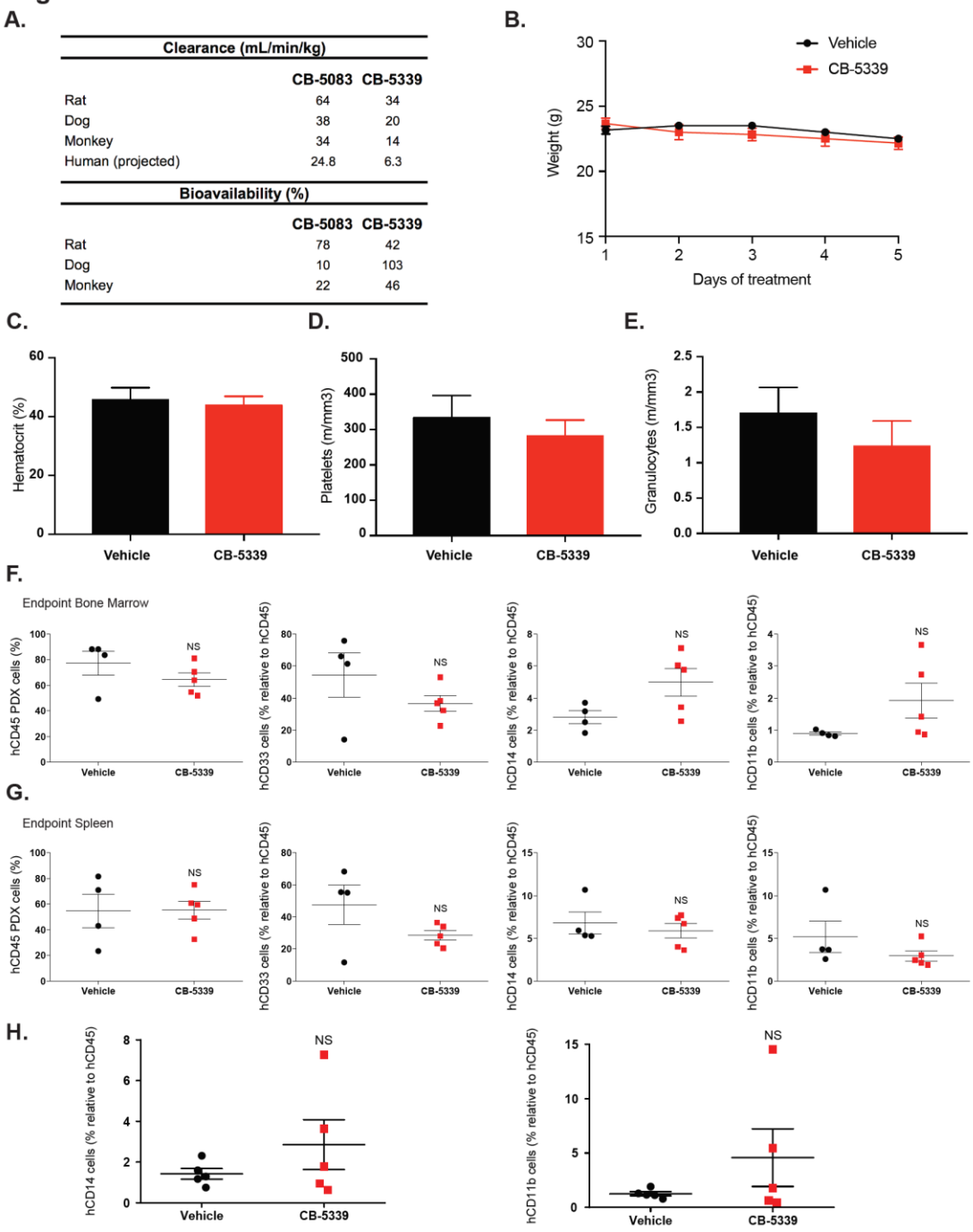

Figure S6. CB-5339 pharmacokinetic properties, tolerability profile and post-treatment relapse characteristics.

(A) CB-5339 clearance and bioavailability compared to CB-5083 across different species.

(B) Weight was measured starting from day 1 of CB-5339 treatment at 90 mg/kg in C57/BL6 mice injected with MLL-AF9 cells (n=6 mice per condition).

(C-E) Complete blood counts were measured at day 5 of treatment with CB-5339 at 90 mg/kg in C57/BL6 mice injected with MLL-AF9 cells (n=6 mice per condition).

(F,G) Percentage of hCD45+, hCD33+, hCD11b+ and hCD14+ leukemic cells in mice bone marrow **(F)** and spleen **(G)**, at time of death post-injection of patient derived primary AML cells (n=4 to 5 mice per condition). CB-5339 treatment was started 10 days post-injection, after engraftment validation. Mann-Whitney test in comparison with vehicle. Error bars represent mean ± SEM.

(H) Percentage of hCD11b+ and hCD14+ leukemic cells in mice bone marrow, 21 days post-injection of patient-derived primary AML cells (n=5 mice per condition). CB-5339 treatment was started 10 days post-injection, after engraftment validation. Mann-Whitney test in comparison with vehicle. Error bars represent mean ± SEM.

SUPPLEMENTARY TABLES

Table S1. List of the top depleted genes identified by the *in vivo* shRNA screening. Gene Normalized Enrichment Scores (NES) and adjusted P-values were calculated using EdgeR/RIGER methods.

Gene rank	Gene	NES	- $\log_{10}$(P value)
1	*Fkbp8*	0.02559	2.769551079
2	*Slc5a1*	0.04327	2.167491087
3	*Mdh2*	0.04838	2.080921908
4	*Rictor*	0.05257	2.022276395
5	*Nbr1*	0.05908	1.931814138
6	*S1pr1*	0.06327	1.866461092
7	*Ptgs2*	0.0649	1.853871964
8	*Rps6kb2*	0.07048	1.769551079
9	*Uvrag*	0.09188	1.554395797
10	*Eef2k*	0.09281	1.55129368
11	*Nos2*	0.09514	1.53165267
12	*Klhl20*	0.1093	1.415668776
13	*Dram1*	0.1096	1.412289035
14	*Fam176a*	0.1112	1.404503778
15	*Aco2*	0.1193	1.348721986
16	*Eno1*	0.1254	1.304518324
17	*Txn1*	0.1282	1.289036881
18	*Gabarap*	0.1291	1.281498311
19	*Tecpr1*	0.1307	1.269217724
20	*2310035C23Rik*	0.1326	1.258848401
21	*Unc45a*	0.1454	1.1837587
22	*Ldha*	0.1489	1.162411562
23	*Nupr1*	0.151	1.282329497
24	*Tlr2*	0.157	1.11577123
25	***Vcp***	**0.1624**	**1.093664958**
26	*Tnfsf10*	0.1645	1.085656843
27	*Ctnnd1*	0.171	1.057000407
28	*Hspb6*	0.174	1.040958608
29	*Pck2*	0.1747	1.037157319
30	*Tlr7*	0.1768	1.029653124
31	*Skp2*	0.1833	1.006123085
32	*Dapk2*	0.1847	0.997833938
33	*Cul3*	0.1863	0.990974258
34	*Nek9*	0.187	0.989700043

Table S2. CB-5083 sensitivity profile across 131 cancer cell lines. Distribution of IC_{50} (concentrations of CB-5083 at which viability was reduced by 50%) in a panel of 131 cancer cell lines treated with CB-5083 in duplicate, for three days. Cell lines are classified by cancer subtype.

Cell line	IC50 (μM)	Cancer sub-type
MOLM-13	0.152	Myeloid Leukemia
ML-1	0.209	Myeloid Leukemia
MV-4-11	0.215	Myeloid Leukemia
HEL 92.1.7	0.220	Myeloid Leukemia
HL-60	0.276	Myeloid Leukemia
K-562	0.224	Myeloid Leukemia
Ramos (RA 1)	0.186	Burkitt's lymphoma
Daudi	0.230	Burkitt's lymphoma
Raji	0.271	Burkitt's lymphoma
AMO1	0.069	Multiple Myeloma
LP-1	0.115	Multiple Myeloma
L-363	0.238	Multiple Myeloma
RPMI8226	0.261	Multiple Myeloma
OPM-2	0.342	Multiple Myeloma
MM1S	0.392	Multiple Myeloma
U266B1	0.452	Multiple Myeloma
SU-DHL-2	0.244	B cell lymphoma
SU-DHL-6	0.250	B cell lymphoma
U-2932	0.311	B cell lymphoma
SJSA1	0.260	Bone
U-2 OS	0.328	Bone
MKN45	0.273	Stomach
NUGC-3	0.343	Stomach
MeWo	0.165	Skin
G-361	0.190	Skin
A101D	0.222	Skin
SK-MEL-5	0.253	Skin
HT-144	0.273	Skin
A375	0.291	Skin
RPMI-7951	0.303	Skin
A2058	0.311	Skin
C32	0.357	Skin
Malme-3M	0.362	Skin
COLO 679	0.367	Skin
SK-MEL-1	0.368	Skin
COLO 829	0.370	Skin
CHL-1	0.566	Skin
Caki-2	0.241	Kidney

A-498	0.338	Kidney
BICR 18	0.234	Upper aerodigestive tract
Detroit 562	0.316	Upper aerodigestive tract
BICR 16	0.327	Upper aerodigestive tract
CAL27	0.340	Upper aerodigestive tract
BICR 31	0.344	Upper aerodigestive tract
PE/CA-PJ34 (clone C12)	0.416	Upper aerodigestive tract
A-253	0.452	Upper aerodigestive tract
FaDu	0.458	Upper aerodigestive tract
PE/CA-PJ41 (clone D2)	0.496	Upper aerodigestive tract
HEC-1-A	0.326	Uterus
SK-UT-1	0.465	Uterus
HCT116	0.158	Colon
C2BBe1	0.225	Colon
H716	0.252	Colon
GP2D	0.287	Colon
LS 174T	0.309	Colon
LoVo	0.344	Colon
SW620	0.369	Colon
DLD1	0.387	Colon
HCT-15	0.424	Colon
HT55	0.441	Colon
HT-29	0.461	Colon
SW948	0.467	Colon
LS1034	0.474	Colon
SW480	0.479	Colon
SNU-C1	0.567	Colon
SK-CO-1	0.617	Colon
LS513	0.684	Colon
H1838	0.133	Lung
H2347	0.153	Lung
H2291	0.161	Lung
H2030	0.185	Lung
H226	0.188	Lung
H2122	0.191	Lung
Calu-1	0.228	Lung
H1792	0.275	Lung
Calu-6	0.277	Lung
H1975	0.287	Lung
H2171	0.304	Lung
H2087	0.305	Lung
LC-2/ad	0.319	Lung
H838	0.319	Lung
MSTO-211H	0.319	Lung

H526	0.322	Lung
H2023	0.338	Lung
H1355	0.340	Lung
H1703	0.347	Lung
A549	0.353	Lung
H510A	0.363	Lung
H358	0.385	Lung
H1944	0.393	Lung
H2126	0.393	Lung
H441	0.395	Lung
H446	0.402	Lung
COLO 668	0.416	Lung
ChaGo-K-1	0.425	Lung
H1650	0.425	Lung
COR-L23	0.443	Lung
HLF-a	0.444	Lung
H2228	0.446	Lung
H1793	0.460	Lung
H647	0.470	Lung
H460	0.483	Lung
H1299	0.494	Lung
H841	0.497	Lung
H1693	0.516	Lung
H209	0.520	Lung
H1836	0.614	Lung
H661	0.644	Lung
H28	0.652	Lung
H146	0.840	Lung
H2081	0.910	Lung
H1092	0.965	Lung
H1770	1.115	Lung
HepG2	0.317	Liver
SK-HEP-1	0.348	Liver
SNU-449	0.407	Liver
Hep 3B2.1-7	0.426	Liver
SNU-475	0.568	Liver
PLC/PRF/5	0.630	Liver
HCC1143	0.352	Breast
MDA-MB435	0.362	Breast
HCC1954	0.383	Breast
HCC70	0.563	Breast
HCC1187	0.572	Breast
HCC1937	0.619	Breast
SK-N-DZ	0.445	Neural Crest

SK-N-FI	0.535	Neural Crest
MIA PaCa	0.222	Pancreas
Capan-1	0.232	Pancreas
BxPC-3	0.276	Pancreas
QGP-1	3.040	Pancreas

Table S3. Patients characteristics. Cytogenetics, molecular and clinical characteristics of patient samples used in this study. n/a: data not available.

# ID	Age	Sex	Diagnosis	Disease Status	FLT3	NPM1	Cytogenetics	Colony formation	Viability	PDX	CB-5339 IC50 (µM)
1	88	M	Therapy related AML	new	FLT3-ITD	WT	n/a	no	yes	no	n/a
2	n/a	M	AML	n/a	n/a	n/a	n/a	no	yes	no	n/a
3	66	M	MDS RAEB-1	new	WT	WT	46, XY	no	yes	no	n/a
4	64	M	Secondary AML (prior CMML)	new	WT	WT	86-92, XXYY, -2 -5 +22 +3mar	no	yes	no	n/a
5	58	M	AML	new	FLT3-ITD	mutant	46, XY	no	yes	no	n/a
6	49	F	AML	new	FLT3-ITD	mutant	46, XX	no	yes	no	n/a
7	65	F	AML	relapsed	FLT3-ITD	WT	46, XX	no	yes	no	n/a
8	11	M	AML	new	FLT3-ITD	n/a	46, XY add(6)(q21), add(9)(p24)	no	yes	no	n/a
9	60	F	AML	relapsed	WT	n/a	47, XX, +13	no	yes	no	n/a
10	74	M	AML	relapsed	WT	mutant	46, XY, del(5q)	no	yes	no	n/a
11	26	M	AML	new	WT	WT	45, X, -Y, t(8;21)(q22;q22), idem, (12-5)	no	yes	no	n/a
12	68	M	AML	new	WT	WT	46, XY	no	yes	no	n/a
13	67	F	AML	primary refractory	N843K	WT	46, XX, del(7)(q22)	no	yes	no	n/a
14	53	M	APL	new	FLT3-ITD	WT	46, XY t(15;17)	no	yes	no	n/a
15	65	M	AML	relapsed	WT	WT	46, XY inv(16)	no	yes	no	n/a
16	n/a	n/a	AML	n/a	n/a	n/a	n/a	no	yes	no	n/a
17	66	M	Secondary AML (prior MDS)	new	WT	WT	47, XY, +8[47],idem, +1, der(1;13)(q10;q10)	yes	no	no	n/a
18	64	M	AML with MDS changes	new	WT	WT	complex karyotype	yes	no	no	n/a
19	81	F	Therapy related AML	new	WT	WT	complex karyotype	yes	no	no	n/a
20	70	M	AML	relapsed	WT	WT	complex karyotype (+8, t(9;11), 20q del, etc)	yes	no	no	n/a
21	83	F	Secondary AML (prior MDS)	new	WT	WT	46, XX	yes	no	no	n/a
22	59	F	Therapy related AML	new	N676T	WT	46,XX,t(9;11)(p22;q23)[3]/47,idem,+8[8]/ 50,idem,+6,+8,+9,der(9)(t(9;11) (p22;q23),+13[cp5]	no	no	yes	n/a
23	n/a	M	AML	new	WT	WT	41-46,XY,-Y,-1,del(3)(q21q26),+2, -5, -7, add(8)(q24), add(9)(q21), -10, -11, -12, -15, add(16)(p10), add(19)(q13.3), +1-4mar [cp20]	no	yes	no	208.00
24	n/a	F	AML	new	WT	WT	46,XX, del(7)(q22q36) [15]	no	yes	no	211.80
25	n/a	M	AML	new	FLT3-ITD	WT	46, XY	no	yes	no	219.50
26	55	M	AML	new	FLT3-ITD	WT	46, XY	no	yes	no	236.80
27	59	F	AML	relapsed	FLT3-ITD	mutant	n/a	no	yes	no	274.30
28	54	F	AML	new	FLT3-ITD	mutant	46, XX	no	yes	no	275.30
29	n/a	M	AML with MDS changes	primary refractory	V579A	WT	46, XY	no	yes	no	306.90
30	66	M	AML with MDS changes	new	WT	WT	46, XY, del(20)(q11.2q13.3) [20]	no	yes	no	362.20
31	79	M	AML	new	n/a	mutant	46, XY	no	yes	no	394.90
32	75	F	AML with MDS changes	new	FLT3-ITD	WT	47, XX, inv(16)(p11.2q21.2)c, +13 [6]/46XX, inv(16)(p11.2q21.2)c [14]	no	yes	no	412.50
33	39	M	AML	new	FLT3-ITD	mutant	46, XY	no	yes	no	485.00
34	75	M	AML	new	WT	WT	46, XY, t(9;11)(p22;q23), add(11)(q24) [5]/46 XY [5]	no	yes	no	500.10
35	n/a	M	AML	relapsed	WT	WT	45, XY, t(3;3)(q21q26), del(7)(p13), del(17)(p12), -21 [20]	no	yes	no	512.50
36	41	F	AML	new	FLT3-ITD	mutant	46, XX	no	yes	no	568.40
37	n/a	M	AML	new	WT	WT	44, XY, der(3)(t(3;11)(p21;q2), del(5)(q75q?34), del(6)(q2?), der(7)(t(6;7)(q12;p15), -11, der(17)(t(11;17)(p11.2;p11.2), -18 [11]/44, idem, -del(6)(q12), +i(6)(p10)[5]/44, idem, -Y, +i(Y)(q10), del(6)(q12), +i(6)(p10) [4]	no	yes	no	626.80
38	53	M	AML	primary refractory	WT	WT	46, XY, del(2)(p13p23), t(4;19)(q31q34), add(4)(q25), del(6)(q13q25), t(9;22)(q34;q11.2), del(10)(q24), add(16)(q24) [20]	no	yes	no	752.10

Table S4. List of VCP-interacting partners identified by mass spectrometry-based interactome analysis in the MV4-11 AML cell line. Results are presented as Log(FC) for each replicate relative to empty vector and rank ordered based on P-value. Nuclear localization is specified for each protein.

Gene name	Accession number	logFC rep1	logFC rep2	average logFC	p value	FDR	Nuclear localization
RPA1	P27694	2.104	1.869	1.9865	0.0000	0.0102	yes
VCP	P55072	1.771	1.957	1.864	0.0000	0.0102	yes
ARMCX3	Q9UH62	1.601	1.553	1.577	0.0001	0.0102	no
U2AF2	P26368	-1.52	-1.74	-1.632	0.0001	0.0102	yes
RPA3	P35244	1.908	1.512	1.71	0.0001	0.0102	yes
UBXN2B	Q14CS0	1.632	1.432	1.532	0.0001	0.0102	yes
NPLOC4	Q8TAT6-2	1.433	1.444	1.4385	0.0001	0.0102	yes
UBXN6	Q9BZV1	1.408	1.429	1.4185	0.0001	0.0102	yes
FKBP1A	P62942	1.411	1.418	1.4145	0.0001	0.0102	no
NSFL1C	Q9UNZ2	1.36	1.274	1.317	0.0002	0.0132	yes
TRAFD1	O14545	1.735	1.285	1.51	0.0002	0.0132	no
APEX1	P27695	1.505	1.208	1.3565	0.0002	0.0142	yes
RAE1	P78406	1.617	1.197	1.407	0.0003	0.0142	yes
MYO5A	F8W6H6	1.416	1.156	1.286	0.0003	0.0142	no
CSNK1A1	P48729-2	-1.15	-1.29	-1.22	0.0003	0.0142	yes
DBT	P11182	-1.13	-1.37	-1.25	0.0003	0.0142	no
RPS29	P62273	-1.13	-1.47	-1.302	0.0003	0.0142	no
EFCAB14	O75071	-1.1	-1.41	-1.255	0.0004	0.0142	no
UCHL5	Q5LJA5	1.11	1.275	1.1925	0.0004	0.0142	yes
FAM104A	Q969W3-2	1.516	1.088	1.302	0.0004	0.0155	no
ASPSCR1	Q9BZE9-2	1.383	1.055	1.219	0.0005	0.0159	yes
SNRPE	P62304	1.194	0.988	1.091	0.0006	0.0210	yes
NGLY1	Q96IV0	1.028	1.071	1.0495	0.0006	0.0210	no
UBXN2A	P68543	1.141	0.973	1.057	0.0007	0.0217	no
UBP1	Q9NZI7	1.493	0.977	1.235	0.0007	0.0217	yes
GMFG	O60234	1.326	0.932	1.129	0.0008	0.0233	no
MYL6	P60660	0.908	1.075	0.9915	0.0010	0.0257	no
MYL6	G3V1V0	0.903	1.089	0.996	0.0010	0.0257	no
PARP1	P09874	1.06	0.883	0.9715	0.0011	0.0257	yes
INPP5D	Q92835	-0.91	-0.99	-0.951	0.0011	0.0257	no
GRB2	P62993	-0.86	-1.16	-1.009	0.0011	0.0257	yes
SEC16A	O15027	-0.86	-1.16	-1.01	0.0011	0.0257	no
MYL9	P24844	1.19	0.853	1.0215	0.0012	0.0257	no
FAF2	Q96CS3	1.399	0.863	1.131	0.0012	0.0257	no
MIOS	Q9NXC5	1.026	0.863	0.9445	0.0013	0.0257	no

UNC45A	Q9H3U1	0.861	1.419	1.14	0.0013	0.0257	yes
RPA2	P15927	1.819	0.955	1.387	0.0013	0.0257	yes
CIT	O14578-4	-0.87	-0.99	-0.929	0.0013	0.0257	no
ARPC2	O15144	0.934	0.89	0.912	0.0014	0.0261	no
TNKS1BP1	Q9C0C2	-0.93	-0.86	-0.893	0.0015	0.0286	yes
VCPIP1	Q96JH7	1.036	0.808	0.922	0.0016	0.0286	no
MRPS12	O15235	-0.84	-0.94	-0.888	0.0016	0.0286	no
CIT	O14578-3	-0.82	-0.96	-0.888	0.0017	0.0286	no
PGAM1	P18669	0.792	1.025	0.9085	0.0017	0.0286	no
MYH11	P35749-2	0.99	0.797	0.8935	0.0018	0.0286	no
MYL6	P60660-2	0.822	0.916	0.869	0.0018	0.0286	no
UFD1L	Q92890-1	2.232	1.004	1.618	0.0019	0.0286	yes
PEO1	Q96RR1	0.94	0.802	0.871	0.0019	0.0286	no
GLUL	P15104	0.836	0.877	0.8565	0.0019	0.0286	no
TTN	Q8WZ42-12	1.094	0.759	0.9265	0.0020	0.0291	yes
DCD	P81605	-0.8	-1.53	-1.162	0.0020	0.0295	no
SAMHD1	Q9Y3Z3	1.198	0.749	0.9735	0.0021	0.0295	yes
UBA52	P62987	1.501	0.775	1.138	0.0022	0.0314	yes
RPL31	P62899	-0.79	-0.85	-0.818	0.0024	0.0328	no
MYH9	P35579	0.935	0.743	0.839	0.0024	0.0328	no
MYL12A	P19105	1.335	0.717	1.026	0.0026	0.0352	no
HMGB3	O15347	1.248	0.7	0.974	0.0028	0.0359	yes
LRRC59	Q96AG4	0.792	0.786	0.789	0.0028	0.0359	yes
RPS11	P62280	-0.72	-0.89	-0.806	0.0029	0.0359	no
LIG3	P49916	0.776	0.79	0.783	0.0029	0.0359	yes
HSPE1	P61604	-0.83	-0.75	-0.787	0.0029	0.0359	no
SYVN1	Q86TM6	0.72	1.506	1.113	0.0030	0.0360	no
FAU	P62861	-0.68	-1.22	-0.95	0.0030	0.0360	no
RPL34	P49207	-0.69	-0.95	-0.819	0.0031	0.0364	no
TMOD3	Q9NYL9	1.03	0.67	0.85	0.0032	0.0366	no
SRSF6	Q13247	-0.89	-0.69	-0.793	0.0032	0.0366	yes
APRT	P07741	0.702	0.855	0.7785	0.0033	0.0369	no
P4HB	P07237	-0.72	-0.8	-0.761	0.0035	0.0381	no
UBXN7	O94888	0.931	0.663	0.797	0.0036	0.0382	yes
GSN	P06396	1.079	0.641	0.86	0.0037	0.0382	no
ACTC1	P68032	0.914	0.659	0.7865	0.0037	0.0382	no
MYH14	Q7Z406	1.082	0.638	0.86	0.0038	0.0382	no
HSPA6	P17066	1.058	0.635	0.8465	0.0038	0.0382	no
TFEB	B0QYS7	0.654	0.903	0.7785	0.0039	0.0382	yes
TFE3	P19532	0.654	0.903	0.7785	0.0039	0.0382	yes
TFCP2	Q12800	1.493	0.671	1.082	0.0039	0.0382	yes
ACTB	P60709	0.926	0.642	0.784	0.0040	0.0384	no
HNRNPF	P52597	1.073	0.626	0.8495	0.0040	0.0384	yes
RPL13	P26373	-0.7	-0.76	-0.727	0.0043	0.0399	no
MYO18A	Q92614-2	0.921	0.629	0.775	0.0043	0.0399	no
YBX1	P67809	-0.63	-0.89	-0.761	0.0044	0.0409	yes

RPL28	P46779	-0.65	-0.81	-0.73	0.0046	0.0409	no
ACTG1	P63261	0.925	0.615	0.77	0.0046	0.0409	no
RPLP2	P05387	0.77	0.669	0.7195	0.0046	0.0409	no
ARPC1A	Q92747	1.676	0.659	1.1675	0.0049	0.0432	no
PPIB	P23284	-0.63	-0.81	-0.72	0.0050	0.0433	no
RPL29	P47914	-0.65	-0.76	-0.707	0.0051	0.0433	no
DYNLL1	P63167	-0.58	-0.99	-0.784	0.0053	0.0448	yes
RPS6	P62753	-0.61	-0.82	-0.715	0.0055	0.0460	no
SF3B2	Q13435	-0.58	-0.93	-0.752	0.0056	0.0461	yes
MSN	P26038	-0.7	-0.66	-0.676	0.0060	0.0490	no
RPL36A	J3KQN4	-0.54	-1.13	-0.839	0.0064	0.0518	no
BOP1	Q14137	-0.66	-0.67	-0.663	0.0065	0.0519	yes
RPS23	P62266	-0.56	-0.85	-0.708	0.0066	0.0519	no
ATAD3B	Q5T9A4	-0.77	-0.57	-0.67	0.0072	0.0557	no
FARSA	Q9Y285	-0.94	-0.53	-0.736	0.0072	0.0557	no
ARPC3	O15145	1.1	0.512	0.806	0.0077	0.0584	no
RPS19	P39019	-0.69	-0.6	-0.644	0.0077	0.0584	yes
BANF1	O75531	-0.56	-0.76	-0.661	0.0078	0.0585	yes
HMGB2	P26583	-0.77	-0.54	-0.659	0.0082	0.0607	yes
RPL36AL	Q969Q0	-0.5	-1.12	-0.808	0.0083	0.0608	no
SEC13	P55735	-0.5	-0.91	-0.708	0.0086	0.0622	yes
CEBPA	P49715	0.797	0.526	0.6615	0.0086	0.0622	yes
OLA1	J3KQ32	-0.57	-0.68	-0.626	0.0089	0.0636	yes
SENP3	Q9H4L4	-0.8	-0.52	-0.658	0.0090	0.0636	yes
MAX	P61244	1.022	0.484	0.753	0.0091	0.0636	yes
CNOT1	A5YKK6	-0.6	-0.62	-0.613	0.0094	0.0651	yes
UTP23	Q9BRU9	-0.47	-1.06	-0.764	0.0099	0.0683	yes
CDC5L	Q99459	-0.51	-0.75	-0.629	0.0103	0.0698	yes
ACTBL2	Q562R1	1.002	0.461	0.7315	0.0104	0.0698	no
MYL4	P12829	-0.46	-1.17	-0.817	0.0104	0.0698	no
RPS27A	P62979	1.362	0.458	0.91	0.0111	0.0736	yes
RPL22L1	Q6P5R6	-0.67	-0.52	-0.599	0.0112	0.0739	no
FARSB	Q9NSD9	-0.46	-0.89	-0.671	0.0114	0.0747	no
RAB27A	P51159	0.507	0.686	0.5965	0.0118	0.0762	no
VPS29	F8VXU5	-0.84	-0.45	-0.646	0.0121	0.0777	no
HMGB1	P09429	-0.8	-0.46	-0.626	0.0126	0.0798	yes
WDR1	O75083	0.668	0.499	0.5835	0.0128	0.0803	no
RPL38	P63173	-0.44	-0.83	-0.638	0.0129	0.0803	no
KIF23	Q02241	-0.58	-0.55	-0.564	0.0134	0.0822	yes
TRIP6	Q15654	-0.43	-0.86	-0.645	0.0134	0.0822	yes
PAICS	P22234-2	0.666	0.488	0.577	0.0136	0.0822	no
EIF5A	P63241	0.474	0.696	0.585	0.0136	0.0822	yes
RPS9	P46781	-0.49	-0.66	-0.573	0.0139	0.0837	no
BTBD10	Q9BSF8-2	-0.4	-1.31	-0.851	0.0151	0.0893	yes
ATIC	P31939	0.445	0.705	0.575	0.0155	0.0893	no
CNOT2	Q9NZN8	-0.48	-0.64	-0.556	0.0155	0.0893	yes

MYL6B	P14649	0.403	0.871	0.637	0.0156	0.0893	no
HERC2	O95714	0.976	0.391	0.6835	0.0156	0.0893	yes
RPL19	P84098	-0.55	-0.54	-0.543	0.0157	0.0893	no
RPL21	P46778	-0.5	-0.59	-0.546	0.0157	0.0893	no
FCGR1A	P12314	-0.44	-0.7	-0.573	0.0159	0.0893	no
LARS	Q9P2J5	0.395	0.888	0.6415	0.0161	0.0893	no
HIST2H3A	Q71DI3	-0.38	-1.24	-0.812	0.0162	0.0893	yes
H3F3A	P84243	-0.38	-1.25	-0.813	0.0162	0.0893	yes
RPL37A	P61513	-0.42	-0.75	-0.585	0.0163	0.0894	no
RUNX1	Q01196-8	0.668	0.447	0.5575	0.0166	0.0901	yes
ALDH1B1	P30837	0.722	0.42	0.571	0.0172	0.0922	no
MT2A	P02795	-0.51	-0.55	-0.531	0.0173	0.0922	no
RPL10	F8W7C6	-0.52	-0.54	-0.53	0.0174	0.0922	no
PSMD4	P55036	0.451	0.638	0.5445	0.0175	0.0922	no
RPL26	P61254	-0.64	-0.44	-0.542	0.0181	0.0946	no
CNOT3	O75175	-0.67	-0.43	-0.548	0.0183	0.0950	yes
PPP1R7	Q15435	1.381	0.358	0.8695	0.0184	0.0953	yes
HCLS1	P14317	-0.43	-0.64	-0.539	0.0188	0.0959	no
RSL1D1	O76021	-0.91	-0.36	-0.637	0.0189	0.0959	yes
ACTR2	P61160	0.837	0.374	0.6055	0.0190	0.0959	no
POTEF	A5A3E0	0.967	0.355	0.661	0.0192	0.0965	no
DERL1	Q9BUN8	0.38	0.764	0.572	0.0200	0.0994	no
HIST1H1E	P10412	-0.55	-0.48	-0.514	0.0200	0.0994	yes
ADAR	P55265-4	0.591	0.447	0.519	0.0203	0.0997	yes
ZYX	Q15942	-0.59	-0.44	-0.519	0.0204	0.0997	yes
SLTM	Q9NWH9	-0.42	-0.63	-0.526	0.0205	0.0998	yes
GNB2L1	P63244	0.433	0.607	0.52	0.0207	0.1002	no
FLT3	P36888	-0.6	-0.44	-0.516	0.0211	0.1006	no
HIST1H1C	P16403	-0.54	-0.47	-0.507	0.0211	0.1006	yes
HMGN2	P05204	-1.88	-0.36	-1.117	0.0214	0.1006	yes
RPL10	P27635	-0.49	-0.51	-0.504	0.0214	0.1006	no
RPL17	P18621-3	-0.48	-0.53	-0.503	0.0216	0.1009	no
XRCC1	P18887	0.459	0.545	0.502	0.0221	0.1028	yes
RPL13A	P40429	-0.51	-0.49	-0.499	0.0222	0.1028	no
RPLP1	P05386	1.226	0.316	0.771	0.0224	0.1028	no
RPS25	P62851	-0.79	-0.35	-0.568	0.0229	0.1045	no
STT3B	Q8TCJ2	-0.35	-0.77	-0.56	0.0231	0.1048	no
RPL36	Q9Y3U8	-0.47	-0.52	-0.494	0.0233	0.1051	no
HIST2H2BC	Q6DN03	-0.38	-0.68	-0.528	0.0236	0.1056	yes
RPL35	P42766	-0.31	-1	-0.659	0.0237	0.1056	no
LRRFIP2	Q9Y608	0.434	0.556	0.495	0.0240	0.1061	no
HIST1H4A	P62805	-0.32	-0.92	-0.621	0.0242	0.1066	yes
MYO1C	O00159	0.827	0.331	0.579	0.0244	0.1069	yes
HIST1H1B	P16401	-0.76	-0.34	-0.549	0.0250	0.1090	yes
RPL23A	P62750	-0.36	-0.69	-0.523	0.0256	0.1108	no
ANLN	Q9NQW6	-0.35	-0.71	-0.529	0.0261	0.1121	yes

RPL27A	P46776	-0.53	-0.43	-0.48	0.0268	0.1145	no
EEF1A1P5	Q5VTE0	0.448	0.503	0.4755	0.0269	0.1145	no
BCKDK	O14874	-0.4	-0.56	-0.478	0.0283	0.1190	no
PGAM5	Q96HS1	-0.59	-0.38	-0.484	0.0284	0.1190	no
MRPL22	J3KQY1	-0.52	-0.42	-0.47	0.0287	0.1190	no
RPL3	P39023	-0.53	-0.41	-0.471	0.0289	0.1190	yes
FXR1	P51114	0.427	0.509	0.468	0.0289	0.1190	no
SSBP1	Q04837	1.986	0.28	1.133	0.0290	0.1190	no
CAT	P04040	0.529	0.406	0.4675	0.0298	0.1219	no
SSB	P05455	0.949	0.276	0.6125	0.0300	0.1221	yes
RPL26L1	Q9UNX3	-0.44	-0.48	-0.46	0.0303	0.1224	no
DOCK8	Q8NF50	0.44	0.479	0.4595	0.0305	0.1224	no
MAP7D1	Q3KQU3	0.343	0.64	0.4915	0.0306	0.1224	no
GTPBP4	Q9BZE4	-0.3	-0.74	-0.522	0.0319	0.1267	yes
RPS14	P62263	-0.42	-0.48	-0.453	0.0324	0.1284	no
SERBP1	Q8NC51	-0.26	-0.93	-0.593	0.0331	0.1304	yes
AURKAIP1	Q9NWT8	-0.38	-0.53	-0.453	0.0343	0.1343	yes
RPS4Y1	P22090	-0.46	-0.42	-0.444	0.0346	0.1345	no
GSPT1	P15170-3	0.476	0.413	0.4445	0.0347	0.1345	no
CUL3	Q13618	0.494	0.394	0.444	0.0355	0.1363	yes
RPLP0	P05388	0.377	0.517	0.447	0.0356	0.1363	yes
TPM1	P09493-9	-0.22	-1.38	-0.799	0.0358	0.1363	no
RPL4	P36578	-0.41	-0.47	-0.441	0.0359	0.1363	no
LGALS1	P09382	0.492	0.391	0.4415	0.0362	0.1363	no
RPL39	P62891	-0.28	-0.74	-0.512	0.0363	0.1363	no
COMT	P21964	0.579	0.331	0.455	0.0377	0.1408	no
NEURL4	Q96JN8	0.766	0.265	0.5155	0.0380	0.1415	no
FLII	Q13045	0.628	0.306	0.467	0.0384	0.1417	yes
IMPDH2	P12268	0.618	0.309	0.4635	0.0386	0.1417	yes
GPX1	P07203	0.513	0.362	0.4375	0.0388	0.1417	no
FAM8A1	Q9UBU6	0.202	2.408	1.305	0.0389	0.1417	no
RPS18	P62269	-0.45	-0.41	-0.428	0.0394	0.1421	no
MRPS18B	Q9Y676	-0.29	-0.65	-0.471	0.0395	0.1421	no
LGALS9	O00182	0.293	0.648	0.4705	0.0395	0.1421	yes
PDIA6	Q15084-2	0.417	0.435	0.426	0.0399	0.1426	no
ATAD2	Q6PL18	-0.46	-0.4	-0.427	0.0401	0.1426	yes
RPSA	P08865	0.469	0.38	0.4245	0.0414	0.1459	yes
AIMP2	Q13155	1.192	0.192	0.692	0.0414	0.1459	yes
RPS7	P62081	-0.39	-0.46	-0.423	0.0416	0.1460	no
LYN	P07948	-0.29	-0.63	-0.459	0.0423	0.1465	yes
RPL27	P61353	-0.25	-0.74	-0.497	0.0423	0.1465	no
BRIX1	Q8TDN6	-0.37	-0.48	-0.423	0.0423	0.1465	yes
FUOM	A2VDF0	-0.24	-0.8	-0.517	0.0429	0.1477	no
RPN1	P04843	0.492	0.353	0.4225	0.0434	0.1485	no
ITPR1	Q14643	-0.33	-0.53	-0.43	0.0435	0.1485	no
LGALS8	O00214-2	-0.45	-0.39	-0.416	0.0438	0.1489	no

PSMC2	P35998	1.019	0.195	0.607	0.0441	0.1491	yes
KRT2	P35908	-0.27	-0.65	-0.461	0.0445	0.1493	no
TUFM	P49411	0.565	0.306	0.4355	0.0446	0.1493	no
EIF3I	Q13347	-0.85	-0.22	-0.531	0.0456	0.1519	no
RNH1	P13489	0.328	0.515	0.4215	0.0457	0.1519	no
ARPC4	P59998	0.916	0.199	0.5575	0.0465	0.1528	no
HRNR	Q86YZ3	-0.54	-0.31	-0.426	0.0465	0.1528	no
PCBP1	Q15365	0.533	0.314	0.4235	0.0466	0.1528	yes
RRP12	Q5JTH9	0.429	0.385	0.407	0.0470	0.1532	yes
RPL24	P83731	-0.34	-0.49	-0.414	0.0471	0.1532	no
TPM3	P06753-2	0.752	0.227	0.4895	0.0478	0.1548	no
FAM83H	Q6ZRV2	-0.36	-0.44	-0.402	0.0496	0.1597	no
ESYT1	Q9BSJ8-2	0.584	0.276	0.43	0.0499	0.1600	no
RPL32	F8W727	-0.44	-0.36	-0.401	0.0502	0.1603	no
RPL11	P62913	-0.36	-0.45	-0.401	0.0504	0.1604	yes
GPX4	P36969	0.447	0.351	0.399	0.0512	0.1623	no
PPA1	Q15181	0.153	1.105	0.629	0.0516	0.1624	no
ACTR3	P61158	0.578	0.272	0.425	0.0517	0.1624	no
DSG1	Q02413	-0.16	-1.04	-0.599	0.0524	0.1637	no
ARHGDIB	P52566	0.367	0.417	0.392	0.0533	0.1660	no
NDUFS4	O43181	-0.56	-0.27	-0.418	0.0538	0.1666	no
LUC7L2	Q9Y383	-1.55	-0.11	-0.827	0.0540	0.1666	yes
CNOT7	Q9UIV1	-0.26	-0.59	-0.425	0.0543	0.1668	yes
TPM1	H0YK48	-0.13	-1.19	-0.661	0.0552	0.1686	no
PCNA	P12004	0.577	0.26	0.4185	0.0553	0.1686	yes
LUC7L	Q9NQ29	-1.37	-0.11	-0.741	0.0564	0.1711	no
RREB1	Q92766-2	-0.43	-0.34	-0.387	0.0566	0.1711	yes
ATP5F1	P24539	-0.23	-0.62	-0.429	0.0573	0.1727	no
HNRNPH2	P55795	0.746	0.192	0.469	0.0584	0.1751	yes
KRT13	P13646	-0.41	-0.35	-0.38	0.0596	0.1780	no
MYL3	P08590	0.551	0.251	0.401	0.0619	0.1836	no
TRIM28	Q13263	0.745	0.181	0.463	0.0620	0.1836	yes
SRSF7	Q16629	1.997	0.042	1.0195	0.0622	0.1836	yes
HSPA8	P11142	0.485	0.282	0.3835	0.0633	0.1862	yes
UBXN1	Q04323-2	0.276	0.487	0.3815	0.0649	0.1901	no
TPM3	P06753-6	0.741	0.171	0.456	0.0658	0.1920	no
TMA16	Q96EY4	-0.32	-0.42	-0.369	0.0663	0.1927	no
RCC2	Q9P258	0.201	0.634	0.4175	0.0672	0.1946	yes
RPL30	P62888	0.292	0.447	0.3695	0.0681	0.1963	no
PCBP2	Q15366-2	0.533	0.24	0.3865	0.0687	0.1969	yes
SMN1	Q16637	0.948	0.116	0.532	0.0688	0.1969	yes
RPL6	Q02878	-0.28	-0.45	-0.366	0.0709	0.2022	no
UBAC2	Q8NBM4	0.75	0.153	0.4515	0.0714	0.2029	no
TIMM50	Q3ZCQ8-2	-0.13	-0.82	-0.476	0.0720	0.2038	yes
JUP	P14923	-1.71	-0.01	-0.861	0.0728	0.2052	no
TPM3	J3KN67	0.747	0.149	0.448	0.0733	0.2057	no

TPM4	P67936	0.739	0.149	0.444	0.0741	0.2074	no
VDAC3	Q9Y277-2	0.529	0.225	0.377	0.0751	0.2087	no
HSPH1	Q92598	0.412	0.296	0.354	0.0755	0.2087	no
PIP	P12273	-0.23	-0.51	-0.373	0.0758	0.2087	no
G6PD	P11413-2	0.327	0.373	0.35	0.0759	0.2087	no
TPI1	P60174	-0.39	-0.31	-0.351	0.0760	0.2087	no
SHC1	P29353-6	-0.11	-0.87	-0.489	0.0774	0.2117	no
EIF3F	O00303	0.609	0.183	0.396	0.0779	0.2119	no
GNB1	P62873	-0.38	-0.31	-0.348	0.0780	0.2119	no
VARS	P26640	-0.29	-0.4	-0.348	0.0790	0.2134	no
XRCC6	P12956	0.493	0.234	0.3635	0.0791	0.2134	yes
FAF1	Q9UNN5	1.332	0.02	0.676	0.0811	0.2178	yes
SSRP1	Q08945	-0.59	-0.18	-0.385	0.0814	0.2179	yes
RPS24	P62847-4	-0.33	-0.35	-0.34	0.0823	0.2194	no
DBN1	Q16643-3	1.178	0.035	0.6065	0.0834	0.2214	no
KEAP1	Q14145	0.343	0.333	0.338	0.0836	0.2214	yes
KRT9	P35527	-0.6	-0.17	-0.387	0.0840	0.2216	no
H2AFX	P16104	-1.01	-0.06	-0.533	0.0857	0.2254	yes
IGKC	P01834	0.905	0.071	0.488	0.0890	0.2332	no
RPS13	P62277	-0.28	-0.39	-0.332	0.0908	0.2370	no
MAT2A	P31153	-0.58	-0.17	-0.373	0.0912	0.2373	no
PPP2R1A	P30153	0.549	0.178	0.3635	0.0916	0.2373	no
HSD17B10	Q99714	0.801	0.09	0.4455	0.0918	0.2373	no
DGKZ	Q13574	-0.15	-0.57	-0.362	0.0989	0.2545	yes
XRCC5	P13010	0.226	0.432	0.329	0.0993	0.2548	yes
RPL5	P46777	0.442	0.218	0.33	0.1002	0.2561	yes
PPIA	P62937	-0.37	-0.27	-0.319	0.1007	0.2565	no
HADHA	P40939	0.205	0.46	0.3325	0.1012	0.2570	no
RBM39	Q14498	-0.51	-0.18	-0.342	0.1019	0.2578	yes
RPS4X	P62701	-0.31	-0.31	-0.313	0.1039	0.2620	no
FAM98B	Q52LJ0-2	-0.3	-0.32	-0.312	0.1044	0.2624	yes
RPS3A	P61247	-0.27	-0.36	-0.313	0.1056	0.2646	yes
COPA	P53621-2	0.329	0.291	0.31	0.1065	0.2658	no
RECQL4	O94761	-0.42	-0.22	-0.319	0.1082	0.2689	yes
HSPA1L	P34931	0.745	0.07	0.4075	0.1097	0.2689	no
LAP3	P28838	0.469	0.184	0.3265	0.1097	0.2689	no
ERLIN1	O75477	0.445	0.198	0.3215	0.1097	0.2689	no
EIF5B	O60841	0.419	0.214	0.3165	0.1100	0.2689	no
SND1	Q7KZF4	0.292	0.319	0.3055	0.1105	0.2689	yes
RPL18A	Q02543	-0.33	-0.28	-0.305	0.1113	0.2689	no
RUNX3	Q13761-2	0.292	0.317	0.3045	0.1114	0.2689	yes
DARS	P14868	0.331	0.279	0.305	0.1114	0.2689	no
FLNA	P21333	0.522	0.153	0.3375	0.1115	0.2689	no
TMOD1	P28289	-0.07	-0.75	-0.406	0.1117	0.2689	no
TPM2	P07951-2	-0.09	-0.67	-0.381	0.1125	0.2697	no
DDX39B	Q13838-2	0.223	0.398	0.3105	0.1129	0.2697	yes

MTA2	O94776	0.334	0.273	0.3035	0.1131	0.2697	yes
RPL23	P62829	-0.16	-0.51	-0.333	0.1135	0.2698	no
CS	O75390	-0.39	-0.22	-0.309	0.1139	0.2699	no
QARS	P47897	0.11	0.605	0.3575	0.1151	0.2717	no
IQCB1	Q15051	-0.12	-0.58	-0.349	0.1160	0.2732	no
LAT2	Q9GZY6	0.56	0.125	0.3425	0.1175	0.2752	no
HMGA1	P17096	-0.46	-0.17	-0.318	0.1181	0.2752	yes
ACP1	P24666	-0.24	-0.36	-0.301	0.1185	0.2752	no
IDH2	P48735	-0	0.943	0.4705	0.1188	0.2752	no
NONO	Q15233	-0.02	1.016	0.498	0.1189	0.2752	yes
PSMD7	P51665	0.443	0.183	0.313	0.1191	0.2752	no
YBX3	P16989	0.542	0.129	0.3355	0.1201	0.2766	yes
DNAJA1	P31689	0.011	0.878	0.4445	0.1208	0.2768	yes
NUP153	P49790-3	-0.06	-0.71	-0.387	0.1209	0.2768	yes
ARPC5	O15511	0.555	0.121	0.338	0.1213	0.2769	no
RBM12B	Q8IXT5	-0.2	-0.41	-0.305	0.1222	0.2781	no
KRT1	P04264	-0.61	-0.1	-0.352	0.1234	0.2791	no
FAM104B	Q5XKR9-3	0.354	0.237	0.2955	0.1236	0.2791	no
DHX15	O43143	0.187	0.424	0.3055	0.1238	0.2791	yes
RPS8	P62241	-0.19	-0.42	-0.303	0.1251	0.2812	no
S100A4	P26447	0.272	0.306	0.289	0.1272	0.2849	no
PPP1CA	P62136-2	-0.3	-0.28	-0.289	0.1275	0.2849	yes
TBL2	Q9Y4P3	-0.44	-0.17	-0.304	0.1293	0.2880	no
AARS	P49588	-0.29	-0.28	-0.286	0.1302	0.2883	no
MYH10	P35580-3	0.342	0.235	0.2885	0.1305	0.2883	no
CANX	P27824-2	-0.26	-0.31	-0.286	0.1309	0.2883	no
PABPC4	Q13310-3	0.36	0.22	0.29	0.1310	0.2883	no
SBSN	Q6UWP8	-0.59	-0.08	-0.338	0.1348	0.2957	no
RAN	B5MDF5	-0.47	-0.14	-0.305	0.1355	0.2965	yes
PAK2	Q13177	0.469	0.141	0.305	0.1364	0.2976	yes
NOP56	O00567	-0.31	-0.26	-0.281	0.1371	0.2982	yes
ECM1	Q16610-4	-0.55	-0.1	-0.323	0.1384	0.2994	no
PFN1	P07737	-0.2	-0.37	-0.285	0.1388	0.2994	no
KHDRBS1	Q07666	-0.1	-0.55	-0.323	0.1388	0.2994	yes
LSP1	P33241-3	0.72	0.026	0.373	0.1408	0.3027	no
POLR2A	P24928	0.105	0.524	0.3145	0.1416	0.3028	yes
CSE1L	P55060	-0.34	-0.22	-0.279	0.1416	0.3028	yes
NOP58	Q9Y2X3	-0.36	-0.21	-0.281	0.1425	0.3033	yes
KIF14	Q15058	-0.37	-0.2	-0.282	0.1427	0.3033	yes
RPS16	P62249	-0.15	-0.44	-0.294	0.1434	0.3040	no
TXN	P10599	-0.22	-0.34	-0.278	0.1443	0.3049	yes
H2AFZ	P0C0S5	-0.69	-0.03	-0.362	0.1450	0.3055	yes
ARPC1B	O15143	0.366	0.193	0.2795	0.1458	0.3064	no
HIST1H2AD	P20671	-0.98	0.063	-0.459	0.1465	0.3071	yes
ACADVL	P49748-3	0.348	0.204	0.276	0.1475	0.3080	no
HIST1H2AB	P04908	-0.93	0.05	-0.439	0.1478	0.3080	yes

CBX3	Q13185	-0.16	-0.41	-0.285	0.1486	0.3088	yes
NHP2L1	B1AHD1	-0.17	-0.39	-0.281	0.1492	0.3088	no
RAD50	Q92878-2	0.396	0.167	0.2815	0.1494	0.3088	yes
EIF1AX	P47813	-0.21	-0.34	-0.273	0.1500	0.3092	no
AIMP1	Q12904-2	0.243	0.295	0.269	0.1512	0.3102	yes
HSPB1	P04792	0.247	0.29	0.2685	0.1515	0.3102	yes
SMC1A	Q14683	0.243	0.294	0.2685	0.1518	0.3102	yes
LMNA	P02545	-0.24	-0.29	-0.268	0.1529	0.3117	yes
RAC1	P63000-2	-0.26	-0.27	-0.267	0.1536	0.3123	no
ENO2	P09104	0.538	0.081	0.3095	0.1542	0.3127	no
ACAA1	P09110	-0.94	0.064	-0.436	0.1547	0.3127	no
PLAA	Q9Y263	0.025	0.666	0.3455	0.1552	0.3127	no
GSTP1	P09211	0.314	0.22	0.267	0.1555	0.3127	yes
FLOT1	O75955	0.029	-0.82	-0.394	0.1559	0.3127	no
EIF3B	P55884-2	0.53	0.08	0.305	0.1580	0.3159	no
CHAF1A	Q13111	-0.04	-0.63	-0.331	0.1584	0.3159	yes
DNAJC13	O75165	-0.72	0	-0.36	0.1589	0.3159	no
GPT2	Q8TD30	0.033	0.632	0.3325	0.1592	0.3159	no
HBB	P68871	-0.49	-0.1	-0.293	0.1598	0.3162	no
CSTB	P04080	0.013	-0.75	-0.369	0.1602	0.3162	yes
GANAB	Q14697	0.543	0.069	0.306	0.1617	0.3182	no
GMPS	P49915	-0.45	-0.12	-0.284	0.1624	0.3186	no
SUZ12	Q15022	-0.33	-0.2	-0.264	0.1627	0.3186	yes
ATAD3A	Q9NVI7-2	-0.77	0.024	-0.372	0.1638	0.3199	no
UHRF1	Q96T88-2	-0.2	-0.32	-0.26	0.1672	0.3256	yes
ERLIN2	O94905	0.328	0.192	0.26	0.1678	0.3259	no
MCM6	Q14566	0.317	0.2	0.2585	0.1684	0.3263	yes
MRPL33	O75394	-0.07	-0.52	-0.296	0.1694	0.3266	no
PTBP1	P26599-3	0.176	0.346	0.261	0.1695	0.3266	yes
RPL35A	P18077	-0.62	-0.02	-0.323	0.1711	0.3289	no
KRT10	P13645	-0.16	-0.36	-0.261	0.1733	0.3323	no
HIST1H1D	P16402	-0.49	-0.08	-0.284	0.1769	0.3383	yes
MRPL51	Q4U2R6	0.089	0.46	0.2745	0.1807	0.3434	no
MYL1	P05976	0.38	0.138	0.259	0.1809	0.3434	no
RPL15	P61313	-0.34	-0.17	-0.253	0.1809	0.3434	no
RRP7A	Q9Y3A4	-0.1	-0.44	-0.269	0.1825	0.3455	no
ERH	P84090	-0.22	-0.27	-0.246	0.1842	0.3455	no
CDK1	P06493	-0.56	-0.03	-0.297	0.1844	0.3455	yes
RPS10	P46783	-1.04	0.141	-0.448	0.1846	0.3455	yes
PA2G4	Q9UQ80	-0.27	-0.22	-0.245	0.1848	0.3455	yes
CHMP5	Q9NZZ3	-0.06	-0.51	-0.283	0.1848	0.3455	no
NACAP1	Q9BZK3	0.417	0.109	0.263	0.1854	0.3457	no
CSTA	P01040	-0.19	-0.3	-0.246	0.1868	0.3469	no
PRDX1	Q06830	0.33	0.167	0.2485	0.1870	0.3469	no
UQCRH	P07919	0.274	0.211	0.2425	0.1892	0.3501	no
HSPA9	P38646	0.281	0.202	0.2415	0.1915	0.3535	yes

CALM3	M0QZ52	0.173	0.313	0.243	0.1934	0.3561	no
GNAI3	P08754	0.422	0.095	0.2585	0.1953	0.3588	no
F2	P00734	-1.14	0.192	-0.472	0.1980	0.3628	no
CALM1	P62158	0.204	0.269	0.2365	0.1989	0.3637	no
CSK	P41240	-0.22	-0.25	-0.235	0.2002	0.3651	no
MYH7	P12883	-1.02	0.161	-0.429	0.2016	0.3666	no
NSF	P46459	0.677	-0.04	0.318	0.2045	0.3711	no
DOT1L	Q8TEK3	0.297	0.173	0.235	0.2051	0.3712	yes
ABCF2	Q9UG63-2	0.28	0.186	0.233	0.2063	0.3726	no
CLTC	Q00610	0.293	0.173	0.233	0.2081	0.3746	no
RPS20	P60866-2	0.65	-0.03	0.308	0.2084	0.3746	no
RPS12	P25398	0.195	0.264	0.2295	0.2110	0.3782	no
HSP90B1	P14625	-0.27	-0.19	-0.229	0.2132	0.3813	no
HCK	P08631	-0.1	-0.39	-0.242	0.2144	0.3826	yes
YWHAE	P62258	-0.23	-0.22	-0.226	0.2164	0.3852	yes
TMED3	Q9Y3Q3	0.282	0.171	0.2265	0.2188	0.3885	no
AHCY	P23526	-0.36	-0.11	-0.234	0.2209	0.3905	no
EIF3D	O15371	-0.2	-0.25	-0.224	0.2210	0.3905	no
PKM	P14618	0.214	0.229	0.2215	0.2237	0.3945	yes
NHP2	Q9NX24	0.189	0.25	0.2195	0.2287	0.4021	yes
KRT16	P08779	-0.28	1.252	0.487	0.2292	0.4021	no
PTPN6	P29350-3	0.125	-0.81	-0.345	0.2299	0.4024	yes
RPS17L	P0CW22	-0.11	-0.33	-0.224	0.2353	0.4109	no
LASP1	Q14847-2	-0.16	-0.27	-0.217	0.2364	0.4120	no
RPL9	P32969	-0.05	-0.42	-0.238	0.2385	0.4133	no
TUBB6	Q9BUF5	0.124	0.315	0.2195	0.2398	0.4133	no
MRPL11	Q9Y3B7	-0.09	0.702	0.3055	0.2406	0.4133	no
NOP2	P46087-4	-0.42	-0.05	-0.235	0.2410	0.4133	yes
SNRPD2	P62316	-0.06	-0.41	-0.233	0.2420	0.4133	yes
HNRNPDL	O14979	-0.41	-0.06	-0.233	0.2421	0.4133	yes
MRPS7	Q9Y2R9	-0.31	-0.12	-0.218	0.2423	0.4133	no
STIP1	P31948-2	-0.21	-0.21	-0.212	0.2428	0.4133	yes
ARHGEF1	M0QZR4	-0.09	0.699	0.3035	0.2428	0.4133	no
SQRDL	Q9Y6N5	0.227	0.196	0.2115	0.2431	0.4133	no
CAD	P27708	0.288	0.142	0.215	0.2433	0.4133	yes
EEF1A2	Q05639	0.274	0.153	0.2135	0.2440	0.4134	yes
PTK2B	Q14289	0.251	0.171	0.211	0.2460	0.4160	yes
TUBA4A	P68366	0.244	0.176	0.21	0.2474	0.4165	no
MATR3	P43243	0.732	-0.11	0.3105	0.2474	0.4165	yes
TUBB4A	P04350	0.195	0.222	0.2085	0.2490	0.4182	no
MCM7	P33993	0.117	0.312	0.2145	0.2500	0.4189	yes
MYO1F	O00160	-0.1	-0.34	-0.216	0.2532	0.4233	no
TUBB4B	P68371	0.195	0.217	0.206	0.2540	0.4238	no
PPP2R2A	P63151-2	0.29	0.127	0.2085	0.2581	0.4296	no
ANP32A	P39687	-0.91	0.2	-0.355	0.2621	0.4353	yes
ATP5C1	P36542	-0.02	-0.44	-0.228	0.2654	0.4398	no

TUBB	P07437	0.192	0.205	0.1985	0.2698	0.4461	no
IARS	P41252	0.31	0.1	0.205	0.2714	0.4477	no
RPL18	Q07020	-0.24	-0.16	-0.198	0.2728	0.4491	no
ATP5B	P06576	0.141	0.257	0.199	0.2735	0.4492	no
TUBA1A	Q71U36-2	0.229	0.164	0.1965	0.2757	0.4517	no
ARPC5L	Q9BPX5	-0.35	-0.06	-0.208	0.2792	0.4565	no
UNC13D	Q70J99-3	0.639	-0.1	0.2685	0.2813	0.4581	no
KRT14	P02533	-0.4	1.363	0.483	0.2814	0.4581	yes
CALR	P27797	-0.14	-0.25	-0.194	0.2838	0.4610	no
RPL22	P35268	0.11	0.28	0.195	0.2878	0.4662	no
KCTD10	Q9H3F6	0.498	-0.04	0.2315	0.2883	0.4662	yes
TAF6L	Q9Y6J9	-0.08	-0.31	-0.197	0.2924	0.4718	yes
H2AFY	O75367	0.066	0.331	0.1985	0.2942	0.4738	yes
TUBA1B	P68363	0.234	0.143	0.1885	0.2953	0.4745	no
SRSF3	P84103	-0.17	-0.2	-0.187	0.2961	0.4748	yes
ADK	P55263	-0.23	-0.14	-0.188	0.2975	0.4760	yes
HNRNPR	O43390	0.025	-0.47	-0.221	0.2986	0.4767	yes
FASN	P49327	0.343	0.051	0.197	0.3025	0.4819	no
PDIA3	P30101	-0.21	-0.16	-0.184	0.3048	0.4839	no
NAT10	Q9H0A0	0.013	-0.44	-0.212	0.3062	0.4839	yes
RTCB	Q9Y3I0	0.178	0.187	0.1825	0.3065	0.4839	yes
RPL7	P18124	-0.1	-0.27	-0.187	0.3065	0.4839	no
HNRNPA2B1	P22626	-0	-0.41	-0.207	0.3070	0.4839	yes
RRS1	Q15050	0.127	-0.64	-0.257	0.3088	0.4858	yes
PES1	O00541	-0.01	-0.39	-0.202	0.3099	0.4864	yes
COPB1	P53618	0.131	0.233	0.182	0.3115	0.4880	no
RNPS1	Q15287	-0.22	-0.14	-0.181	0.3127	0.4888	yes
HNRNPL	P14866	0.224	0.136	0.18	0.3155	0.4920	yes
HNRNPH1	P31943	0.427	-0.02	0.205	0.3188	0.4956	yes
TBC1D15	Q8TC07	0.707	-0.17	0.269	0.3191	0.4956	no
CSDE1	O75534-4	0.253	0.107	0.18	0.3204	0.4967	no
RPS5	M0R0R2	-0.37	-0.02	-0.195	0.3220	0.4981	no
KRT17	Q04695	-0.48	1.397	0.46	0.3264	0.5037	no
MRTO4	Q9UKD2	-0.89	0.26	-0.313	0.3273	0.5042	yes
RPS26	P62854	0.068	-0.5	-0.215	0.3299	0.5072	no
PML	P29590	-0.45	0.039	-0.204	0.3317	0.5089	yes
PSMA1	P25786-2	-0.61	1.692	0.5415	0.3341	0.5105	yes
SUPT16H	Q9Y5B9	-0.53	0.089	-0.22	0.3343	0.5105	yes
DNAJA2	O60884	-0.02	-0.36	-0.188	0.3348	0.5105	no
EEF2	P13639	0.254	0.092	0.173	0.3399	0.5171	yes
TPM2	P07951	0.159	-0.65	-0.244	0.3430	0.5207	no
RARS	P54136	0.057	0.292	0.1745	0.3463	0.5242	no
MRPL47	Q9HD33	-0.28	-0.06	-0.174	0.3466	0.5242	no
PRKCD	Q05655-2	0.036	-0.42	-0.193	0.3492	0.5270	yes
RAVER1	E9PAU2	-0.16	-0.17	-0.165	0.3527	0.5312	yes
HIST1H2BN	U3KQK0	-0.44	0.048	-0.194	0.3536	0.5315	yes

RAC2	P15153	0.301	0.043	0.172	0.3566	0.5349	no
TOP2B	Q02880-2	-0.02	-0.33	-0.175	0.3586	0.5349	yes
KRT77	Q7Z794	-0.5	0.093	-0.206	0.3588	0.5349	no
CFL1	P23528	0.211	0.116	0.1635	0.3588	0.5349	yes
ZFP91	Q96JP5	-0.14	-0.17	-0.157	0.3752	0.5571	yes
DDX39A	O00148	0.07	0.251	0.1605	0.3757	0.5571	yes
ETFA	P13804	-0.05	0.412	0.182	0.3759	0.5571	no
PAFAH1B3	Q15102	0.024	0.306	0.165	0.3795	0.5614	no
HSPD1	P10809	0.122	0.187	0.1545	0.3823	0.5641	no
ITGAL	P20701-2	-0.37	0.023	-0.173	0.3829	0.5641	no
RHOG	P84095	-0.12	0.526	0.201	0.3837	0.5642	no
DNAJB1	P25685	-0.04	-0.29	-0.161	0.3847	0.5646	yes
DSP	P15924	-0	0.339	0.167	0.3867	0.5663	no
PDCD6IP	Q8WUM4	0.273	0.039	0.156	0.3961	0.5790	no
PGK1	P00558	-0.13	-0.17	-0.147	0.4048	0.5905	no
SUN2	Q9UH99-2	-0.51	0.13	-0.19	0.4067	0.5922	yes
NPM1	P06748	0.12	0.168	0.144	0.4127	0.5998	yes
TK1	P04183	-0.13	-0.15	-0.143	0.4151	0.5999	no
RBBP4	Q09028	-0.11	-0.18	-0.144	0.4153	0.5999	yes
RBBP7	Q16576-2	-0.11	-0.18	-0.144	0.4153	0.5999	yes
HNRNPA1	P09651	-0.16	-0.12	-0.142	0.4202	0.6049	yes
PFKL	P17858	-0.06	-0.23	-0.145	0.4203	0.6049	no
HPX	P02790	0.13	0.151	0.1405	0.4229	0.6051	no
RPS15A	P62244	0.159	0.122	0.1405	0.4232	0.6051	no
RPS2	P15880	-0.16	-0.12	-0.141	0.4235	0.6051	no
MYO1G	B0I1T2	-0.07	-0.21	-0.143	0.4238	0.6051	no
SNRPB	P14678-3	-0.26	-0.03	-0.146	0.4273	0.6090	yes
HNRNPM	P52272	0.066	0.216	0.141	0.4293	0.6108	yes
PABPC1	P11940	0.343	-0.04	0.1535	0.4316	0.6121	yes
CNBP	P62633-6	-0.15	-0.13	-0.138	0.4323	0.6121	no
HNRNPUL1	Q9BUJ2	-0.13	0.472	0.1735	0.4337	0.6121	yes
BOLA2	Q9H3K6	0.392	-0.07	0.16	0.4339	0.6121	yes
ILVBL	A1L0T0	0.415	-0.09	0.1635	0.4344	0.6121	no
HNRNPD	Q14103	-0.09	-0.18	-0.137	0.4368	0.6144	yes
CCT2	P78371	0.173	0.099	0.136	0.4389	0.6162	no
SLC25A5	P05141	0.204	0.07	0.137	0.4402	0.6168	no
SLIRP	Q9GZT3	-0.12	-0.15	-0.133	0.4468	0.6249	yes
WARS	P23381	0.338	-0.04	0.1475	0.4494	0.6273	no
RAB14	P61106	0.111	0.152	0.1315	0.4521	0.6299	no
ACOT9	Q9Y305-4	-0.61	0.228	-0.192	0.4586	0.6378	no
PSMC3	P17980	0.075	-0.37	-0.15	0.4595	0.6378	yes
KIAA0101	Q15004	1.176	-0.55	0.3135	0.4645	0.6425	no
RPS15	P62841	-0.13	0.454	0.1605	0.4646	0.6425	no
ZNF593	O00488	-0.02	0.3	0.138	0.4659	0.6431	yes
MCM2	P49736	-0	0.273	0.134	0.4697	0.6465	yes
MCM4	P33991	-0.08	-0.18	-0.127	0.4701	0.6465	yes

MCM3	P25205	-0.05	-0.2	-0.126	0.4786	0.6570	yes
RPL7A	P62424	-0.12	-0.13	-0.123	0.4799	0.6576	no
ALB	P02768	0.264	-0	0.13	0.4808	0.6576	no
FKBP8	Q14318-2	0.483	-0.17	0.159	0.4849	0.6617	no
CLEC11A	Q9Y240	-0.94	0.442	-0.25	0.4856	0.6617	no
CAPZA1	P52907	0.249	0.004	0.1265	0.4885	0.6633	no
PSMC6	P62333	-0.06	-0.18	-0.122	0.4886	0.6633	yes
TFAM	Q00059	-0.23	-0.02	-0.125	0.4906	0.6639	no
RALA	P11233	0.05	0.193	0.1215	0.4922	0.6639	no
MRPL14	Q6P1L8	-0	-0.25	-0.125	0.4930	0.6639	no
EHD1	Q9H4M9	0.309	-0.7	-0.197	0.4933	0.6639	no
PSMD3	O43242	-0.17	-0.07	-0.12	0.4939	0.6639	no
PSMD11	O00231-2	-0.23	-0.02	-0.123	0.4958	0.6639	yes
HSP90AB2P	Q58FF8	-0.07	-0.17	-0.12	0.4961	0.6639	no
ZNF559	Q9BR84	-0.02	0.277	0.127	0.4962	0.6639	yes
TARDBP	Q13148	0.434	-0.14	0.1465	0.4997	0.6675	yes
ATP5O	P48047	0.181	0.056	0.1185	0.5009	0.6676	no
MDH2	P40926	-0.28	0.028	-0.126	0.5024	0.6676	no
EIF4A1	P60842	0.12	0.113	0.1165	0.5025	0.6676	no
DDX17	H3BLZ8	0.09	0.14	0.115	0.5087	0.6739	yes
MNDA	P41218	-0.06	0.31	0.127	0.5090	0.6739	yes
NACA	E9PAV3	0.046	0.186	0.116	0.5109	0.6752	yes
CCT4	P50991	-0.2	-0.03	-0.115	0.5184	0.6832	no
ZNF788	Q6ZQV5	-0.79	0.383	-0.205	0.5188	0.6832	yes
EFTUD2	Q15029	0.152	0.07	0.111	0.5244	0.6893	yes
CMPK1	P30085	0.212	0.014	0.113	0.5279	0.6920	yes
HNRNPUL2	Q1KMD3	-0.02	-0.21	-0.113	0.5283	0.6920	yes
GAPDH	P04406	0.04	0.181	0.1105	0.5306	0.6937	yes
TRA2B	P62995	0.084	-0.33	-0.123	0.5320	0.6945	yes
FERMT3	Q86UX7	0.038	0.181	0.1095	0.5343	0.6958	no
FKBP4	Q02790	-0.1	-0.11	-0.108	0.5349	0.6958	yes
NCL	P19338	0.16	0.055	0.1075	0.5385	0.6993	yes
HADHB	P55084	0.117	0.095	0.106	0.5406	0.7007	no
GNB2	P62879	-0.21	-0.01	-0.109	0.5433	0.7030	no
SRSF9	Q13242	0.118	-0.37	-0.124	0.5444	0.7032	yes
PCMT1	H7BY58	0.169	0.042	0.1055	0.5475	0.7055	no
EEF1G	P26641	0.28	-0.59	-0.157	0.5491	0.7055	no
B4DLN1	B4DLN1	0.054	0.155	0.1045	0.5493	0.7055	no
COPB2	P35606	-0.47	0.199	-0.138	0.5500	0.7055	no
ENO3	P13929	-0	-0.21	-0.107	0.5511	0.7056	no
CCT7	Q99832	0.049	-0.27	-0.112	0.5520	0.7057	no
HSP90AB1	P08238	0.144	0.062	0.103	0.5538	0.7067	yes
LRPPRC	P42704	-0.03	0.242	0.1075	0.5574	0.7090	yes
NIFK	Q9BYG3	-0.12	-0.09	-0.102	0.5575	0.7090	yes
PPP1CC	P36873-2	0.917	-0.5	0.2095	0.5630	0.7130	yes
ATP2A3	Q93084-5	0.202	0.004	0.103	0.5639	0.7130	yes

ATP2A2	P16615	0.202	0.004	0.103	0.5639	0.7130	no
HNRNPU	Q00839	-0.08	-0.12	-0.1	0.5654	0.7130	yes
TCP1	P17987	0.122	0.077	0.0995	0.5654	0.7130	no
SQSTM1	Q13501	0.099	0.099	0.099	0.5667	0.7134	yes
MRPL57	Q9BQC6	-0.15	-0.05	-0.099	0.5699	0.7162	no
SMC4	Q9NTJ3	0.241	-0.03	0.1035	0.5726	0.7184	yes
COPG1	Q9Y678	0.078	0.114	0.096	0.5786	0.7247	no
VAV1	P15498	0.066	0.125	0.0955	0.5812	0.7267	no
RPS27	P42677	-0.06	-0.13	-0.094	0.5897	0.7352	no
VASP	P50552	-0.47	0.219	-0.125	0.5906	0.7352	no
ENO1	P06733	-0.02	-0.17	-0.095	0.5909	0.7352	yes
BAZ1A	Q9NRL2	-0.15	-0.03	-0.093	0.5940	0.7360	yes
PTGES3	Q15185	0.001	0.188	0.0945	0.5944	0.7360	no
FBL	P22087	-0.36	0.137	-0.109	0.5945	0.7360	yes
PLEC	Q15149	0.374	-0.15	0.1105	0.5972	0.7379	no
PYCRL	Q53H96	-0.11	-0.07	-0.091	0.5980	0.7379	no
DYNC1H1	Q14204	-0.01	-0.17	-0.09	0.6113	0.7530	no
GLTSCR2	Q9NZM5	0.25	-0.06	0.094	0.6131	0.7538	yes
TXNL1	O43396	0.041	0.134	0.0875	0.6140	0.7538	yes
RUVBL2	Q9Y230	0.137	0.037	0.087	0.6164	0.7555	yes
SMARCA5	O60264	-0.18	0	-0.088	0.6184	0.7567	yes
SNRNP200	O75643	-0.17	-0	-0.088	0.6195	0.7568	yes
HDAC1	Q13547	0.215	-0.44	-0.111	0.6230	0.7580	yes
KRT6B	P04259	-0.6	0.987	0.194	0.6232	0.7580	no
SMCHD1	A6NHR9	-0.24	0.057	-0.091	0.6235	0.7580	no
SYNCRIP	O60506	0.065	0.101	0.083	0.6299	0.7642	yes
RQCD1	Q92600-2	-0.21	0.418	0.1065	0.6307	0.7642	no
BTK	Q06187-2	0.331	-0.14	0.096	0.6340	0.7670	yes
HUWE1	Q7Z6Z7	0.324	-0.57	-0.125	0.6377	0.7702	yes
HSD17B11	Q8NBQ5	-0.06	0.228	0.086	0.6390	0.7706	no
ACLY	P53396	-0.16	0.002	-0.081	0.6451	0.7759	no
CDC42	P60953-1	-0.34	0.149	-0.094	0.6456	0.7759	no
UBA1	P22314	-0.04	0.206	0.0825	0.6477	0.7773	yes
S100A9	P06702	0.048	0.109	0.0785	0.6489	0.7774	no
TARS	P26639	-0.32	0.141	-0.09	0.6551	0.7835	no
UPF1	Q92900	0.03	-0.19	-0.08	0.6563	0.7835	yes
PSMD2	Q13200	-0.2	0.042	-0.08	0.6572	0.7835	no
HNRNPA3	P51991	-0.07	-0.08	-0.076	0.6603	0.7852	yes
CDC37	Q16543	-0.01	-0.14	-0.077	0.6606	0.7852	no
MRPL4	Q9BYD3	-0.25	0.086	-0.082	0.6618	0.7853	no
DDX50	Q9BQ39	0.22	-0.06	0.079	0.6658	0.7883	yes
GALK1	P51570-2	-0.01	-0.14	-0.075	0.6665	0.7883	no
RRM1	P23921	-0.15	-0	-0.074	0.6719	0.7930	no
PRPF8	Q6P2Q9	-0.41	0.225	-0.094	0.6735	0.7930	yes
DDX1	Q92499	-0.1	0.262	0.08	0.6736	0.7930	yes
TFAP4	Q01664	0.264	-0.11	0.0795	0.6763	0.7949	yes

SRP9	P49458	0.217	-0.07	0.076	0.6776	0.7952	no
CORO1C	Q9ULV4-3	0.187	-0.04	0.074	0.6791	0.7957	no
KDM1A	O60341-2	0.189	-0.36	-0.087	0.6820	0.7974	yes
DAZAP1	Q96EP5	-0.11	-0.03	-0.071	0.6827	0.7974	yes
MRPL30	Q8TCC3-2	-0.25	0.1	-0.076	0.6871	0.8012	no
TOP2A	P11388-4	-0.38	0.212	-0.086	0.6919	0.8048	yes
HSPA5	P11021	-0.03	-0.11	-0.068	0.6931	0.8048	no
CLIC1	O00299	0.085	0.05	0.0675	0.6941	0.8048	yes
KPRP	Q5T749	0.062	0.072	0.067	0.6960	0.8048	no
MYH7B	A7E2Y1	-0.55	0.824	0.137	0.6965	0.8048	no
DPYSL2	Q16555	0.321	-0.16	0.079	0.6966	0.8048	no
PGD	P52209	-0.13	0.001	-0.067	0.7024	0.8094	no
BTF3	P20290	-0.01	0.147	0.0665	0.7041	0.8094	yes
WDR43	Q15061	0.359	-0.56	-0.102	0.7044	0.8094	yes
PFKP	Q01813	0.018	-0.15	-0.066	0.7067	0.8094	no
PRPF19	Q9UMS4	-0.12	-0.01	-0.065	0.7070	0.8094	yes
ATP5A1	P25705	0.137	-0.01	0.0655	0.7071	0.8094	no
FLNB	O75369-8	0.123	0.006	0.0645	0.7098	0.8112	no
RPL12	P30050	0.082	0.044	0.063	0.7134	0.8141	no
DDX3Y	O15523	-0.14	0.013	-0.064	0.7162	0.8148	yes
POLRMT	O00411	-0.01	0.14	0.0635	0.7162	0.8148	no
EIF3CL	B5ME19	0.327	-0.18	0.0735	0.7202	0.8181	no
TKT	P29401-2	-0.01	0.131	0.0605	0.7282	0.8259	no
TALDO1	P37837	0.094	-0.22	-0.064	0.7314	0.8283	no
SRSF5	Q13243	0.028	-0.15	-0.06	0.7326	0.8284	yes
RUVBL1	Q9Y265	0.05	0.063	0.0565	0.7413	0.8369	yes
YWHAB	P31946	-0.11	-0	-0.056	0.7457	0.8405	no
PRKDC	P78527	0.05	0.06	0.055	0.7479	0.8405	yes
DDX6	P26196	0.049	0.061	0.055	0.7479	0.8405	yes
GART	P22102	-0.14	0.268	0.062	0.7494	0.8407	no
PRPS1	P60891	0.141	-0.26	-0.062	0.7505	0.8407	no
DDX5	P17844	0.126	-0.02	0.055	0.7519	0.8407	yes
HSP90AA1	P07900-2	0.022	-0.13	-0.055	0.7526	0.8407	no
EEF1D	P29692	0.182	-0.31	-0.064	0.7544	0.8415	yes
CLTA	P09496-2	-0.18	0.07	-0.056	0.7557	0.8417	no
GNAI2	P04899	0.382	-0.25	0.068	0.7582	0.8432	no
ALDOA	P04075-2	0.085	-0.19	-0.055	0.7645	0.8489	no
NEK9	Q8TD19	-0.57	0.41	-0.08	0.7728	0.8561	yes
LMNB1	P20700	0.174	-0.29	-0.058	0.7733	0.8561	yes
DDX3X	O00571	-0.14	0.04	-0.05	0.7758	0.8576	yes
KRT6A	P02538	-0.6	0.804	0.1	0.7793	0.8602	no
CCT8	P50990	0.02	0.074	0.047	0.7838	0.8607	no
RPS3	P23396	0.018	0.076	0.047	0.7839	0.8607	yes
HNRNPA3	P51991-2	-0.01	-0.08	-0.047	0.7842	0.8607	yes
SNW1	Q13573	-0.21	0.106	-0.05	0.7863	0.8607	yes
CCT3	P49368	0.248	-0.14	0.052	0.7863	0.8607	no

HBA1	P69905	-0.11	0.209	0.05	0.7869	0.8607	no
HNRNPAB	Q99729-3	-0.05	-0.04	-0.046	0.7878	0.8607	yes
SLC25A1	P53007	-0.13	0.039	-0.046	0.7926	0.8647	no
HNRNPK	P61978-2	0.142	-0.24	-0.049	0.7973	0.8685	yes
RAP1A	P62834	-0.32	0.216	-0.053	0.7993	0.8694	no
RNF5	Q99942	-0.03	-0.06	-0.043	0.8014	0.8694	no
ASS1	P00966	0.1	-0.01	0.043	0.8033	0.8694	no
DNM2	P50570	-0.06	-0.03	-0.043	0.8036	0.8694	no
PDS5B	Q9NTI5	0.108	-0.02	0.043	0.8039	0.8694	yes
USP4	Q13107	-0.33	0.229	-0.051	0.8093	0.8739	yes
GARS	P41250	-0.32	0.225	-0.05	0.8135	0.8772	no
EIF3L	B0QY89	-0.21	0.309	0.0475	0.8181	0.8808	no
DIMT1	Q9UNQ2	0.133	-0.22	-0.042	0.8228	0.8846	yes
RPL10A	P62906	0.119	-0.04	0.0385	0.8253	0.8860	no
CBFB	Q13951-2	0.14	-0.06	0.0385	0.8273	0.8861	yes
SFPQ	P23246	-0.25	0.341	0.0465	0.8288	0.8861	yes
CCT5	P48643	0.154	-0.08	0.0385	0.8290	0.8861	no
EIF3G	O75821	0.19	-0.11	0.038	0.8359	0.8923	yes
ACTN4	O43707	0.184	-0.26	-0.04	0.8395	0.8948	yes
RPL8	P62917	-0.06	-0.01	-0.034	0.8423	0.8965	no
TOP1	P11387	-0.03	0.094	0.034	0.8439	0.8969	yes
SLC25A6	P12236	0.308	-0.23	0.04	0.8475	0.8979	no
HSD17B4	P51659	-0.02	0.089	0.033	0.8482	0.8979	no
ZC3HAV1	C9J6P4	0.927	-0.77	0.079	0.8484	0.8979	yes
CHMP4B	Q9H444	-0.18	0.109	-0.033	0.8560	0.9046	yes
MCM5	P33992	0.135	-0.2	-0.033	0.8593	0.9064	yes
RBM25	P49756	0.237	-0.17	0.034	0.8601	0.9064	yes
PREB	Q9HCU5	0.132	-0.08	0.0285	0.8718	0.9174	yes
ACTR3B	Q9P1U1	-0.16	0.102	-0.028	0.8764	0.9209	no
TCEB1	Q15369	0.198	-0.14	0.0285	0.8784	0.9218	no
MAPK1	P28482	-0.24	0.299	0.0305	0.8834	0.9257	yes
CAPZB	P47756-2	0.138	-0.09	0.024	0.8926	0.9330	no
CORO1A	P31146	0.047	-0	0.023	0.8929	0.9330	no
SNAP23	O00161	0.135	-0.18	-0.025	0.8944	0.9333	no
CRKL	P46109	-0.15	0.107	-0.023	0.9004	0.9383	no
HSPA4	P34932	0.412	-0.48	-0.032	0.9037	0.9402	no
BAG6	P46379-3	0.178	-0.22	-0.023	0.9048	0.9402	yes
TRAP1	Q12931	-0.08	0.038	-0.02	0.9076	0.9418	no
E7EVH7	E7EVH7	-0.12	0.156	0.0205	0.9097	0.9426	no
KRT5	P13647	-0.5	0.44	-0.028	0.9170	0.9468	no
EIF4A3	P38919	0.045	-0.08	-0.018	0.9170	0.9468	yes
DDX21	Q9NR30	-0.15	0.111	-0.019	0.9181	0.9468	yes
OTUB1	Q96FW1	0.302	-0.26	0.0215	0.9188	0.9468	no
TLN1	Q9Y490	0.035	-0	0.0165	0.9229	0.9497	no
ATP13A1	Q9HD20	0.147	-0.18	-0.018	0.9248	0.9503	no
HNRNPA0	Q13151	0.087	-0.12	-0.016	0.9300	0.9541	yes

RAB35	Q15286	0.251	-0.29	-0.018	0.9310	0.9541	no
DIAPH1	O60610	-0.05	0.077	0.014	0.9354	0.9572	no
FYTTD1	Q96QD9	-0.33	0.299	-0.017	0.9403	0.9610	yes
DECR1	Q16698	-0.1	0.118	0.0115	0.9481	0.9676	no
RPL14	P50914	0.058	-0.04	0.009	0.9582	0.9766	no
HNRNPC	P07910-2	0.145	-0.16	-0.008	0.9652	0.9811	yes
TECR	Q9NZ01	0.147	-0.16	-0.008	0.9653	0.9811	no
SUCLG1	P53597	-0.1	0.109	0.007	0.9683	0.9828	no
DHX9	Q08211	-0.03	0.042	0.0065	0.9697	0.9829	yes
ELAVL1	Q15717-2	0.265	-0.28	-0.007	0.9713	0.9832	yes
PSMC4	P43686	0.207	-0.19	0.0065	0.9730	0.9836	yes
U2AF1	Q01081-2	-0.17	0.18	0.006	0.9744	0.9837	yes
EPRS	P07814	0.081	-0.07	0.005	0.9770	0.9850	no
PTDSS1	P48651	0.016	-0.03	-0.005	0.9790	0.9856	no
MTHFD1	F5H2F4	-0.09	0.102	0.004	0.9818	0.9872	no
EDC4	Q6P2E9	0.491	-0.5	-0.004	0.9885	0.9925	yes
YARS	P54577	-0.38	0.386	0.003	0.9900	0.9927	no
EIF3A	Q14152	0.317	-0.31	0.002	0.9928	0.9941	no
CCT6A	P40227	-0.02	0.015	-5E-04	0.9977	0.9977	no

Table S5. List of enriched pathways among VCP interactome. VCP-interacting network identified by mass spectrometry-based analysis of VCP interactome was interrogated in a functional enrichment overlapping analysis across the MsigDB database (C2 collection). All significantly enriched pathways are listed (-log10 (FDR)>1) and selected pathways involved in DNA repair, synthesis and cell cycle are highlighted in bold characters. Results are rank ordered based on -log10 (FDR).

MSigDB Pathways	-log10(FDR)
KEGG_REGULATION_OF_ACTIN_CYTOSKELETON	5.43
BIOCARTA_SALMONELLA_PATHWAY	5.43
BIOCARTA_RHO_PATHWAY	5.43
BIOCARTA_CDC42RAC_PATHWAY	5.43
BIOCARTA_ACTINY_PATHWAY	4.99
REACTOME_G1_S_TRANSITION	**4.87**
REACTOME_DNA_REPAIR	**4.87**
REACTOME_S_PHASE	**4.87**
REACTOME_M_G1_TRANSITION	**4.66**
REACTOME_SEMA4D_INDUCED_CELL_MIGRATION_AND_GROWTH_CONE_COLLAPSE	4.63
KEGG_PATHOGENIC_ESCHERICHIA_COLI_INFECTION	4.37
REACTOME_SEMA4D_IN_SEMAPHORIN_SIGNALING	4.37
REACTOME_SYNTHESIS_OF_DNA	**4.37**
REACTOME_MITOTIC_G1_G1_S_PHASES	**4.37**
BIOCARTA_MPR_PATHWAY	4.23
REACTOME_CELL_CYCLE_CHECKPOINTS	**3.65**
KEGG_MISMATCH_REPAIR	**3.47**
KEGG_TIGHT_JUNCTION	3.47
REACTOME_SMOOTH_MUSCLE_CONTRACTION	3.38
REACTOME_TGF_BETA_RECEPTOR_SIGNALING_ACTIVATES_SMADS	3.29
KEGG_HOMOLOGOUS_RECOMBINATION	**3.18**
REACTOME_REMOVAL_OF_THE_FLAP_INTERMEDIATE_FROM_THE_C_STRAND	3.08
REACTOME_SIGNALING_BY_TGF_BETA_RECEPTOR_COMPLEX	3.07
REACTOME_CYCLIN_E_ASSOCIATED_EVENTS_DURING_G1_S_TRANSITION_	**3.02**
REACTOME_SEMAPHORIN_INTERACTIONS	2.99
REACTOME_MITOTIC_M_M_G1_PHASES	**2.93**
REACTOME_RESOLUTION_OF_AP_SITES_VIA_THE_SINGLE_NUCLEOTIDE_REPLACEMENT_PATHWAY	**2.91**
KEGG_BASE_EXCISION_REPAIR	**2.91**
KEGG_DNA_REPLICATION	**2.87**
KEGG_VIRAL_MYOCARDITIS	2.87
REACTOME_REPAIR_SYNTHESIS_FOR_GAP_FILLING_BY_DNA_POL_IN_TC_NER	**2.76**
REACTOME_DNA_REPLICATION	**2.71**
REACTOME_PROCESSIVE_SYNTHESIS_ON_THE_LAGGING_STRAND	**2.69**
REACTOME_TGF_BETA_RECEPTOR_SIGNALING_IN_EMT_EPITHELIAL_TO_MESENCHYMAL_TRANSITION	2.61
REACTOME_HOMOLOGOUS_RECOMBINATION_REPAIR_OF_REPLICATION_INDEPENDENT_DOUBLE_STRAND_BREAKS	**2.54**
REACTOME_MUSCLE_CONTRACTION	2.51
REACTOME_CDK_MEDIATED_PHOSPHORYLATION_AND_REMOVAL_OF_CDC6	**2.48**
REACTOME_BASE_EXCISION_REPAIR	**2.44**
REACTOME_LAGGING_STRAND_SYNTHESIS	**2.44**
KEGG_FC_GAMMA_R_MEDIATED_PHAGOCYTOSIS	2.43
REACTOME_P53_INDEPENDENT_G1_S_DNA_DAMAGE_CHECKPOINT	**2.43**
REACTOME_AUTODEGRADATION_OF_THE_E3_UBIQUITIN_LIGASE_COP1	2.43
REACTOME_SCF_BETA_TRCP_MEDIATED_DEGRADATION_OF_EMI1	2.43
REACTOME_DOWNREGULATION_OF_SMAD2_3_SMAD4_TRANSCRIPTIONAL_ACTIVITY	2.43
REACTOME_VIF_MEDIATED_DEGRADATION_OF_APOBEC3G	2.43
REACTOME_DESTABILIZATION_OF_MRNA_BY_AUF1_HNRNP_D0	2.41
PID_RAC1_PATHWAY	2.38
REACTOME_CDT1_ASSOCIATION_WITH_THE_CDC6_ORC_ORIGIN_COMPLEX	2.34
REACTOME_SCFSKP2_MEDIATED_DEGRADATION_OF_P27_P21	2.34
REACTOME_P53_DEPENDENT_G1_DNA_DAMAGE_RESPONSE	**2.32**
REACTOME_DOWNREGULATION_OF_TGF_BETA_RECEPTOR_SIGNALING	2.31
REACTOME_REGULATION_OF_APOPTOSIS	2.31
REACTOME_FORMATION_OF_INCISION_COMPLEX_IN_GG_NER	**2.31**
REACTOME_CELL_CYCLE_MITOTIC	**2.29**
REACTOME_DOUBLE_STRAND_BREAK_REPAIR	**2.28**
REACTOME_METABOLISM_OF_RNA	2.26
REACTOME_ER_PHAGOSOME_PATHWAY	2.26
REACTOME_ACTIVATION_OF_NF_KAPPAB_IN_B_CELLS	2.20
REACTOME_AUTODEGRADATION_OF_CDH1_BY_CDH1_APC_C	2.20
REACTOME_SIGNALING_BY_WNT	2.18
REACTOME_ASSEMBLY_OF_THE_PRE_REPLICATIVE_COMPLEX	**2.18**
REACTOME_EXTENSION_OF_TELOMERES	**2.17**
REACTOME_ORC1_REMOVAL_FROM_CHROMATIN	2.15

PID_CDC42_PATHWAY	2.08
REACTOME_DNA_STRAND_ELONGATION	**2.06**
REACTOME_APC_C_CDH1_MEDIATED_DEGRADATION_OF_CDC20_AND_OTHER_APC_C_CDH1_TARGETED_PROTEINS_IN_LATE_MITOSIS_EARLY_G1	2.05
REACTOME_ACTIVATION_OF_THE_PRE_REPLICATIVE_COMPLEX	**2.03**
REACTOME_APC_C_CDC20_MEDIATED_DEGRADATION_OF_MITOTIC_PROTEINS	2.03
REACTOME_HOST_INTERACTIONS_OF_HIV_FACTORS	2.02
REACTOME_ANTIGEN_PROCESSING_CROSS_PRESENTATION	1.98
REACTOME_PURINE_METABOLISM	**1.97**
REACTOME_GLOBAL_GENOMIC_NER_GG_NER	**1.90**
REACTOME_REGULATION_OF_MRNA_STABILITY_BY_PROTEINS_THAT_BIND_AU_RICH_ELEMENTS	1.84
KEGG_HYPERTROPHIC_CARDIOMYOPATHY_HCM	1.83
REACTOME_TRANSCRIPTIONAL_ACTIVITY_OF_SMAD2_SMAD3_SMAD4_HETEROTRIMER	1.83
REACTOME_REGULATION_OF_MITOTIC_CELL_CYCLE	**1.83**
REACTOME_IRAK2_MEDIATED_ACTIVATION_OF_TAK1_COMPLEX_UPON_TLR7_8_OR_9_STIMULATION	1.83
REACTOME_APOPTOSIS	1.83
REACTOME_ACTIVATION_OF_ATR_IN_RESPONSE_TO_REPLICATION_STRESS	**1.83**
KEGG_RIBOSOME	1.80
REACTOME_MEMBRANE_BINDING_AND_TARGETTING_OF_GAG_PROTEINS	1.76
KEGG_DILATED_CARDIOMYOPATHY	1.74
REACTOME_CELL_CYCLE	**1.74**
REACTOME_NFKB_IS_ACTIVATED_AND_SIGNALS_SURVIVAL	1.70
REACTOME_PURINE_RIBONUCLEOSIDE_MONOPHOSPHATE_BIOSYNTHESIS	**1.70**
REACTOME_REGULATION_OF_THE_FANCONI_ANEMIA_PATHWAY	**1.70**
KEGG_NUCLEOTIDE_EXCISION_REPAIR	**1.69**
REACTOME_DOWNSTREAM_SIGNALING_EVENTS_OF_B_CELL_RECEPTOR_BCR	1.69
REACTOME_TRANSCRIPTION_COUPLED_NER_TC_NER	**1.68**
REACTOME_G2_M_CHECKPOINTS	**1.68**
REACTOME_DOWNREGULATION_OF_ERBB2_ERBB3_SIGNALING	1.66
REACTOME_P75NTR_RECRUITS_SIGNALLING_COMPLEXES	1.66
REACTOME_RECEPTOR_LIGAND_BINDING_INITIATES_THE_SECOND_PROTEOLYTIC_CLEAVAGE_OF_NOTCH_RECEPTOR	1.66
PID_ERBB1_DOWNSTREAM_PATHWAY	1.59
REACTOME_SPRY_REGULATION_OF_FGF_SIGNALING	1.55
REACTOME_ASSOCIATION_OF_LICENSING_FACTORS_WITH_THE_PRE_REPLICATIVE_COMPLEX	**1.55**
REACTOME_P75NTR_SIGNALS_VIA_NFKB	1.55
REACTOME_NUCLEOTIDE_EXCISION_REPAIR	**1.55**
REACTOME_ACTIVATION_OF_IRF3_IRF7_MEDIATED_BY_TBK1_IKK_EPSILON	1.55
REACTOME_TRAF6_MEDIATED_INDUCTION_OF_TAK1_COMPLEX	1.55
KEGG_VASCULAR_SMOOTH_MUSCLE_CONTRACTION	1.51
REACTOME_NRIF_SIGNALS_CELL_DEATH_FROM_THE_NUCLEUS	1.50
KEGG_LEUKOCYTE_TRANSENDOTHELIAL_MIGRATION	1.44
REACTOME_METABOLISM_OF_MRNA	1.44
BIOCARTA_HIVNEF_PATHWAY	1.43
REACTOME_INFLUENZA_LIFE_CYCLE	1.38
REACTOME_SIGNALING_BY_CONSTITUTIVELY_ACTIVE_EGFR	1.37
REACTOME_SIGNALING_BY_THE_B_CELL_RECEPTOR_BCR	1.37
REACTOME_OXYGEN_DEPENDENT_PROLINE_HYDROXYLATION_OF_HYPOXIA_INDUCIBLE_FACTOR_ALPHA	1.37
REACTOME_HIV_INFECTION	1.36
PID_PDGFRB_PATHWAY	1.34
REACTOME_ANTIGEN_PROCESSING_UBIQUITINATION_PROTEASOME_DEGRADATION	1.32
REACTOME_ANTIVIRAL_MECHANISM_BY_IFN_STIMULATED_GENES	1.30
REACTOME_INSULIN_SYNTHESIS_AND_PROCESSING	1.25
REACTOME_METABOLISM_OF_NUCLEOTIDES	**1.20**
PID_E2F_PATHWAY	1.17
REACTOME_TELOMERE_MAINTENANCE	**1.16**
REACTOME_CYTOSOLIC_TRNA_AMINOACYLATION	1.16
REACTOME_REGULATION_OF_HYPOXIA_INDUCIBLE_FACTOR_HIF_BY_OXYGEN	1.13
REACTOME_EGFR_DOWNREGULATION	1.13
REACTOME_FANCONI_ANEMIA_PATHWAY	**1.13**
REACTOME_PEPTIDE_CHAIN_ELONGATION	1.12
REACTOME_APC_C_CDC20_MEDIATED_DEGRADATION_OF_CYCLIN_B	1.11
REACTOME_AXON_GUIDANCE	1.10
PID_SMAD2_3NUCLEAR_PATHWAY	1.09
REACTOME_ACTIVATED_NOTCH1_TRANSMITS_SIGNAL_TO_THE_NUCLEUS	1.09
REACTOME_SMAD2_SMAD3_SMAD4_HETEROTRIMER_REGULATES_TRANSCRIPTION	1.09
REACTOME_ENDOSOMAL_SORTING_COMPLEX_REQUIRED_FOR_TRANSPORT_ESCRT	1.09
REACTOME_INTERFERON_SIGNALING	1.08
REACTOME_CLASS_I_MHC_MEDIATED_ANTIGEN_PROCESSING_PRESENTATION	1.08
REACTOME_MRNA_PROCESSING	1.07
REACTOME_APC_CDC20_MEDIATED_DEGRADATION_OF_NEK2A	1.07
REACTOME_MEIOTIC_RECOMBINATION	**1.05**
REACTOME_INFLUENZA_VIRAL_RNA_TRANSCRIPTION_AND_REPLICATION	1.01

Table S6. List of VCP-interacting partners identified by mass spectrometry-based interactome analysis in the MV4-11 AML cell line compared to the HEK-293T cell line. VCP-interacting proteins are listed according to their mass-spectrometry detection in the MV4-11 cell line, in the HEK-293T cell line or in both cellular contexts. High confidence VCP-interacting proteins are also listed according to the cellular context.

All_MV411 specific (n=441)	All_HEK specific (n=474)	All_HEK_MV411 common (n=294)	High confidence_MV411 specific (n=80)	High confidence_HEK specific (n=26)	High confidence_HEK _MV411 common (n=12)
ACTN4	C17orf103	RPS11	ACTB	METTL21D	VCP
CNBP	RPS17	ACTR3	HERC2	CSTF2	RAE1
TKT	LTV1	RAE1	PEO1	TOR1AIP2	UBXN2B
PFKP	C22orf28	HSPB1	AIMP2	CSTF3	ASPSCR1
ATP5F1	RYR3	RPL10A	RPA2	OTUD6A	NPLOC4
DECR1	IRS4	QARS	DERL1	IGHG1	PPP1R7
MYL4	U2SURP	RPS18	APRT	LGALS7B	NGLY1
MRPL4	SLC25A3	BRIX1	HSPA6	UBE4B	UBXN6
ESYT1	AIFM1	HSD17B10	ARPC2	KRT74	UBXN2A
RAC1	RNF25	DAZAP1	TMOD3	SPRR2E	VCPIP1
ATP13A1	G3BP1	RPL19	NEURL4	FAF1	NSFL1C
MTA2	HSD17B2	MATR3	ACTBL2	SPRR2F	UFD1L
SLTM	LMAN1	DDX5	SNRPE	FAM136A	
TLN1	DDB1	VCPIP1	FKBP1A	CSTF1	
RAP1A	ANXA1	DSP	MYL6B	IGKC	
HMGB3	CSTF1	GALK1	RPLP1	AKAP9	
GNAI3	UGGT1	EIF3B	UBXN7	SERPINB3	
SQRDL	IGF2BP3	RPS5	FAF2	CSTF2T	
DPYSL2	SEC23B	RPL7A	FAM104A	RAD23B	
PTK2B	MTM1	UBA1	LRRC59	KRT15	
MAX	UBB	FASN	ARPC4	UBL7	
MSN	TIA1	DARS	MYH11	SPRR1B	
DNAJB1	USP47	SFPQ	ALDH1B1	HTRA2	
RPL36A	SMARCC2	PSMA1	SSB	S100A9	
RRP7A	G2E3	RPL29	ARPC3	SERPINB4	
NAT10	PKP1	KRT1	MYH9	S100A8	
GNAI2	SMARCC1	RPL35	MYL6		
SHC1	CD2BP2	CLTA	RAB27A		
HERC2	THRAP3	RPS23	RUNX1		
FARSB	ATP5D	HSPA1L	SAMHD1		
RUNX3	AADACL2	TRA2B	RPA1		
IMPDH2	LRRN1	HIST1H1E	TFEB		
SQSTM1	SRPK1	LGALS1	GLUL		
RAC2	ACAD8	PCMT1	POTEF		
PDIA3	ZFP106	SLC25A5	EIF5A		
ANLN	PUF60	YWHAE	XRCC1		
CHMP5	PRDX6	HSPD1	TTN		
KRT13	ILF2	RPL12	MYO5A		

PSMC2	KV402_HUMAN	TUBB	ADAR
MYL12A	RIOK1	HNRNPR	PSMD4
TPI1	ASCC3	CCT2	PGAM1
SLC25A1	ACTL6A	NUP153	LARS
DOCK8	LARP7	PSMD3	HNRNPF
MRPL33	KPNA2	MYH9	UCHL5
MYO1C	SMC3	ATP5B	HMGB3
WDR1	SNRNP70	HSD17B4	GSN
SRSF6	ACAT1	NPM1	APEX1
GRB2	NUDT1	XRCC6	UBA52
TPM3	SMAD3	NOP2	MYL9
HIST1H2AD	MRPS34	PSMD11	MYH14
BOP1	PLK1	LARS	SSBP1
CDK1	TAGLN2	CNOT1	ARPC1A
PRPF19	DAP3	CCT8	GNB2L1
RPA2	RBM10	RPS4X	CEBPA
GLTSCR2	BCLAF1	LUC7L2	PSMC2
FAM98B	GOLGA3	RPS3	RPS27A
HSP90AB2P	FAM98A	ACTC1	SYVN1
MRPL47	PRKAR2A	ATAD3B	MYL12A
COPA	RAD23B	PRDX1	LIG3
EIF1AX	SKP1	UFD1L	PAICS
RPLP1	EXOSC2	RPL32	MAX
WDR43	HIST2H4A	HSPA4	TRAFD1
COPG1	A2ML1	SMC1A	GMFG
B4DLN1	TIAL1	HSPA8	UBP1
NDUFS4	KT81L_HUMAN	DHX15	ATIC
CSDE1	GAN	RPS13	RPA3
RAB35	SRI	RPSA	ACTR2
ERLIN2	MRPL24	GSTP1	TFE3
HSD17B11	PELO	RCC2	ACTC1
IDH2	TUBB2C	AHCY	PARP1
ASS1	CSTF3	RPS8	MYO18A
RAB14	CCAR1	TUBA1B	FAM8A1
SND1	POLR2B	PSMC6	ACTG1
RPS27A	RPS28	KRT17	MYO1C
MRPS12	FABP5	RPL4	WDR1
GMFG	OTUD4	HNRNPUL2	RPLP2
PTGES3	IGHG2	DCD	MIOS
EFTUD2	USP7	RPL10	ARMCX3
BTF3	YWHAQ	PPP1CC	TFCP2
CS	OTUD3	RPS2	UNC45A
DYNC1H1	KIF11	CCT4	
FERMT3	PSMB6	SNRPE	

ABCF2	ACOX1	MTHFD1
TECR	KIF5B	FAF1
UBXN7	UBXN4	RPL7
PRKCD	NKRF	DDX39A
ARPC3	C17orf79	HNRNPA0
MYL6	SUPT5H	PCBP1
RUNX1	XRN2	GSN
SMC4	FUS	TCP1
NOP58	PWP2	KRT77
RPL22L1	ELAC2	TUBA1A
FKBP4	DNAH12	EIF3D
ECM1	SPTBN1	PCNA
MNDA	CAMK2D	RBBP4
KIF14	EIF3M	RPL22
EIF4A3	LDHB	EPRS
RTCB	LTBP1	HSPA6
FAM83H	SNRPA	MYH10
HUWE1	CCDC108	RPS26
BTK	DHX30	RUVBL1
PFKL	EHMT2	ASPSCR1
MRPL57	EXOSC10	PRPS1
HCK	PRDX4	HNRNPK
ZC3HAV1	FAM194B	PSMD2
TARS	LSM12	SMCHD1
CSTA	KRT37	ACLY
USP4	SNRPF	HNRNPUL1
ARPC5	SPTAN1	MCM5
MCM3	ATF7	PPIB
SSRP1	NUP88	CUL3
RPS17L	CSDA	RPL17
KDM1A	SEPT2	UBXN2B
ETFA	HP1BP3	PPIA
POLRMT	PEX1	SF3B2
MRPS7	MYH13	MDH2
CHAF1A	HSPA4L	SENP3
NHP2	KV201_HUMAN	TUFM
KCTD10	KCTD5	RPL6
FAU	SF3A3	RPL30
PAFAH1B3	C10orf40	RUVBL2
CSK	CSTF2T	CSNK1A1
BCKDK	FUBP1	RPLP2
HIST1H2BN	HCFC1	RPS24
MRTO4	KRT15	RPL27
LUC7L	EXOSC9	RPL24

GANAB	FN1	VCP
EFCAB14	UBL7	ALDOA
PGAM1	DDX24	SRSF3
SMARCA5	RPS21	PLAA
SEC13	ATP1A1	KRT6A
DGKZ	USP9X	ATAD3A
ZYX	C7orf36	FAM104A
NACAP1	EML5	FAF2
UNC13D	TAB1	CLTC
BOLA2	GAA	PTBP1
PSMC4	METTL21D	DDX50
RPN1	PFN2	HNRNPC
DBT	PRPF39	HSP90AA1
TFE3	LGALS7B	PARP1
CALR	STK38L	DHX9
WARS	SPRR2F	CCT7
AURKAIP1	KIAA1217	KRT2
CORO1C	LIN28B	RPS15
ACADVL	C1QBP	YBX1
F2	PCBP3	RPL26
FUOM	NCCRP1	HNRNPH1
NHP2L1	PRPF6	KRT14
DNAJA1	LYST	PGAM5
ZNF593	CPVL	EEF2
MYH11	ABCC12	KRT9
ALDH1B1	GTF3C5	HNRNPD
RPS29	SF3A2	RPLP0
ENO2	SIRPB1	U2AF2
ITPR1	LARP1	SEC16A
TALDO1	TAB2	ATP5A1
EIF5A	HPS1	RPL36
MYO5A	PSMB2	NSF
SLIRP	VIM	CAPZA1
CNOT7	SNRPC	FAM8A1
CDC42	SNRPD1	SRSF7
LRPPRC	PSMD8	RPS6
TPM1	S100A14	RPS20
PDS5B	LGALS3BP	HNRNPA2B1
RRS1	SERPINB13	RPS10
FLNB	SET	RPL21
PRKDC	FAM120A	IGKC
PDCD6IP	KRT8	EIF3A
MYO18A	LDHA	HNRNPF
ANP32A	SVIP	RPL5

LAT2	EIF2S1	HSPA9
NACA	TMPRSS4	EEF1D
GPX4	RAB5A	EIF4A1
TXNL1	UBXN10	RPS15A
MYL1	PHGDH	UBAC2
RPL39	GRIA1	RPL15
BTBD10	XIAP	RPS3A
ACOT9	AMPD1	HSPA5
EIF3F	HSF4	CFL1
VDAC3	RANBP1	CAD
CSE1L	CAP1	RPS12
RBM12B	YTHDC2	PRPF8
DSG1	GALC	SSB
U2AF1	MRPS22	PABPC4
ERH	SNTA1	DDX6
XRCC1	LCE2B	HNRNPM
GART	HEXB	RPL28
APEX1	EXOSC3	RPA1
MRPL11	PYCR1	IARS
ARPC1A	AP2B1	RPL18A
SUN2	PSMD12	KRT16
UTP23	KCTD17	G6PD
RPS4Y1	PRMT1	NGLY1
H2AFZ	WDR60	HNRNPAB
SUPT16H	PEF1	TOP2A
KEAP1	MRPS9	SYNCRIP
H2AFX	C14orf166	GNB2L1
GNB2	STRAP	RPL3
RQCD1	SRRT	HSP90AB1
RNF5	SNRPG	CCT3
TBL2	SFN	HSPE1
DIMT1	RAPSN	RPL18
RAVER1	KRT74	NCL
AIMP2	RRBP1	VARS
IQCB1	FCAMR	MCM2
LASP1	POFUT2	RPS19
CLIC1	FTSJ3	RPL9
DOT1L	PRSS3	NPLOC4
SRP9	MAP6	TRIM28
RPL36AL	EEF1B2	DDX21
CNOT2	MRPL17	EIF3L
TAF6L	YT001_HUMAN	NSFL1C
CHMP4B	DDX46	RRM1
UPF1	AK2	POLR2A

HMGB2	QPCT	RPL13
SNW1	KCTD2	RRP12
RAN	WDR26	HIST1H2AB
ATP2A3	KRT31	DDX17
BANF1	ILF3	ENO3
MRPL22	ARAP3	ACTB
PES1	S100A16	RPL23
FXR1	S100A8	ENO1
PPP1CA	PLOD2	DDX1
PTDSS1	SEPT6	RNPS1
YWHAB	ZDBF2	SRSF9
FKBP8	EIF3H	RPL35A
KIF23	HNRNPH3	JUP
SUCLG1	SPIN1	CBX3
BAG6	ALS2CR11	UBXN6
EEF1A2	KPNA1	PDIA6
HRNR	PSMC1	RPL13A
ARMCX3	SHMT1	RPS7
ARHGDIB	CLASP2	NONO
TRIP6	SRSF4	HNRNPA3
VPS29	TFG	RPL37A
TMA16	KRT86	ELAVL1
ARPC2	KARS	CANX
TK1	SEC31A	MCM6
COPB2	EEF1A1	CSTB
TUBA4A	PSMD14	PABPC1
H3F3A	SSR4	RPL11
HIST1H1B	ARHGEF40	KRT10
TMED3	TNRC6B	CCT5
PML	SRRM1	RPL8
CBFB	EIF2C1	XRCC5
MYH14	PABPN1	TIMM50
HIST2H2BC	NAP1L1	PSMD7
EIF5B	UBE2G2	SNRPB
LMNB1	ACAP1	PFN1
ACTR3B	EIF4B	KRT5
NIFK	SEC23A	PCBP2
TFAM	NSUN2	RPL23A
LSP1	ANXA2	PSMC3
DNAJA2	PHAX	RARS
TPM4	PSMA4	RPL31
LYN	ROCK1	SNRNP200
ZFP91	FAM87A	KRT6B
ATP5O	MFSD6L	RPS25

HMGN2	BUB3	TXN
S100A4	PDCD6	ALB
NOP56	IVNS1ABP	EIF3I
MAPK1	GLUD1	MYL6B
HIST2H3A	UBXN8	CDC5L
ATAD2	RBM4B	LMNA
SAMHD1	PPP1R15A	HNRNPH2
POTEF	PRDX3	SRSF5
PREB	FAM103A1	GAPDH
RREB1	MOV10	RSL1D1
SNAP23	PFAS	OLA1
MYL3	CARM1	SSBP1
GTPBP4	YWHAG	SERBP1
TFAP4	IGF2BP2	LIG3
FLT3	MARCKS	RPS14
E7EVH7	ASPM	DDX3X
MCM7	SRP14	HNRNPU
HNRNPDL	KRT72	HNRNPL
DDX3Y	DENND2C	RPL38
CMPK1	CLCA4	RPS16
TUBB6	HNRPDL	RPS9
MRPL14	CSTF2	MAP7D1
RALA	HDX	FLNA
TCEB1	ACAD9	RPL14
RPL34	WDR33	HNRNPA1
PPP2R1A	PRMT5	FKBP1A
TNKS1BP1	AMFR	EIF3G
GLUL	SNRPA1	CCT6A
DYNLL1	TNRC6A	TRAP1
DIAPH1	INA	PPP1R7
CORO1A	FAM136A	EEF1G
AIMP1	TRIM21	UBXN2A
PPP2R2A	PPM1B	HMGB1
UBA52	KRT4	S100A9
FARSA	RBM14	SNRPD2
LGALS9	CAPRIN1	RPS27
RBBP7	SEC24B	
ADK	THOC4	
ACAA1	FRG1	
STIP1	SEC24C	
PLEC	LCE3D	
SLC25A6	HOXD10	
EDC4	SERPINB4	
RAD50	KRT6C	

HSP90B1	PURA
GSPT1	PRPF31
ARPC1B	FLG2
DNM2	DHX57
MYH7	ANKFY1
SUZ12	CALML3
DBN1	ABCF1
MCM4	SMARCA4
RPL27A	CPSF6
LRRC59	AGL
ARPC4	Q5HYA3_HUMAN
FBL	NEMF
TARDBP	SLAIN2
HADHB	PSMD6
ADAR	WDR77
PTPN6	SRSF1
PSMD4	UBXN11
ERLIN1	AKAP9
UBXN1	MRPS23
RHOG	HSPBP1
HBB	SF3B1
CEBPA	TRA2A
CDC37	NIF3L1
PA2G4	HPRT1
RPA3	TUBA1C
BAZ1A	PSMA7
INPP5D	DNAJC21
ARHGEF1	HDAC2
HSPH1	MSI2
CALM3	AKR1B1
PEO1	MRPS31
ZNF559	PSMB4
FYTTD1	MTDH
NEURL4	SART1
SMN1	OTUD6A
ILVBL	PSMB5
RNH1	NCOA1
COPB1	IGHG1
OTUB1	EIF3C
TMOD1	UBE4B
LRRFIP2	CHD4
TTN	KRT18
VASP	GRN
YARS	PTS

MYL9	KHSRP
ACP1	GGCT
EHD1	PWP1
CIT	DHX29
PAICS	LAS1L
MYO1F	RAB5C
CAT	NME2P1
PKM	HIST1H2BK
TBC1D15	TNRC6C
TPM2	MED15
ARPC5L	MTA1
PIP	ZNF507
FLOT1	AAGAB
FCGR1A	PRDX2
LAP3	MRPS2
MYO1G	CMBL
TUBB4B	SRSF2
HADHA	EIF2C2
RAB27A	NT5C3
RBM39	PCBD1
TFEB	ZC3H11A
HDAC1	TBC1D7
YBX3	MAP1B
FAM104B	SPATA21
HPX	PKM2
UCHL5	ASH2L
MRPL51	PSMD1
NEK9	EWSR1
SYVN1	RNF219
ATP5C1	RBMX
GNB1	PSMC5
UBP1	ZCCHC11
P4HB	LOX
SBSN	FLG
DDX39B	UNC80
MIOS	MDN1
TFCP2	MAP3K7
TOP2B	BAG4
CNOT3	GTF2I
CLEC11A	HTRA2
DERL1	PTBP2
GMPS	AGAP3
LGALS8	C20orf11
GPT2	HSPA1B

EIF3CL	DDX23
ACTBL2	PSMD13
HIST1H1D	MRPS21
KPRP	LYZ
KHDRBS1	ITCH
UHRF1	ZFR
GPX1	MYCBP
HIST1H1C	TOR1AIP2
RBM25	PPP1R11
KIAA0101	EBNA1BP2
RECQL4	CIRBP
PPA1	SART3
HMGA1	SLC5A1
HIST1H4A	SNRPD3
ATP2A2	TSR1
TRAFD1	KATNAL2
ATIC	AKAP8
MT2A	SF3B14
MRPL30	EIF2S2
ACTG1	RNMT
MYH7B	NFKB1
CALM1	E9PLD3_HUMAN
CRKL	KRT35
UNC45A	TUBB8
PGD	MARS
FLII	MRPL16
RPL26L1	S100A7
APRT	SF3B4
PYCRL	EIF3E
MRPS18B	SKIL
TMOD3	ORC4
EEF1A1P5	EXOSC6
MAT2A	PAF1
AARS	PSMA6
TUBB4A	TAF15
ITGAL	C11orf84
CAPZB	MAP4K4
VAV1	DLAT
UQCRH	SNRNP40
PAK2	KPNB1
COMT	HSDL2
GARS	DCTN2
DNAJC13	CLNS1A
STT3B	PANK4

ZNF788	TUBA4B
HCLS1	PYCR2
ACTR2	DOCK7
TOP1	SERPINB3
PGK1	ARCN1
HBA1	SEC24A
H2AFY	TPR
	GATAD2B
	MAGED2
	KRT85
	PDHB
	SHKBP1
	STK38
	ME1
	ATXN2L
	MPG
	SERPINB12
	DHX36
	RFC5
	RBM28
	SRRM2
	MYBBP1A
	SF3B3
	RANBP9
	SPRR2E
	NUDT21
	SMARCE1
	ARID1A
	BOLA2B
	SDHA
	IGF2BP1
	C21orf70
	SPRR1B
	SEPT8
	CCDC88A
	CKAP4
	CBR1
	OR52K2
	DNAJC10
	PLOD1

Table S7. RAS and TP53 mutational profiles of AML cell lines according to the CCLE database. *KRAS, NRAS* and *TP53* detailed mutational profiles of the 13 AML cell lines available in the CCLE 18Q4 mutations database and treated with various concentrations of NMS-873 for four days (n=13 with four replicates for each condition). Distribution of the NMS-873 IC_{50} is reported.

Cell line	TP53 and RAS mutations	KRAS variant classification	KRAS protein change	KRAS genome change	NRAS variant classification	NRAS protein change	NRAS genome change	TP53 variant classification	TP53 protein change	TP53 genome change
NOMO1	KRAS, TP53	Missense_Mutation	p.G13D	g.chr12:25398281C>T	0	0	0	Frame_Shift_Del	p.S241fs	g.chr17:7577558delG
SKM1	KRAS, TP53	Missense_Mutation	p.K117N	g.chr12:25378647T>G	0	0	0	Missense_Mutation	p.R248Q	g.chr17:7577538C>T
NB4	KRAS, TP53	Missense_Mutation	p.A18D	g.chr12:25398266G>T	0	0	0	Missense_Mutation	p.R248Q	g.chr17:7577538C>T
MOLM13	none	0	0	0	0	0	0	0	0	0
MV411	none	0	0	0	0	0	0	0	0	0
EOL1	none	0	0	0	0	0	0	0	0	0
HL60	NRAS, TP53	0	0	0	Missense_Mutation	p.Q61L	g.chr1:115256529T>A	Missense_Mutation	p.C242F	g.chr17:7577556C>A
THP1	NRAS, TP53	0	0	0	Missense_Mutation	p.G12D	g.chr1:115258747C>T	Frame_Shift_Del	p.RRCPHHERC174fs	g.chr17:7578385_7578410delCAGCGCTCATGGTGGGGGCAGCGCCT
TF1	NRAS, TP53	0	0	0	Missense_Mutation	p.Q61P	g.chr1:115256529T>G	Splice_Site	NA	g.chr17:7577610T>C
M07E	NRAS	0	0	0	Missense_Mutation	p.Q61K	g.chr1:115256530G>T	0	0	0
KASUMI1	TP53	0	0	0	0	0	0	Missense_Mutation	p.R248Q	g.chr17:7577538C>T
UT7	TP53	0	0	0	0	0	0	Splice_Site	NA	g.chr17:7577017A>C
U937	TP53	0	0	0	0	0	0	Splice_Site	NA	g.chr17:7578370C>T

Table S8. Mutational and functional co-occurrence of RAS activation and TP53 deficiency in pan-cancer TCGA cohorts. Co-occurrence frequency of RAS activation and TP53 deficiency assessed based on non-silent mutations and functional classifiers across pan-cancer TCGA database (10, 294 patient samples, 33 tumor lineages). TCGA tumor type acronyms and patients cohort size are detailed.

TCGA ID	Tumor type	TCGA cohort size	RAS and TP53 mutations (% co-occurrence)	RAS activation and TP53 depletion based on classifier scores (% co-occurrence)
PAAD	Pancreatic adenocarcinoma	183	53.55	72.37
UCS	Uterine carcino-sarcoma	57	24.56	37.5
READ	Rectum adenocarcinoma	171	21.05	88.14
LUAD	Lung adenocarcinoma	576	19.62	49.2
COAD	Colon adenocarcinoma	495	17.58	73.31
GBM	Glioblastoma multiforme	174	13.79	7.5
BLCA	Bladder urothelial carcinoma	427	8.43	24.37
KICH	Kidney chromophobe	91	7.69	21.54
SKCM	Skin cutaneous melanoma	474	7.17	15.7
STAD	Stomach adenocarcinoma	450	6.89	48.04
LUSC	Lung squamous cell carcinoma	554	6.86	15.73
ESCA	Esophageal carcinoma	196	6.12	32.54
ACC	Adrenocortical carcinoma	79	5.06	2.63
HNSC	Head and Neck squamous cell carcinoma	566	4.42	7.19
SARC	Sarcoma	265	4.15	7.86
UCEC	Uterine corpus endometrial carcinoma	567	3.70	14.79
LGG	Brain lower grade glioma	534	2.43	2.56
CHOL	Cholangiocarcinoma	45	2.22	16.67
BRCA	Breast invasive carcinoma	1218	1.72	20.08
CESC	Cervical squamous cell carcinoma and endocervical adenocarcinoma	310	1.61	5.51
LIHC	Liver hepatocellular carcinoma	424	0.94	9.2
KIRC	Kidney renal clear cell carcinoma	606	0.66	1.7
TGCT	Testicular germ cell tumors	156	0.64	26.39
LAML	**Acute myeloid leukemia**	**173**	**0.58**	**1.74**
OV	Ovarian serous cystadenocarcinoma	309	0.32	31.25
PRAD	Prostate adenocarcinoma	550	0.18	6.68
DLBC	Lymphoid neoplasm Diffuse large B-cell lymphoma	48	0.00	2.7
KIRP	Kidney renal papillary cell carcinoma	323	0.00	0.37
MESO	Mesothelioma	87	0.00	7.32
PCPG	Pheochromocytoma and paraganglioma	187	0.00	0
THCA	Thyroid carcinoma	572	0.00	0
THYM	Thymoma	122	0.00	0
UVM	Uveal melanoma	80	0.00	0